Engineering Journal

American Institute of Steel Construction

Third Quarter 2011 Volume 48, No. 3

www.aisc.org

ENGINEERING JOURNAL

AMERICAN INSTITUTE OF STEEL CONSTRUCTION

Dedicated to the development and improvement of steel construction, through the interchange of ideas, experiences and data.

ENGINEERING JOURNAL (ISSN 0013-8029) is published quarterly. Subscriptions: Members: one subscription, $40 per year, included in dues; Additional Member Subscriptions: $40 per year. Non-Members U.S.: $160 per year. International Members (including Canada and Mexico): $160 per year. International Non-Members (including Canada and Mexico): $320. Published by the American Institute of Steel Construction at One East Wacker Drive, Suite 700, Chicago, IL 60601.

Periodicals postage paid at Chicago, IL and additional mailing offices. **Postmaster:** Send address changes to ENGINEERING JOURNAL in care of the American Institute of Steel Construction, One East Wacker Drive, Suite 700, Chicago, IL 60601.

Hybrid Moment-Resisting Steel Frames

FINLEY A. CHARNEY and OZGUR ATLAYAN

ABSTRACT

A new type of moment-resisting steel frame, called a hybrid moment-resisting frame, is described. Unlike a typical moment frame, where all member sizes and connection details fit a specific set of rules (e.g., for a special moment frame), the hybrid frame contains members and connections with a variety of detailing rules, including those typically associated with ordinary, intermediate and special moment frames. Elements that have special detailing are designed to yield at force levels well below the design basis earthquake and thereby provide some inelastic energy dissipation that helps to control dynamic amplification. Elements with ordinary detailing are designed to remain elastic during the design basis earthquake and to provide enough positive stiffness to counteract P-delta effects. The resulting system can be designed to perform better than the traditional special moment frame and to be more economical than the special moment frame because a limited number of elements and connections have special detailing. The behavior of the system is demonstrated through incremental nonlinear dynamic response history analysis.

Keywords: seismic design, moment-resisting frames, structural steel.

The current specifications for seismic resistant design (AISC, 2005a; AISC, 2005b; ASCE, 2010) require that special detailing be used in virtually all moment-resisting frame systems that are to be constructed in high seismic hazard regions. This detailing requires the use of designated flexural yielding regions with limited width-to-thickness ratios, highly ductile prequalified connection types, limited panel zone yielding and adherence to a strong-column weak-beam design philosophy. The structure must be designed such that first significant yield occurs at lateral force levels that are at or above the design basis earthquake (DBE) forces. The sequencing of plastic hinging is usually not explicitly designed, and hence, there is no guarantee that the slope of the structure's force-deformation response (pushover curve), including P-delta effects, is continuously positive up to the maximum expected drift. This a critical design issue, because it is much more likely that dynamic instability will occur when the post-yield stiffness is negative (Gupta and Krawinkler, 2000). This fact led to a significant revision in the 2003 NEHRP provisions (FEMA, 2004), where it is required that the pushover curve be continuously positive up to 1.5 times the target displacement if the stability ratio, based on initial elastic stiffness and on design level gravity loads, exceeds 0.10. This requirement was proposed for inclusion in ASCE 7-10, but was not adopted. Another consequence of not explicitly designing the hinging sequence is that the expected overstrength, which is implicitly included in the system's response modification coefficient, R, is not guaranteed. Indeed, there is nothing in the current design provisions that prevents a designer from developing a system for which a nonlinear static pushover analysis indicates that all of the hinges form nearly simultaneously.

In a hybrid moment frame (HMF), the hinging sequence is explicitly designed to ensure a continuously positive post-yield pushover response. The HMF shares many of the features of the special moment frame (SMF), with the following exceptions:

1. The yielding sequence is set such that the first plastic hinges form at load levels well below the design basis earthquake, and the last hinges form at load levels consistent with the maximum considered earthquake. The inelastic energy dissipation provided through early yielding is expected to improve the performance of the structure subjected to earthquakes of intensity less than the design basis earthquake. The near-elastic response of the late-forming hinges is intended to guarantee a positive pushover response.
2. The detailing for the lateral load resisting components and their connections depends on the level of inelastic rotation that is expected in the various plastic hinges. The hinges that form first have the highest ductility demand and are detailed according to the rules for special moment frames. It is noted that these hinges may have ductility demands that exceed those expected from traditional SMF designs. The hinges that form last have the lowest ductility demand and are detailed

Finley A. Charney, Professor, Via Department of Civil and Environmental Engineering, Virginia Polytechnic Institute and State University, Blacksburg, VA (corresponding author). E-mail: fcharney@vt.edu

Ozgur Atlayan, Graduate Research Assistant, Via Department of Civil and Environmental Engineering, Virginia Polytechnic Institute and State University, Blacksburg, VA. E-mail: oatlayan@vt.edu

according to the rules for intermediate or ordinary moment frames.

Hewitt et al. (2009) compared the cost of an ordinary moment frame (OMF) with an SMF supposing that material and labor represent 30 and 70% of the total cost of the frame, respectively; that 50% of the labor cost is due to special connections; and that there are additional special inspection requirements for the connections. As a result of this scenario, the cost premium for an SMF over an OMF is about 22%. Even though this is a very rough estimate (because the foundation costs were ignored and moment frames were assumed as strength controlled), labor cost associated with fabrication and inspection of the connections is significant. Because HMF discussed in this paper limits the number of special connections and elements, it is expected to be more economical than a SMF.

The hybrid frame concept may be used for any structural system, such as concentrically braced frames or buckling restrained braced frames, as well as for moment-resisting frames. The concept of hybrid buckling restrained frames is particularly attractive because of the ability to tightly control the inelastic behavior of the yielding elements.

The advantages of hybrid frames will be demonstrated through two examples. The first example is of a simple hybrid braced frame and is used only to demonstrate the concepts and to introduce some of the features used in the analysis. The second example is of a nine-story steel moment resisting frame. Frames of this type are the main focus of this paper.

DEMONSTRATION OF CONCEPTS: A HYBRID BRACED FRAME

In this demonstration, a simple one-story braced frame is analyzed. This fictitious frame, shown in Figure 1, is intended to have the dynamic characteristics of a 15-story building, with a first mode period of vibration of 2.0 s. Two different versions of the frame are presented. The first frame, called the *normal frame,* has six identical diagonal braces; each with an axial strength of 141 kips. The second frame, called the *hybrid frame,* has bracing bars of the following strengths: bar 1 = 47 kips, bar 2 = 94 kips, bars 3 and 4 = 141 kips, bar 5 = 188 kips and bar 6 = 235 kips. The lateral strength of both structures, exclusive of P-delta

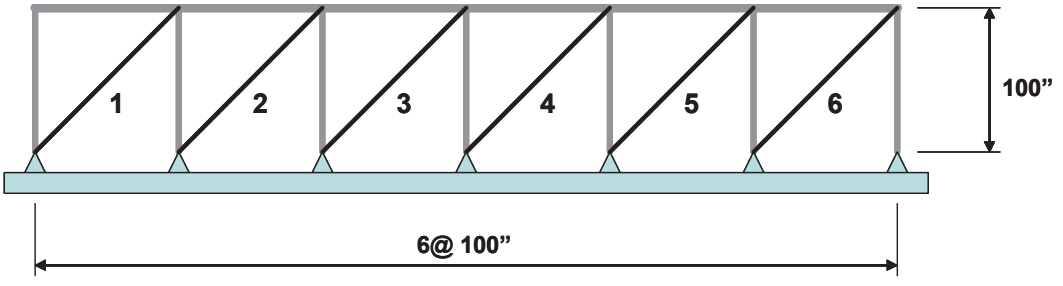

Fig. 1. A simple braced frame.

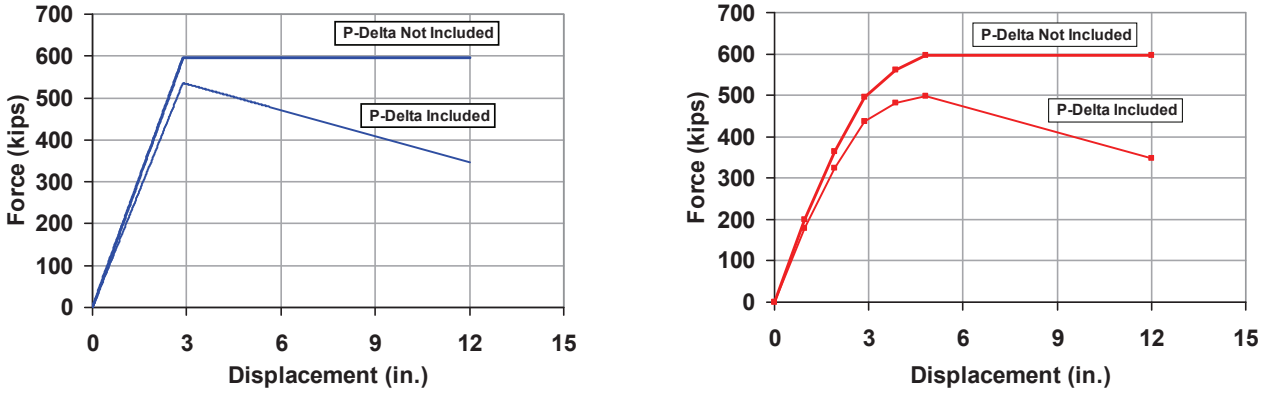

Fig. 2. Nonlinear static pushover curves for braced frame structure: (a) normal frame; (b) hybrid frame.

effects, is 600 kips. The axial stiffness of each of the bars, whether in the normal or hybrid frame, is 68.9 kips/in. The initial lateral stiffness of each frame is 207 kips/in. The force-deformation behavior of the bars was assumed to be elastic-plastic, without strain-hardening.

Nonlinear static pushover plots of the normal and hybrid frames are shown in Figures 2a and 2b, respectively. Response curves with and without P-delta effects are shown in the figures. Where included, the P-delta analysis emulates a structure with an average story stability ratio of 0.10.

To investigate the dynamic behavior, the normal and hybrid structures, with and without P-delta effects included, were subjected to the 1940 Imperial Valley ground motion, with a peak ground acceleration of 0.35 g. For each case, the structure was repeatedly subjected to this ground motion, with each analysis using an incrementally larger ground-motion multiplier. The multipliers ranged from 0.2 to 2.0, in increments of 0.2. For this example, it was assumed that a multiplier of 1.0 corresponds to the design basis earthquake (DBE) and the factor of 1.5 corresponds to the maximum considered earthquake (MCE).

Analysis was run using NONLIN-Pro (Charney and Barngrover, 2006), which uses the Drain 2D-X (Prakash et al., 1993) analysis engine. All analyses were run with an inherent damping ratio of approximately 0.02. One set of analyses was run without P-delta effects and the other with P-delta effects. When P-delta effects were considered, both the normal and hybrid structures were dynamically unstable when the ground motion multiplier exceeded 1.5.

Plots of the results for the models without P-delta effects are shown in Figures 3a through 3d. Figure 3a plots the ground-motion multiplier on the vertical axis and the computed roof displacement on the horizontal axis. The displacements appear to be similar between the two systems, except that it is noted that the hybrid frame displacements are about 12 to 15% less than the normal frame displacements for the first two increments of loading. For all ground-motion levels less than or equal to the MCE, the residual inelastic

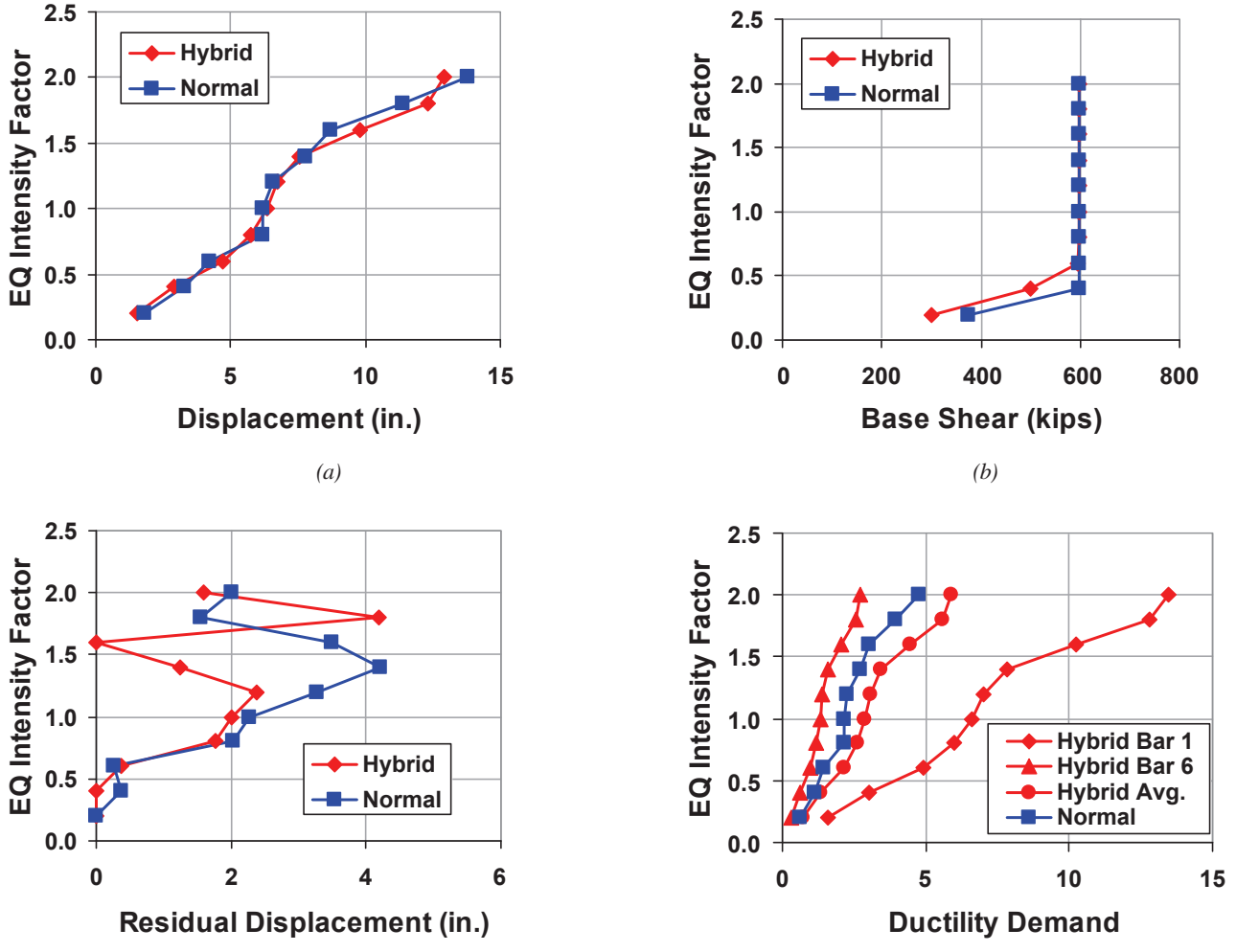

Fig. 3. Results of frame analysis without P-delta analysis.

deformations, presented in Figure 3c, are significantly lower for the hybrid frame when compared to the normal frame. (Residual deformations are the permanent lateral deformations that remain in the structure after ground shaking has ceased.) At the ground motion intensity level of 1.8, however, the residual deformations in the hybrid frame exceed those in the normal frame. The base shears for the hybrid frame, shown in Figure 3b, are also lower than those for the normal frame for the first two increments of ground motion intensity.

Displacement ductility demands for bar 1, bar 6 and for the average of all bars are presented in Figure 3d. For the hybrid frame, bar 1 is the weaker bar, and as expected, the ductility demand is the highest. At the DBE level (multiplier 1.0), the ductility demand for bar 1 is 6.61. At the same intensity, the ductility demand for bar 6 is only 1.32, and the average ductility demand for all hybrid bars is 2.88. For the normal frame, the ductility demand for all bars is the same at each intensity level and is 2.15 at the multiplier of 1.0.

It appears from the results that the hybrid frame is performing as expected. Displacements at low-level ground motions are reduced due to the early yielding and associated hysteretic behavior of bars 1 and 2. Delayed yielding of the stronger bars provides a component of elastic stiffness that controls residual deformations.

When P-delta effects are included, the performance of the hybrid frame is further improved when compared to the normal frame. This is illustrated in Figures 4a through 4d, where it may be seen that the total displacements, Figure 4a, are significantly less in the hybrid frame at all ground motion levels up to the DBE. This improved performance is due to the significant reduction in residual deformations, shown in Figure 4c. As mentioned earlier, both the hybrid and normal frames displayed dynamic instability when the ground motion multiplier exceeded 1.5. This is due to the negative stiffness of the pushover curves (see Figure 2) at larger displacements.

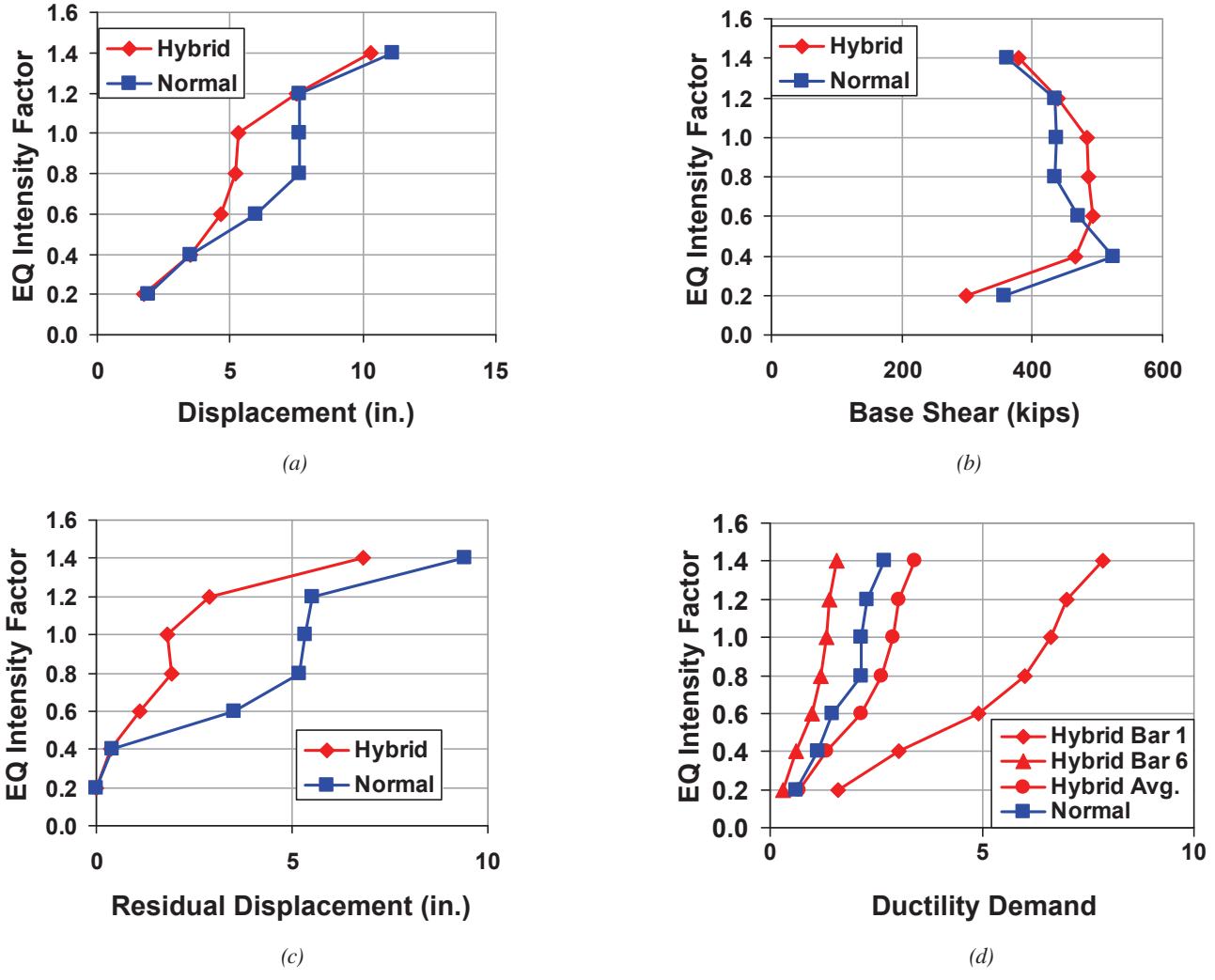

Fig. 4. Results of frame analysis with P-delta analysis.

Table 1. ASCE 7-10 Design Parameters for Hybrid Frame	
Design Parameter	**Value**
0.2-s spectral acceleration, S_S	1.25 g
1.0-s spectral acceleration, S_1	0.5 g
Site class	D
0.2-s design acceleration, S_{DS}	0.83 g
1.0-s design acceleration, S_{D1}	0.5 g
Seismic use group	II
Importance factor	1.0
Seismic design category	D
Effective seismic weight, W	10,500 kips

It is interesting to note from Figure 4b that for ground motion multipliers between 0.6 through 1.0, the base shears for the hybrid frame are somewhat greater than for the normal frame. This is not a disadvantage for the hybrid frame, because the lower base shears for the normal frame are associated with P-delta related strength loss.

ANALYSIS OF A HYBRID MOMENT-RESISTING FRAME

Models and Design Procedures

The hybrid moment frame concept is demonstrated by the analysis of a five-bay, nine-story frame building, located near Seattle, Washington. The geometry of this building is identical to that studied in the SAC Steel Project (FEMA, 2000). The ASCE 7 design parameters used for the design are summarized in Table 1. Four different frame configurations were used in this study. The first configuration, hybrid-0, is closest to the normal frame design, because the same girder sizes were used for each bay in a given story. The other three configurations are the real hybrid designs, referred to hybrid-1, hybrid-2, and hybrid-3 frames, because the girder sizes for these frames are different in different bays. The hybrid-0 frame is the least hybrid (closest in design to the traditional frame), and hybrid-3 frame is the most hybrid (furthest in design concept from the traditional frame). Figure 5 shows the member sizes used for the different frames. Member sizes for the girders are shown above each girder, with the hybrid-0 frame at the bottom and the hybrid-3 frame at the top. The column sizes were the same for all of the designs.

The two exterior girders of the hybrid frames (bays 1 and 5) were designed as special moment frames (SMF), the two interior girders (bays 2 and 4) were designed as intermediate moment frames (IMF) and the middle girder (bay 3) was designed as an ordinary moment frame (OMF). For this reason, a new response reduction factor, R, and deflection amplification factor, C_d, were assumed as 6 and 5, respectively, for hybrid frame design. Note that these values are close to the weighted average R and C_d values of the SMF (two bays), IMF (two bays) and OMF (one bay). After the sections of the hybrid-0 were found by using $R = 6$ and $C_d = 5$, the plastic capacities were changed throughout the story for the other real hybrid frames. The plastic capacities of the exterior girders were decreased by 25, 37.5 and 50% for the hybrid-1, hybrid-2 and hybrid-3 frames, respectively. Because the main idea of the hybrid frame concept is to keep the total strength of the story the same, the plastic capacity of the middle girder was increased by 50, 75 and 100% for the hybrid-1, hybrid-2 and hybrid-3 frames, respectively. Bay-2 and bay-4 girder capacities were kept the same for all the frames. In summary, as the frame identification number gets bigger, the frames become more hybrid, with a greater variation in beam sizes at each story.

The column sections were kept the same for all the designs, but the panel zone doubler plate thicknesses were changed as necessary to meet AISC panel zone rules. Reduced beam sections were used for all the girders except for the girder in the middle bay, which was designed according to the rules for an OMF. The strong column–weak beam requirement was satisfied at the joints of the columns on column lines 1, 2, 5 and 6. Material nonlinearity was considered through assigning a bilinear moment-rotation relationship to beams and columns. Two percent strain hardening was used in the development of moment-rotation relationships. See Atlayan (2008) for a much more detailed description of the step-by-step procedures of beam, column and panel zone design. Panel zones were explicitly represented by use of Krawinkler's model (Charney and Marshall, 2006). P-delta effects were included in all analysis, using a special linear "ghost frame," which captures the entire gravity load tributary to the leaning columns. The inherent damping was determined by setting the critical damping ratio to 2% at the natural period of the structure and at a period of 0.2 s, as it was done in the SAC Report (FEMA, 2000).

Two types of analysis were performed for each frame: nonlinear static pushover analysis (NSP) and incremental dynamic analysis (IDA). For both analyses, gravity loads were followed by the static pushover lateral load pattern or dynamic earthquake load case. All structural analyses were conducted using Perform-3D (CSI, 2006), using a planar frame that is parallel to the design ground motion.

Nonlinear Static Pushover Analysis

Nonlinear static pushover curves for the four different hybrid frames are illustrated in Figure 6. Note that the point of the first significant yield and the point at which the post-yield curve becomes negative are shown on the figure. As expected, the hybrid-3 frame starts yielding first, and the hybrid-0 frame yields last. The more reduction in the plastic

capacity of the exterior bays, the earlier the structure starts yielding. In addition, the negative post-yield stiffness of the pushover curves is reached later, as the frames become more hybrid. It is foreseen that the early yielding of the pushover curve will provide hysteretic energy dissipation to the frame, which will result in a better dynamic behavior under less severe ground motions. Furthermore, negative post-yield stiffness has a significant effect on structures and is a significant contributor to dynamic instability. Although the frames were pushed until they reached 4% roof drift, it is predicted that the hybrid-0 (normal frame) will reach a steeper negative stiffness than the real hybrid frames if the frames are pushed more than 4% reference drift. This behavior may be observed in the last portion of Figure 6.

Having control of plastic hinge sequence is a key concept in hybrid frame design. For this design, the plastic hinges at the exterior bays formed first, and the ones at the middle bay formed last. As a result of pushover analyses, the hinges at the right ends of the exterior bays formed first. This is because the gravity loads were applied initially, and the lateral loads were acting toward the east direction, causing the moments with the same signs to accumulate at the right ends. In other words, if a particular girder had such a preload (due to gravity loads) that the positive moment hinges were near

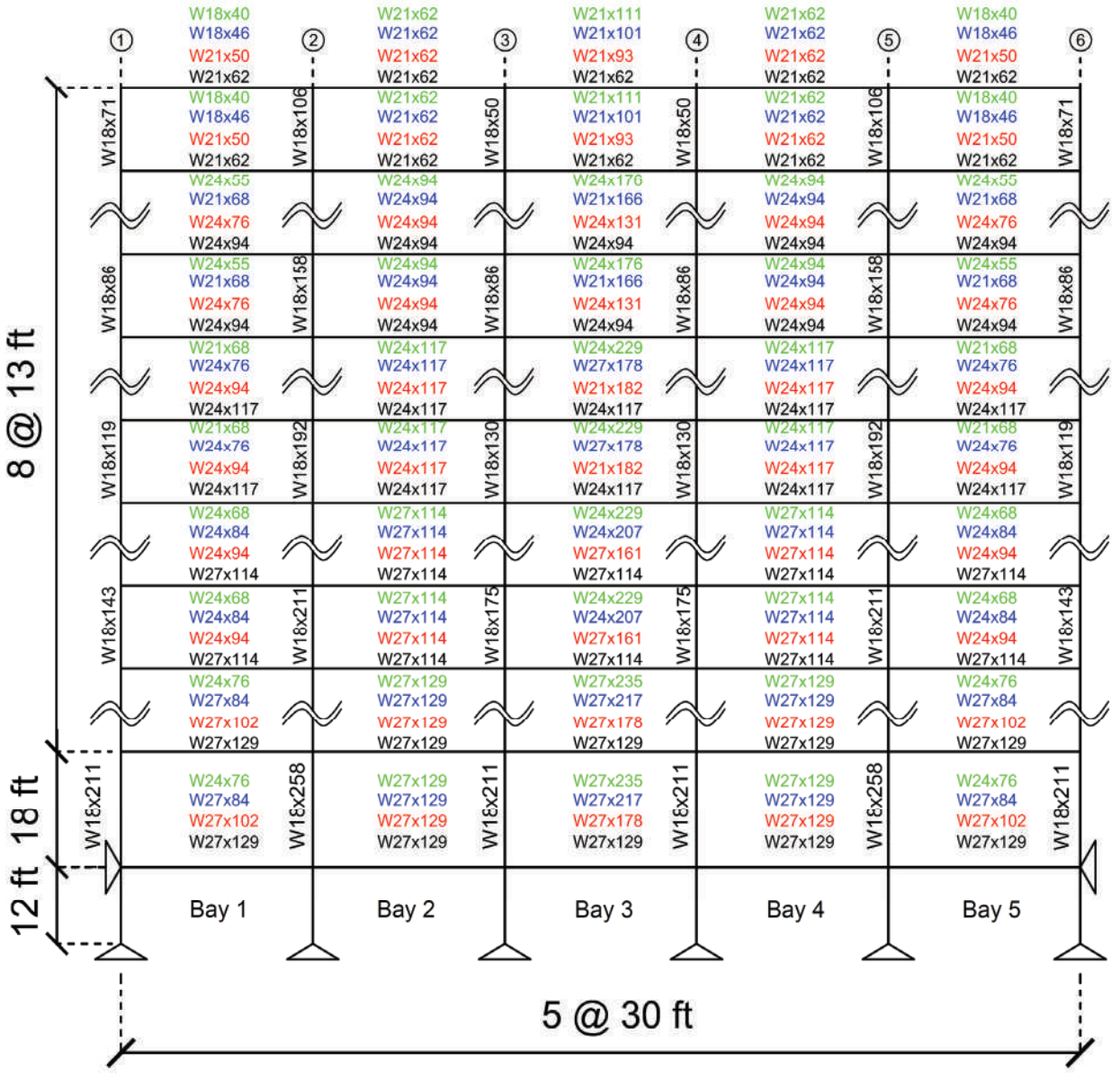

Fig. 5. Member sizes used for hybrid-0 to hybrid-3 frame (bottom to top).

Table 2. Ground-Motion Records Used in Analysis						
EQ No.	SAC Name	EQ Name	Time Step (s)	Newmark Integration Time Step	Scale Factor	Scaled PGA
EQ00	SE 21	Mendocino, 1992	0.020	0.005	0.403	0.311
EQ01	SE 23	Erzincan, 1992	0.005	0.005	0.657	0.313
EQ02	SE 25	Olympia, 1949	0.020	0.005	2.111	0.435
EQ03	SE 27	Seattle, 1965	0.020	0.001	6.214	1.087
EQ04	SE 29	Valparaiso 1, 1985	0.025	0.0025	2.088	1.178
EQ05	SE 31	Valparaiso 2, 1985	0.025	0.001	3.934	1.262
EQ06	SE 33	Deep Interplate	0.020	0.001	4.281	0.888
EQ07	SE 36	Miyagi-Oki, 1978	0.020	0.001	1.189	0.523
EQ08	SE 37	Shallow Interplate 1	0.020	0.005	1.054	0.632
EQ09	SE 40	Shallow Interplate 2	0.020	0.001	1.747	0.879

yield, it would take only a small incremental lateral load to cause yielding in this girder (whereas stronger girders would not have yielded until more lateral load was applied). This is exactly what is happening in the hybrid frames (i.e., the gravity preload influenced the sequence of yielding).

Incremental Dynamic Analysis

Incremental dynamic analysis, sometimes called dynamic pushover analysis, consists of a sequence of nonlinear response history analyses of the structure, with each analysis in the sequence subjecting the structure to the same basic ground motion, but at a higher intensity than the previous analysis in the sequence (Vamvatsikos, 2002). In this study, IDA analysis was conducted for the structure subjected to 10 different earthquake records at intensities of 0.2 to 2.0 times the ground motion scaled to match the design basis earthquake. The ground motions were scaled to match the ASCE 7 design basis spectrum at the structure's fundamental period of vibration. This scaling procedure is recommended for IDA analysis by Shome et al. (1998). The ground

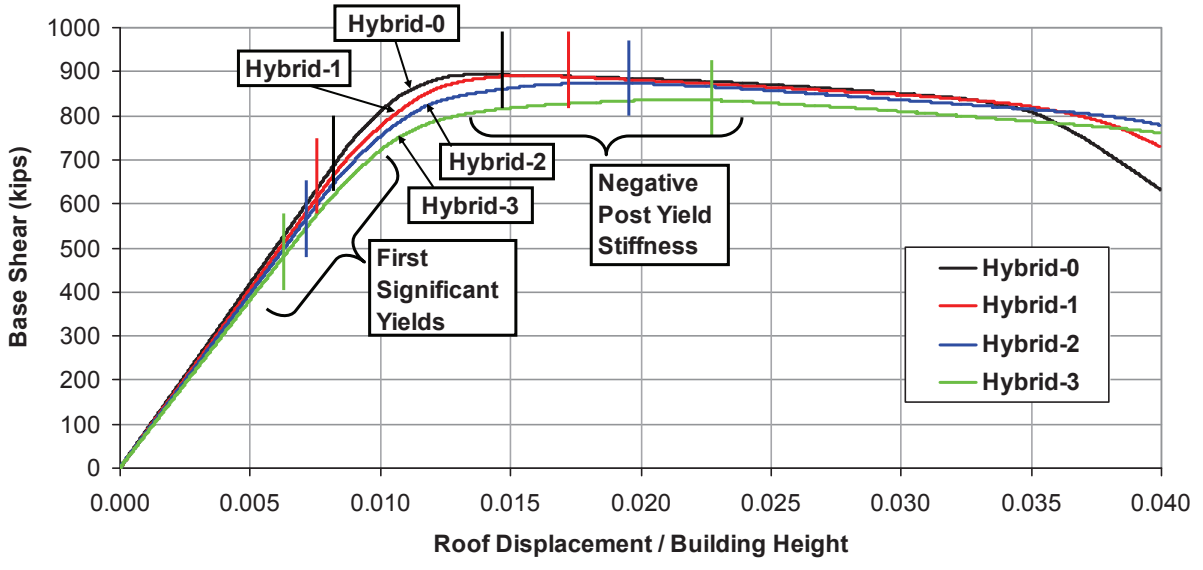

Fig. 6. Static pushover curves for hybrid frames.

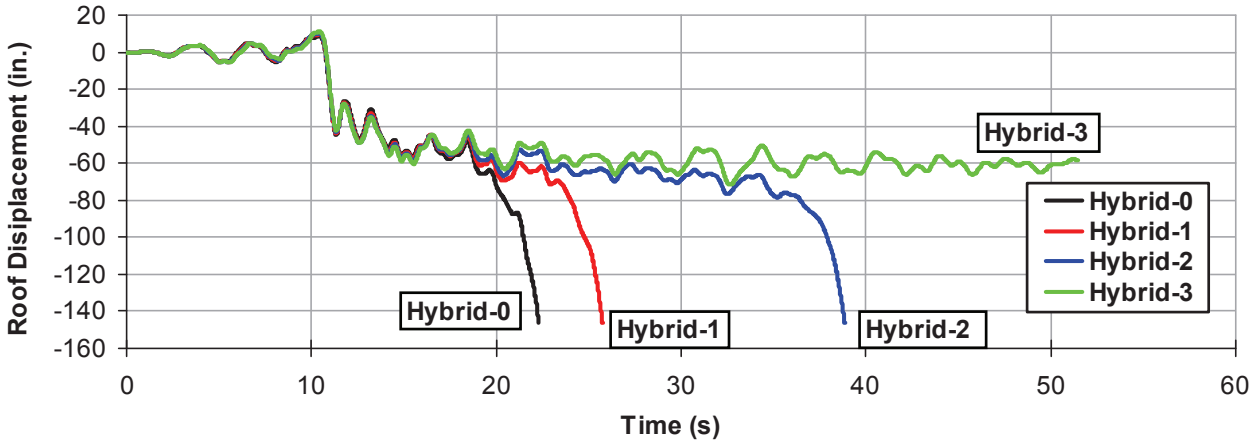

Fig. 7. Roof displacement response history of hybrid frames subject to EQ07 with scale of 2.0 times the anchored design spectrum scale.

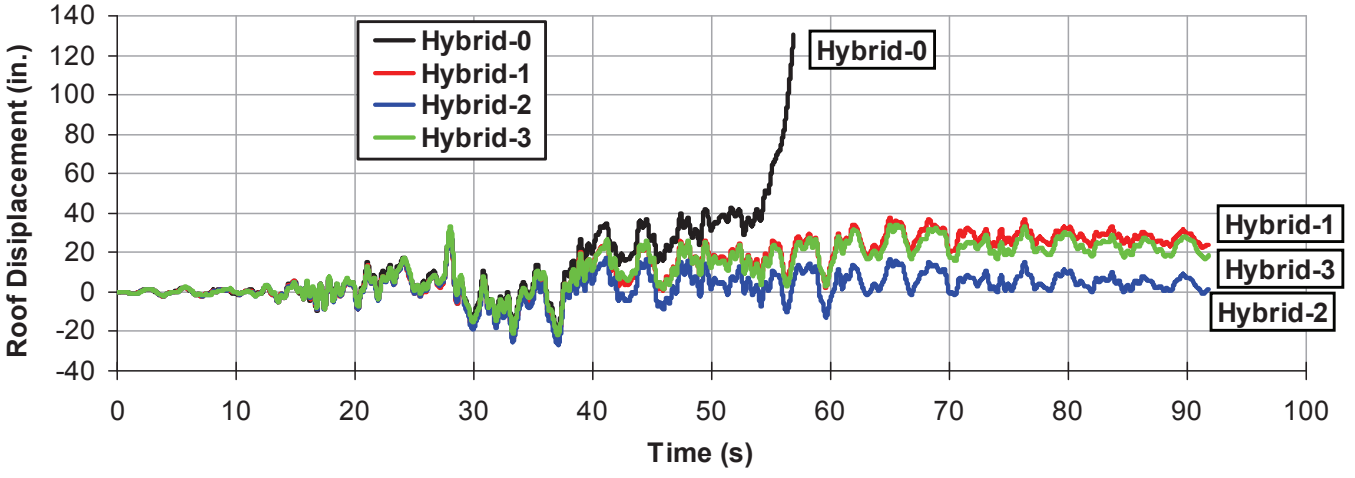

Fig. 8. Roof displacement response history of hybrid frames subject to EQ05 with scale of 1.6 times the anchored design spectrum scale.

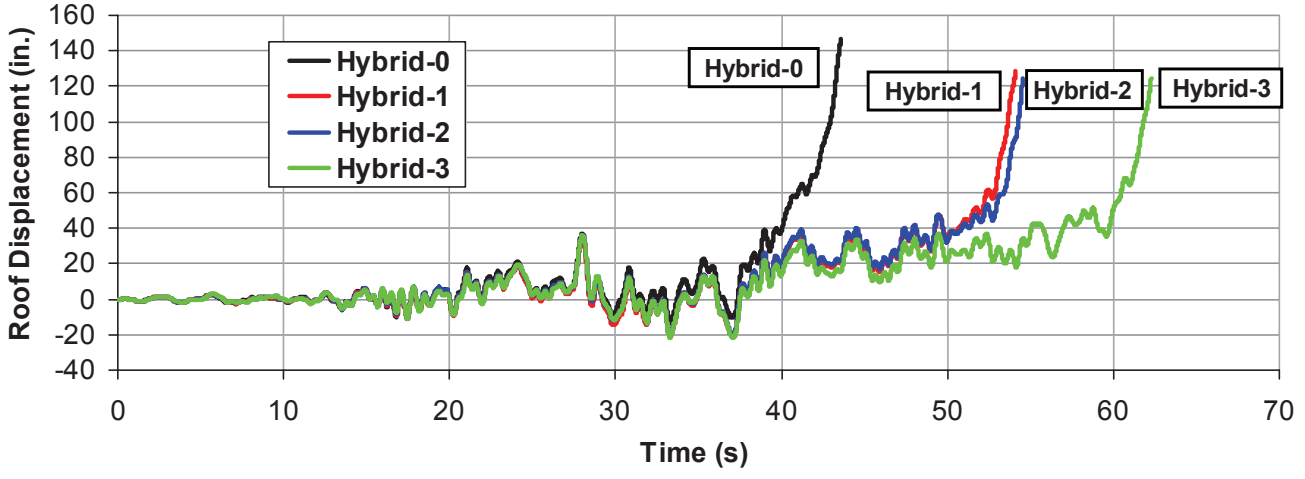

Fig. 9. Roof displacement response history of hybrid frames subject to EQ05 with scale of 1.8 times the anchored design spectrum scale.

motions used in the analysis are summarized in Table 2. It is noted that these ground motions, developed by Somerville (1996), are the same as those used in the original SAC research (FEMA, 2000).

Figures 7 and 8 illustrate the roof displacement response histories of hybrid frames subjected to EQ07 and EQ05 with scale factors of 2.0 and 1.6 times the anchored design spectrum scaling, respectively. These two earthquakes are the most severe ones out of all the earthquakes used in this study. As can be seen from Figure 7, hybrid-0, hybrid-1 and hybrid-2 frames reach dynamic instability, whereas the hybrid-3 frame, the most hybrid frame, resists the collapse with 60 in. residual displacement at the roof level. Similarly, all the real hybrid frames (except the normal frame, hybrid-0) resist the collapse under 1.6 times DBE scaled EQ05 motion (see Figure 8). Note that the hybrid-2 frame results in less residual displacement in Figure 8. When the scale factor of the same ground motion is increased from 1.6 to 1.8 (see Figure 9), all of the hybrid frames collapse; however, as the frames become more hybrid, they resist the collapse more—i.e., collapses occur at a later time.

Figure 10 shows the roof displacement response histories when the frames are subjected to EQ09 with IDA scaling of 2.0. Although none of the frames collapse, the residual

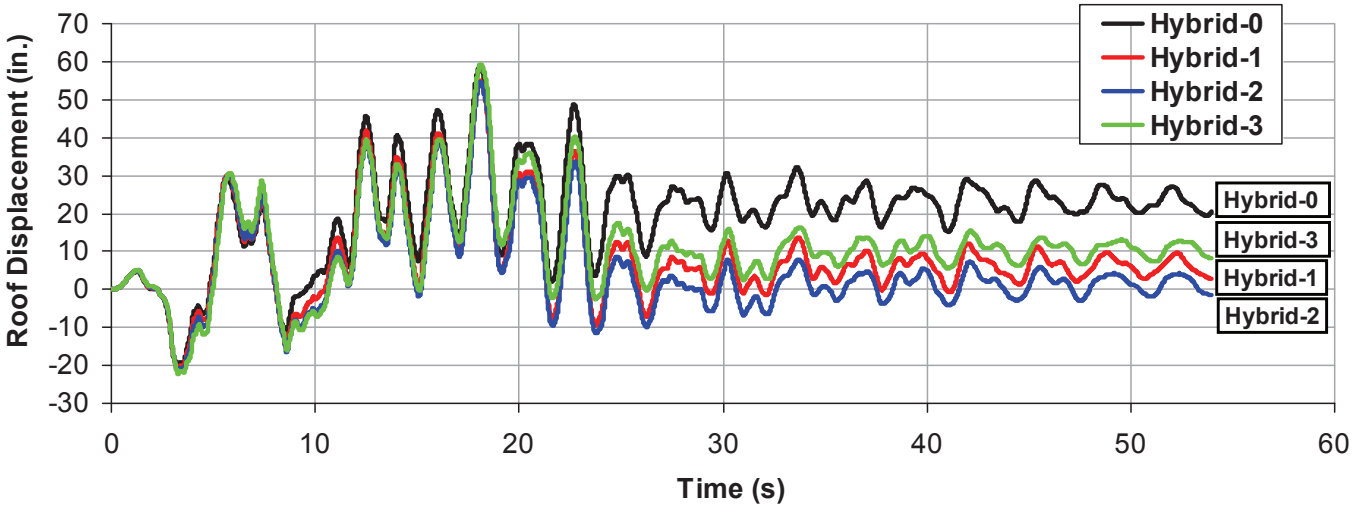

Fig. 10. Roof displacement response history of hybrid frames subject to Shallow Interpolate 2 (EQ09) with scale of 2.0 times the anchored design spectrum scale.

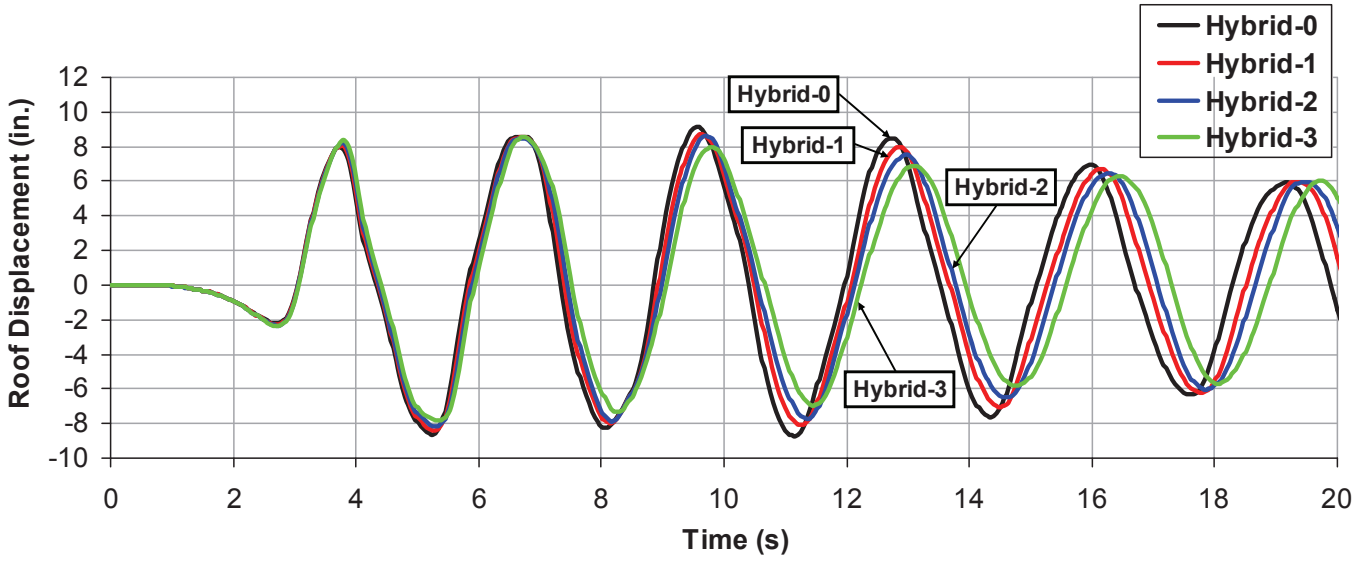

Fig. 11. Roof displacement response history of hybrid frames subject to Mendocino (EQ00) with scale of 0.4 times the anchored design spectrum scale.

displacement is the most for the hybrid-0 frame, which is actually the normal frame. Similar to the behavior in Figure 8, the hybrid-2, instead of the hybrid-3 frame, gives better results in terms of residual displacements. (See Figure 10.)

The effect of early yielding of hybrid frames on pushover curves is observed at low-scaled small magnitude earthquakes. Figure 11 shows an example of this behavior when the frames are subjected to EQ00. As the frames become more hybrid, the maximum displacements decrease due to hysteretic energy dissipation, which is a predicted result of early yielding. Similar results are obtained from EQ01, which is also a small magnitude earthquake.

Figures 12a and 12b illustrate the residual displacement IDA plots when the hybrid frames are subjected to EQ09 and EQ04, respectively. The real hybrid frames (hybrid-1, 2 and 3) result in better results (less residual displacements) for EQ09. The results of EQ04 are close; however, hybrid frames (especially hybrid-2 and 3) result in more residual displacements than the normal frame.

Figures 13a and 13b show the base shear IDA plots for EQ04 and EQ08, respectively. As the frames become more hybrid, the base shear decreases slightly under all the

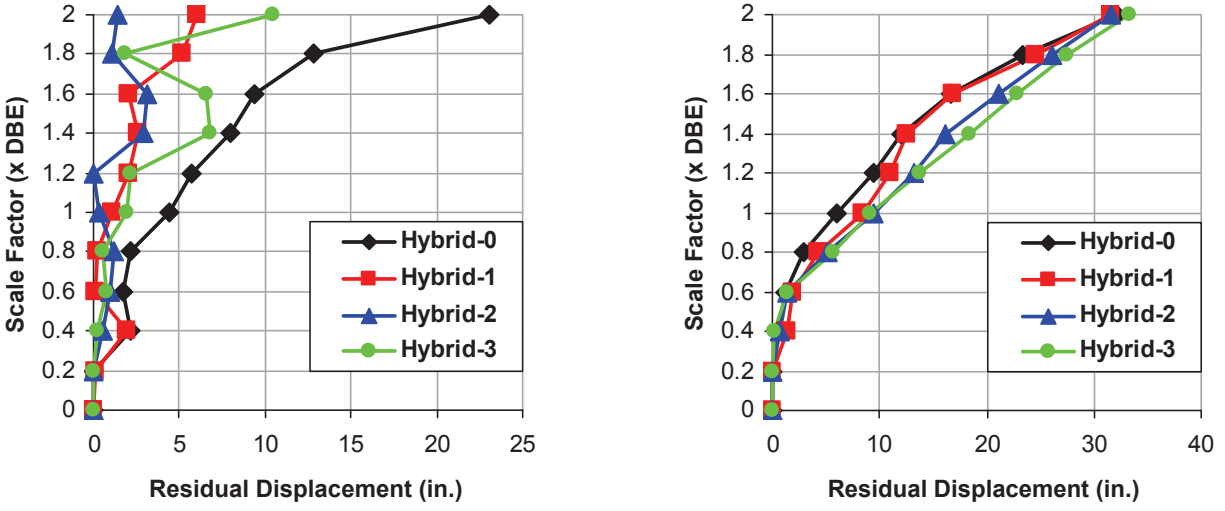

Fig. 12. IDA plots for residual roof displacement using (a) Shallow Interplate 2 (EQ09) and (b) Valparaiso (EQ04) ground motions.

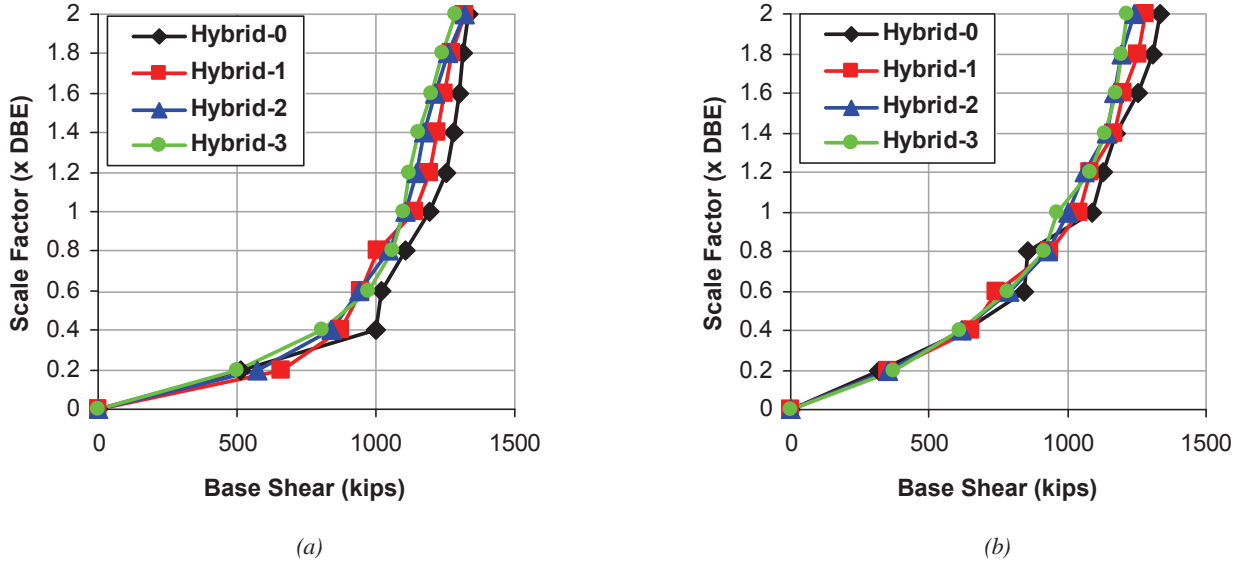

Fig. 13. Base shear IDA plots for (a) Valparaiso 1 (EQ04) and (b) Shallow Interplate1 (EQ08) earthquakes.

earthquakes. In the elastic part of the base shear IDA plots, base shears of different hybrid designs are almost identical. However, in the inelastic part, the normal frame results in slightly more base shear.

In hybrid frames, there is an increase in ductility demand for the elements that are expected to yield early. Figure 14 illustrates the ductility demand IDA plots for the entire hybrid frames subjected to EQ03. Plastic hinge rotations of the first-story bays were used to calculate the ductility demands.

As may be seen in Figure 14, bay-1, the weakest bay referring to SMF, has higher ductility than bay-2 and bay-3, which correspond to IMF and OMF systems, respectively. While bay-1 has the highest ductility demand, bay-3 has the lowest ductility demand for all of the hybrid designs. As the frames become more hybrid (from hybrid-0 to hybrid-3), the ductility demand difference between the bays increases at the same level of ground motion intensity. Because the hybrid-0 frame has the same girder sizes across the same level

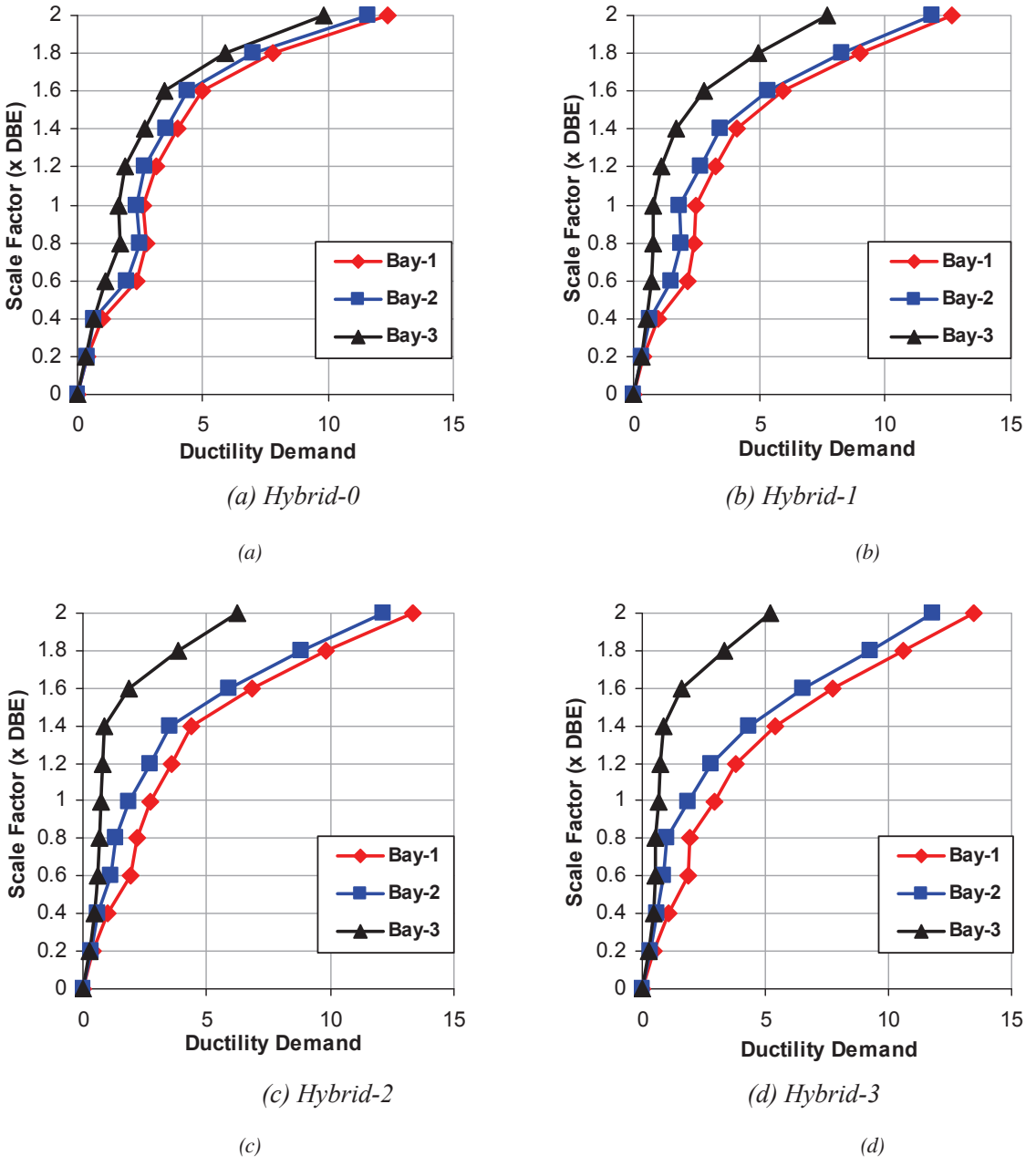

(a) Hybrid-0

(a)

(b) Hybrid-1

(b)

(c) Hybrid-2

(c)

(d) Hybrid-3

(d)

Fig. 14. Rotational ductility demand IDA plots for the first-story bays of hybrid frames (ground motion EQ03): (a) hybrid-0; (b) hybrid-1; (c) hybrid-2; (d) hybrid-3.

(story), the ductility demands of different bays are very close to each other (see Figure 14a).

In addition, the plastic hinges of bay-3 do not yield until the scale factor of 1.4 times the DBE for hybrid-2 frame and until 1.6 times the DBE for hybrid-3 frame. However, the plastic hinges of the same bay yield at a scale factor of 1.0 times the DBE for the hybrid-0 and hybrid-1 frames. As may be seen in Figure 15, as the frames become more hybrid, the ductility demand of bay-3 decreases, and the ductility demand of bay-1 increases (except for the scale factors of 0.6 to 0.8). As a result, the hinges that form first have the highest ductility demand and are detailed according to the rules for SMF systems, and the hinges that form last have the lowest ductility demand and are detailed according to the rules for OMF.

Note that only the first-story IDA ductility demands of Seattle earthquake (EQ03) are displayed in this paper. The Seattle earthquake resulted in about 30 in. residual displacement for all hybrid frame designs when the scale factor of 2.0 times the DBE was used. Different ground motions will result in different ductility demands; however, the general trend in the ductility demand of the different bays (corresponding to different moment frame systems) will be similar.

As a result of this preliminary moment frame study, real hybrid frames (hybrid-1, 2 and 3) always gave better results than hybrid-0 (normal) frame when the structures were subjected to severe earthquakes that caused collapses or significant residual displacements; i.e., hybrid frames are useful in terms of collapse prevention. This structural behavior can be explained with the effect of the relatively late occurrence of negative post-yield stiffness in hybrid frames (see Figure 6). Although hybrid frames could not improve the structural performance when the frames are subjected to EQ01, EQ02 and EQ04, if the overall performance is considered, hybrid frames resulted in better dynamic responses of the system. It is authors' opinion that hybrid frames especially perform better under pulse-type earthquakes where incremental velocities occur and give rise to damage or collapses. Figure 7 displays a nice example of this behavior. As may be seen, the residual displacements begin at the 11th second, and this is where the highest incremental velocity occurs in the Miyagi-Oki (EQ07) earthquake.

This preliminary hybrid moment frame study shows that this new approach may be considered at the design stage of new structures; however, further research is necessary, including an optimization study (where different R and C_d factors can be used with different new design configurations) as well as new strategies for hybrid frame development.

AN ALTERNATIVE STRATEGY FOR DEVELOPING HYBRID BEHAVIOR

In the moment frames studied in this paper, hybrid behavior was obtained by varying the moment capacities of the girders across the bays and by use of gravity preload. Another approach for achieving hybrid behavior would be the use of steels with varying yield strength. The use of low-strength steels and stainless steels might be particularly attractive for the early-yielding components of hybrid frames.

Among carbon steel alloys, two grades have been identified that have a low yield stress and strain and that have excellent ductility. These materials, called LYP steels (for

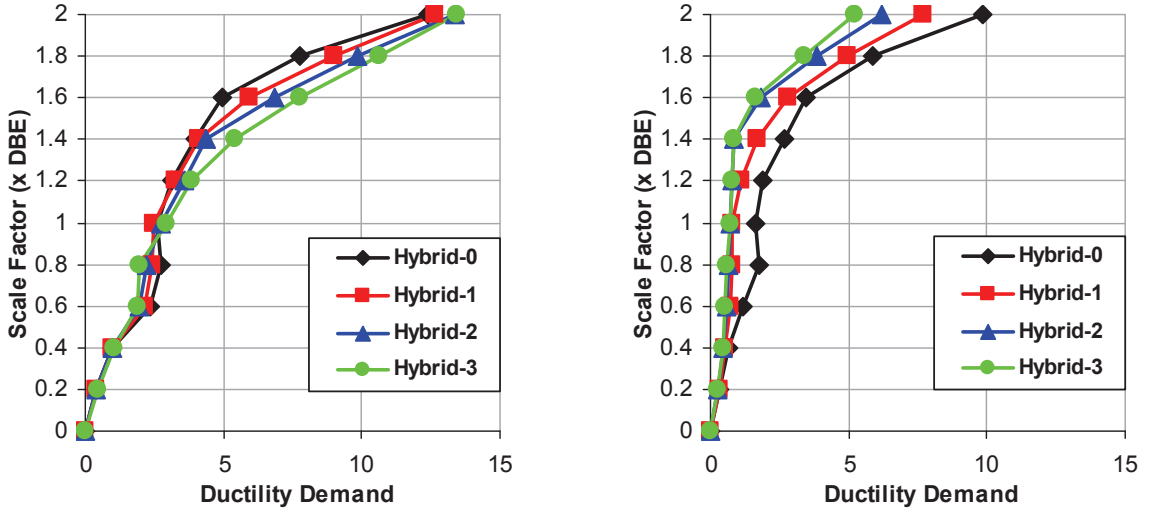

Fig. 15. Rotational ductility demand IDA plots for (a) bay-1 and (b) bay-3 of the first story (ground-motion EQ03).

low yield point), have yield stresses as low as 14.5 ksi (Saeki et al., 1998). The modulus of elasticity of the 14.5 ksi steel is approximately 22,500 ksi. While this modulus is lower than the modulus of structural steels (29,000 ksi), the yield strain of the 14.5 ksi steel (14.5/22,500 = 0.00064 in./in.) is significantly less than that of structural steels (50.0/29,000 = 0.00172 in./in.). Chen et al. (2001) tested four buckling restrained brace specimens using LYP and found them to be particularly effective for systems in which early yielding was desirable. Stainless steels have a relatively low yield stress when compared to structural steels and have excellent energy dissipation capacity. DiSarno et al. (2008) explored the use of stainless steels in both concentrically braced frames and eccentrically braced frames and found that the strain hardening characteristics of the stainless steels delayed inelastic buckling, which contributed to enhanced overstrength in the systems studied.

SUMMARY AND CONCLUSIONS

While the work reported in this paper is preliminary, it appears that there are significant benefits associated with the concept of hybrid frames. By carefully controlling the sequence of yielding, there is a clear indication of improvement in response at all levels of ground shaking, particularly at higher levels where dynamic instability may be more prevalent. At lower levels of shaking, the improvement is less significant, although there is a trend toward reduced displacements and base shears. This behavior is associated with the energy dissipation provided by early yielding of the low-strength plastic hinges.

For the frames studied, there is a significant increase in ductility demand, compared to traditional special moment frames, for those elements and connections that are expected to yield early. Although it is expected that traditional special moment frame detailing will suffice for these locations, additional research needs to be done to determine how much ductility can actually be provided by such connections. It may be necessary to develop special connection details for these areas. The use of special low-strength steels should also be investigated.

Additionally, the hybrid frames described herein were designed on an ad-hoc basis, because no specific rules have been established for assigning the sequence of yielding. It is expected that improved performance can be obtained if the sequence of hinging is more formally optimized. The use of an energy-based procedure is being explored for use in the development of an optimum hinging sequence.

Finally, additional work needs to be done to determine if significant economy is obtained by the hybrid frames. Such economy would be expected even if the performance of the hybrid frames was equivalent to the normal frames. This advantage in economy is due to the reduction in the number of special moment connections in the structure.

REFERENCES

AISC (2005a), *Seismic Provisions for Structural Steel Buildings*, ANSI/AISC 341-05, American Institute of Steel Construction, Chicago, IL.

AISC (2005b), *Prequalified Connections for Special and Intermediate Moment Frames for Seismic Applications*, ANSI/AISC 358-05, American Institute of Steel Construction, Chicago, IL.

ASCE (2010), *Minimum Design Loads for Buildings and Other Structures*, ASCE/SEI 7-10, American Society of Civil Engineers, Reston, VA.

Atlayan, O. (2008), "Effect of Viscous Fluid Dampers on Steel Moment Frames Designed for Strength, and Hybrid Steel Moment Frame Design," M.S. Thesis, Department of Civil Engineering, Virginia Tech, Blacksburg, VA.

Charney, F.A. and Barngrover, B. (2006), *NONLIN-Pro Base Program Description and User's Guide*, Advanced Structural Concepts, Inc., Blacksburg, VA.

Charney, F.A. and Marshall, J.D. (2006), "A Comparison of the Krawinkler and Scissors Models for Including Beam-Column Joint Deformations in the Analysis of Steel Frames," *Engineering Journal*, AISC, Vol. 43, No. 1, pp. 31–48.

Chen, C.C., Chen, S.Y. and Liaw, J.J. (2001), "Application of low yield strength steel on controlled plastification ductile concentrically braced frames," *Canadian Journal of Civil Engineering*, Vol. 28, pp. 823-836.

CSI (2006), *Perform-3D User's Guide, Nonlinear Analysis and Performance Assessment of Structures*, Computers and Structures Inc., Berkeley, CA.

DiSarno, L., Elnashai, A.S. and Nethercot, D.A. (2008), "Seismic Response of Stainless Steel Braced Frames," *Journal of Constructional Steel Research*, Vol. 64, No. 7–8, pp. 914–925.

FEMA (2000), *State of the Art Report on Systems Performance*, FEMA-355C, Federal Emergency Management Agency, Washington, DC.

FEMA (2004), *NEHRP Recommended Provisions for Seismic Regulations for New Buildings and Other Structures*, FEMA 450-1, Federal Emergency Management Agency, Washington, DC.

Gupta, A. and Krawinkler, H. (2000), "Dynamic P-delta Effects for Flexible Inelastic Steel Structures," *Journal of Structural Engineering*, ASCE, Vol. 126, pp. 145–154.

Hewitt, C., Sabelli R. and Bray J. (2009), "Economy of Steel-Framed Buildings for Seismic Loading," *Steel Tips*, Structural Steel Education Council, Moraga, CA.

Prakash, V., Powell, G.H. and Campbell, S. (1993), *Drain 2DX Base Program Description and User's Guide*, University of California, Berkeley, CA.

Saeki, E., Sugisawa, M., Yamaguchi, T. and Wada, A. (1998), "Mechanical Properties of Low Yield Point Steels," *Journal of Materials in Civil Engineering*, Vol. 10, No.3, pp. 143–152.

Shome, N., Cornell, C.A., Bazzurro, P. and Carballo, J.E. (1998), "Earthquakes, Records and Nonlinear Responses," *Earthquake Spectra*, Vol. 14, pp. 469–500.

Somerville, P.G. (1996), "Ground Motion Prediction for Performance Based Seismic Engineering," *Proc. 65th SEAOC Annual Convention*, Structural Engineers' Association of California, Maui, HI, pp. 67–86.

Vamvatsikos, D. (2002), "Seismic Performance, Capacity, and Reliability of Structures as Seen Through Incremental Dynamic Analysis," Ph.D. Thesis, Department of Civil Engineering, Stanford University, Stanford, CA.

Lightly Damped Moment-Resisting Steel Frames: A Design-Based Approach

OZGUR ATLAYAN and FINLEY A. CHARNEY

ABSTRACT

The current U.S. seismic design provisions for steel moment-resisting frames generally result in structures for which stiffness is the controlling factor in the design. The design for stiffness often provides considerable overstrength, which reduces rotational ductility demand on the plastic hinges in the structure. Even though the reduction in ductility demand may be considerable, the design provisions do not allow the detailing rules to be waived, resulting in designs that may not be economically optimized. This paper presents the results of a study in which a variety of steel frames were designed for strength and that used added energy dissipation in the form of linear viscous dampers to control the drift. The goal of the study was to provide only enough damping to control the drift, and to this end, it was found that total system damping of 10% critical was sufficient. As shown in the paper, the added damping provided the required drift control and had the added advantage of minimizing the dispersion, which typically occurs in response history analyses carried out under several appropriately scaled ground motions. Such dispersion control is illustrated through incremental dynamic analysis of damped nine-story buildings in Seattle, Washington.

Keywords: seismic design and performance, viscous fluid dampers, incremental dynamic analysis.

Properly designed moment-resisting steel frames are generally very effective in resisting strong earthquakes. However these systems, designed for strength alone, may not have sufficient stiffness to meet drift or stability limits. Increasing the stiffness increases the strength, and theoretically, the increased strength would reduce the ductility demands. If the ductility demands were reduced enough, it would seem feasible to relax the detailing requirements, and possibly, enhance the economy of the system. Current U.S. design provisions such as the 2005 AISC *Seismic Provisions for Structural Steel Buildings* (AISC, 2005) do not allow such an approach, however.

Another approach would be to simply ignore the drift and stability limits, and design the system for strength alone. Experience has shown that this approach is not feasible because of the potential for developing large residual displacements, or complete dynamic instability (Ruiz-Garcia and Miranda, 2006). The tendency towards dynamic instability is exacerbated by the low amount of inherent damping that is present in steel systems. It has been recognized that the inherent damping is not likely to be in excess of 2% critical (the almost universal practice of modeling such systems with 5% damping is unconservative).

Finley A. Charney, Professor, Via Department of Civil and Environmental Engineering, Virginia Polytechnic Institute and State University, Blacksburg, VA (corresponding author). E-mail: fcharney@vt.edu

Ozgur Atlayan, Graduate Research Assistant, Via Department of Civil and Environmental Engineering, Virginia Polytechnic Institute and State University, Blacksburg, VA. E-mail: oatlayan@vt.edu

If more damping could be justified the excessive residual deformations and dynamic instabilities might be avoided, and the systems could be designed for strength alone. Exactly such a concept is the focus of the research reported in this paper. It is noted, however, that unlike most of the supplemental damping applications (Miyamoto and Singh, 2002; Hwang, 2002; Miyamoto and Gilani, 2008) that concentrate on the effects of added damping that produce total system damping of 20 to 35% critical, this paper concentrates on adding the minimum amount of damping that is required to obtain an acceptable response. As shown in the remainder of the paper, systems with a total of only 10% damping have the desired performance, with the added benefit of increasing the reliability of the structural system.

VISCOUS FLUID DAMPERS

Viscous fluid dampers include a piston head with orifices contained in a hollow cylinder filled with fluid, which is mostly a compound of silicone or similar type of oil. Energy is dissipated in the damper as the piston rod moves through the fluid and forces the fluid to flow through the orifices in the piston head (Lee and Taylor, 2001). Because the fluid flows at high velocities, it causes friction between fluid particles and the piston head, which produces energy dissipation in the form of heat.

The force–velocity relationship for a viscous fluid damper can be expressed as:

$$F_D = C\left|\dot{u}\right|^{\alpha} \operatorname{sgn}(\dot{u}) \tag{1}$$

where F_D is the damper force, C is the damping constant, $\dot{u}$ is the relative velocity between the ends of the damper, α is an exponent that controls the shape of the force–velocity relationship, and sgn is the signum function used to find the sign of the velocity.

In earthquake engineering, viscous fluid dampers with velocity exponent of 0.3 to 1.0 are typically used (Symans et al., 2008). Using a velocity exponent, α, less than 1.0 causes the dampers to yield at high velocities and thus limits the forces transferred into the structure. When $\alpha = 1.0$, the damper force is proportional to the relative velocity, and the device is called a linear viscous damper.

For a given peak force and displacement amplitude, as the velocity exponent, α, of nonlinear dampers reduces below unity, the area in the force-displacement hysteresis loop gets larger and thus the energy dissipated for a cycle of motion is increased. This behavior is shown in Figures 1 and 2. Figure 1 shows the displacement and velocity histories of an applied sine wave with a period of 1 s. Figures 2a and 2b show the damping force-displacement and damping force-velocity relationships, respectively (as a result of the applied sine wave displayed in Figure 1), for three different C and α values. Note that varying the α value, C was adjusted such that the total damping force is the same (200 kips) for all three dampers. Viscous dampers are attractive from the theoretical viewpoint that velocity is out of phase with the displacement. Forces from viscous dampers will not add to the elastic forces in a structure because the maximum damping

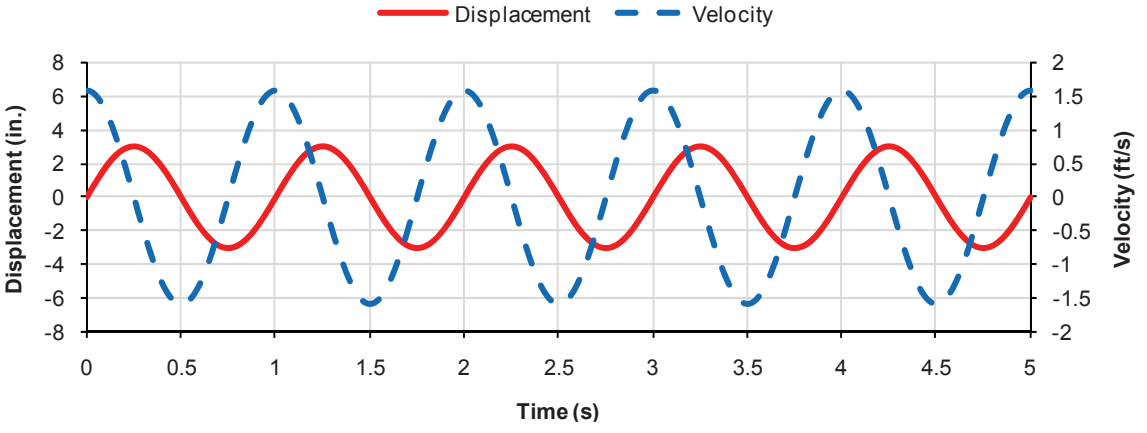

Fig. 1. Phasing of displacement and velocity.

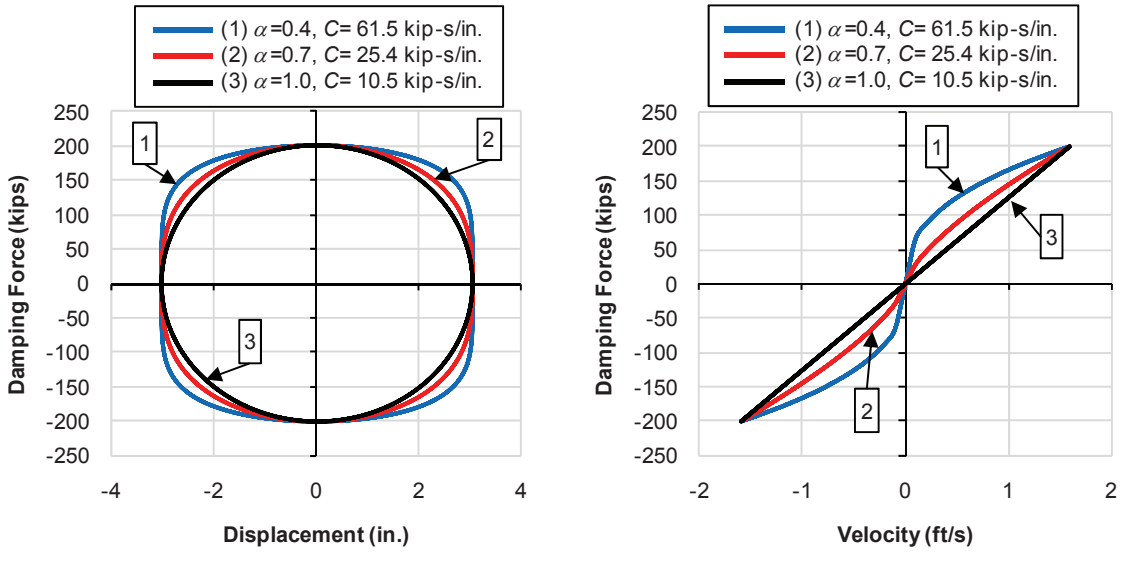

(a) *(b)*

Fig. 2. Damper force-displacement and damper force-velocity relationship for three different dampers.

Table 1. Gravity Loads and Seismic Masses			
Load Type	**Load (psf)**	**Level**	**Mass (kip-s^2/ft)**
Floor dead load	96	Roof	36.55
Roof dead load	83	Floors 2–8	33.93
Penthouse dead load	116	Floor 1	34.52
Exterior wall dead load	25		
Floor/roof reduced live load	20		

forces occur when the elastic forces due to building deformation are small. In practice, however, these two forces do couple to some extent so total force often increases (Kelly, 2001).

The primary advantage of using nonlinear dampers with velocity exponent, α, less than 1.0 is to limit base shears when deformational velocities are large, and the main advantage of using linear dampers is simplified mathematical modeling. In addition, for low-intensity earthquakes, where the structure remains elastic, the damper forces of linear dampers within the story are nearly 90° out of phase with respect to the elastic structural forces. Thus, under certain conditions, the effect of damper forces on the forces at the foundation level will be minimized when linear dampers are used (Symans et al., 2008). In this study, linear viscous dampers with $\alpha = 1.0$ were used.

Dampers can be manufactured to any practically required C and α values. An optimization analysis is required to determine the exact C and α values needed for each damper (Taylor, 2003). In addition, there is always a dilemma between using a large number of small dampers and using a lesser number of large dampers. Architectural restrictions, damper size–cost evaluation, and, obviously, achieving the required structural performance efficiently are important in deciding the number and size of the dampers. Similarly, damper distribution within a structure can be optimized. Wongprasert and Symans (2004) present an optimization technique where frequency-domain objective functions are

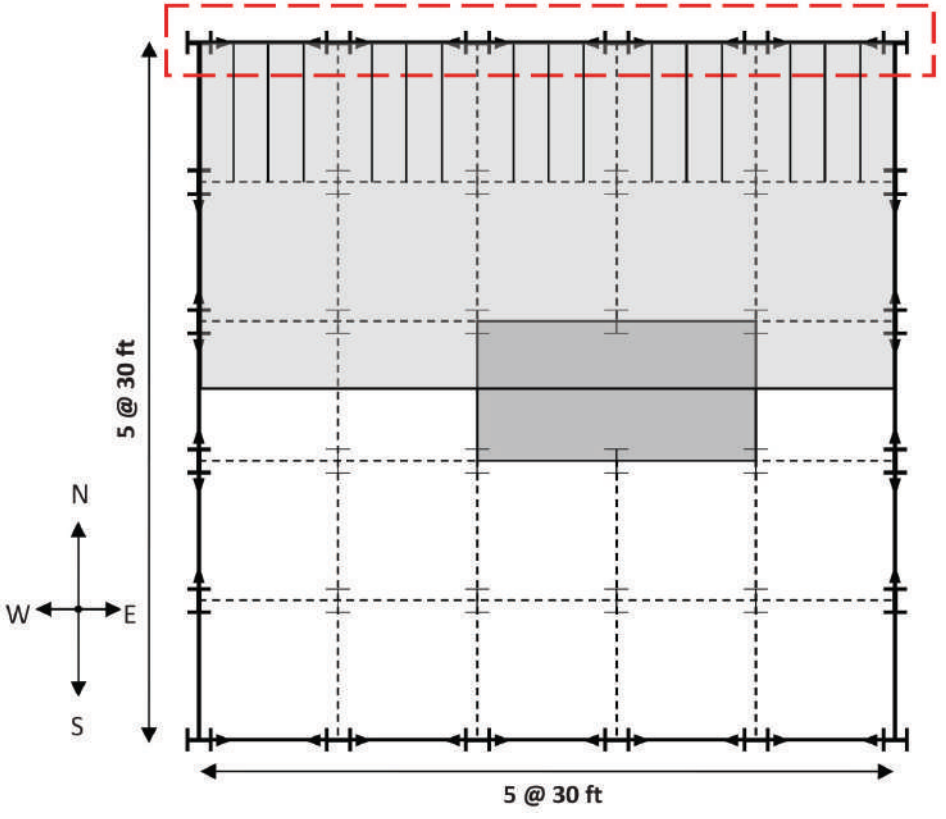

Fig. 3. Plan view of nine-story building.

Table 2. Column and Beam Sections of Strength Controlled Design						
Level	Columns			Beams		
	Exterior	Interior	Middle	Exterior	Interior	Middle
0–1	W18×192	W18×211	W18×192	W27×114	W27×94	W27×94
2–3	W18×130	W18×192	W18×192	W24×103	W24×103	W24×103
4–5	W18×97	W18×158	W18×158	W24×94	W24×94	W24×94
6–7	W18×71	W18×130	W18×130	W24×76	W24×76	W24×76
8–9	W18×50	W18×97	W18×97	W21×62	W21×62	W21×62

Table 3. ASCE 7-05 Design Parameters			
Design Parameter	Value	Design Parameter	Value
0.2 s spectral acceleration, S_S	1.25 g	Seismic Design Category	D
1.0 s spectral acceleration, S_1	0.5 g	Effective seismic weight, W	10,500 kips
Site class	D	Base shear	358 kips
0.2 s design acceleration, S_{DS}	0.83 g	Response modification factor, R	8
1.0 s design acceleration, S_{D1}	0.5 g	Deflection amplification factor, C_d	5.5
Seismic use group	II	Seismic response coefficient, C_S	0.034
Importance factor	1.0	Maximum fundamental period, C_uT_a	1.83 s

considered such that the optimal damper locations are dependent on the building and ground-motion characteristics. In their study, four different objective functions, which have different damper distributions in the structure, are investigated by considering different structural damage measures, and the optimum configuration was decided on the most critical damage measure considered. Note that this optimization was performed under the constraint that the number of dampers and their properties are known parameters.

Dampers can be installed as part of chevron brace, horizontally at top of chevron brace, as diagonal members and as a toggle braced system. In this study, dampers were added horizontally at top of the chevron braces.

MODELS AND DESIGN PROCEDURES

The effect of added viscous fluid dampers was investigated on a five-bay, nine-story steel special moment frame building, located near Seattle, Washington. The building models of the SAC Joint Venture (FEMA, 2000) were used in this study (see Figure 3 for the plan view). The dark gray shaded area in Figure 3 shows the penthouse, and the light gray shaded area shows the total gravity loads applied on the P-delta frame, which will be discussed later. The moment frame used in this study is shown between the dashed lines (E-W direction) in Figure 3. Because two moment frames are used in each lateral direction, each frame resists half of the lateral load in its respective direction. Similar to the SAC Report (FEMA, 2000), it was assumed that sufficient shear resistance is provided between diaphragms and beams so that seismic inertia forces generated at the floor levels can be transferred to the moment frame.

The gravity loads and masses used in this study can be seen in Table 1. The seismic masses shown in Table 1 are for half of the building. Because it is assumed that the loads are carried to the girders with three beams (see Figure 3), the gravity loads were applied as concentrated loads except for the exterior wall dead load, which was applied as a distributed load on the girders of the moment frame.

Strength and Stability Controlled Designs

The purpose of this study was to design a steel moment frame for only strength and then control the drift by using supplemental dampers. Using the mapped acceleration parameters (S_S and S_1), a flexible building design was obtained in Seattle. Because ASCE 7-05 (2006a) permits checking the elastic drift limits by using the lateral forces that are calculated by using the computed period of the structure (instead of the maximum fundamental period at the pre-design stage, C_uT_a), the strength design satisfied the elastic drift requirements of ASCE 7-05 (2006a) under strength-level design earthquake forces. Although the strength-controlled design met the drift requirements, the stability checks (due to P-delta effects) of both ASCE 7-05 and the Commentary to the 2005 AISC *Seismic Provisions* were not satisfied. Using the stability checks of ASCE 7-05 and the seismic provisions Commentary, another moment frame was designed with increased member sizes at the lower levels. Thus, two different nine-story special moment

frames (SMFs) were designed in Seattle, called the stability-controlled and strength-controlled designs. See Table 2 for the column and beam sections of the strength-controlled design for which added dampers will be implemented.

The computed periods for stability-controlled and strength-controlled designs were 3.19 and 3.29 s, respectively. The computed period values were more than expected for a nine-story building. The calculated period in the SAC report (FEMA 2000), for the nine-story building in Seattle, is between 3.06 and 3.17 s, depending on the panel zone modeling. However, periods vary between 2.20 and 2.40 s for a nine-story building in Los Angeles in the same report. The reason for the different periods in Los Angeles is the high demands, due to different S_S and S_1 parameters, which result in a stiffer structure. Thus, it was concluded that the calculated high-period values were reasonable and related with the regional seismic parameters of Seattle. The ASCE 7-05 design parameters used for the designs are summarized in Table 3.

To move the plastic hinges away from the column face, reduced beam sections were used, and the moment rotation properties of each hinge, forming at the reduced sections, were calculated explicitly (Atlayan, 2008). Panel zones were represented by use of Krawinkler's model (Charney and Marshall, 2006). See Atlayan (2008) for a much more detailed description of the step-by-step procedures of beam, column and panel zone design and differences between the stability and strength designs.

P-delta Effects and Damping Modeling

P-delta effects were included in all analyses using a special linear P-delta frame, shown at the right of Figure 4. This frame, sometimes called a ghost column or a leaner column, is needed in two-dimensional analysis because the gravity load tributary to the moment frames (and used for strength design of the frames) is significantly less than the destabilizing gravity load on the system.

All structures have the ability to dissipate energy during free vibration. This energy loss is generally referred as inherent damping. The main sources of inherent damping are material damping due to internal stresses, cracking in the structural materials, and friction in the connections and in the nonstructural components (Charney, 2008). A separate frame, shown to the left in Figure 4, was used to model the inherent damping. Similar to the P-delta frame, the inherent damping frame was laterally constrained to the main structural system. The reason for using the inherent damping frame was to provide an explicit control over the damping in the system.

Inherent damping was calculated by using Rayleigh damping. The total damping in each structure was determined by

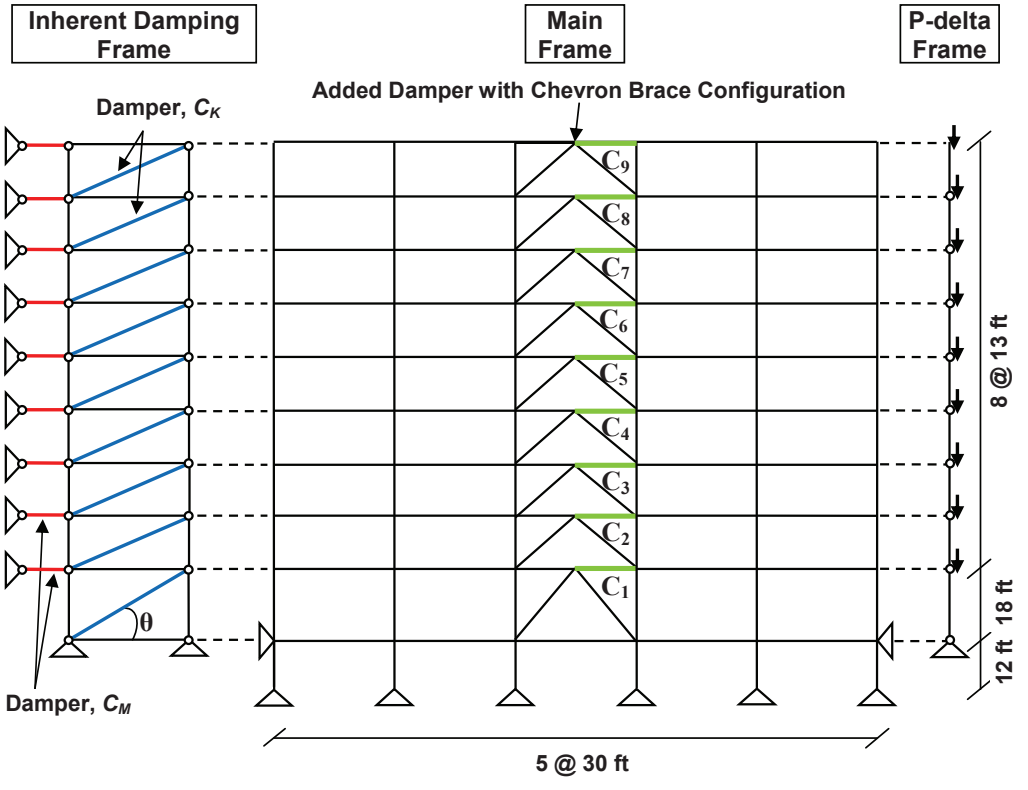

Fig. 4. Inherent damping and P-delta frames constrained to main frame.

Table 4. Inherent and Added Damping Coefficients for Stability and Strength Controlled Designs				
	Strength-Controlled Design		Stability-Controlled Design	
	Mass Proportional Constant	Stiffness Prop. Constant	Mass Proportional Constant	Stiffness Prop. Constant
	$\alpha = 0.071868$	$\beta = 0.001200$	$\alpha = 0.073938$	$\beta = 0.001198$
Story	C_M (kip-s/in.)	C_K (kip-s/in.)	C_M (kip-s/in.)	C_K (kip-s/in.)
9th story	0.219	0.499	0.226	0.495
8th story	0.203	1.035	0.209	1.032
7th story	0.203	0.949	0.209	0.945
6th story	0.203	1.344	0.209	1.346
5th story	0.203	1.292	0.209	1.291
4th story	0.203	1.646	0.209	1.645
3rd story	0.203	1.720	0.209	1.720
2nd story	0.203	1.962	0.209	2.104
1st story	0.207	1.036	0.213	1.256
Damping coefficient for 5% total damping (same at each story)	12.57			
Damping coefficient for 10% total damping (same at each story)	35.62			

setting the critical damping ratio to 2% at the natural period of the structure and at a period of 0.2 s. Using mass proportional constant α and stiffness proportional constant β, the desired level of inherent damping (2% of critical) was achieved. The damping coefficients C_M and C_K were calculated by using the following formulas at each story:

$$C_M = \alpha M_x \tag{2}$$

$$C_K = \beta K_x / \cos^2(\theta) \tag{3}$$

where M_x is the total story mass and K_x is the total story stiffness. The virtual work method was used to find the story stiffnesses. Because the stiffness proportional dampers were used in a diagonal configuration, the damping coefficients were modified using the angle between the braces and the horizontal plane to account for the effective reduction of the diagonal damper, as shown in Equation 3. The stiffness and mass damping coefficients in Table 4 (without added dampers) provide 2% inherent damping when assigned to the inherent damping frame for the corresponding strength or stability controlled designs.

Added Dampers

In order to increase the total system damping, viscous fluid dampers were added to the strength-controlled frame, producing two additional frames, which will be called the 5% and 10% total damped strength designs. These dampers represent physical linear viscous fluid damping devices that would be incorporated into the structural system.

The added damping coefficients were found by using the modal strain energy tools that are included in the NONLIN-Pro computer program (Charney and Barngrover, 2006). The added damper coefficients were updated until the total damping of the strength design reached 5 and 10% of critical. The added dampers were distributed equally at each story, and a chevron brace configuration was used to support the dampers, as shown in Figure 4. The chevron brace configuration was used to provide complete control over the modeling of inherent damping and thereby avoid the potentially adverse consequences of modeling inherent damping as a viscous mechanism (Charney, 2008). See Table 4 for the damping coefficients used in this study.

ANALYSIS OF A NINE-STORY MOMENT-RESISTING STEEL FRAME WITH AND WITHOUT ADDED DAMPERS

Two types of analysis were performed for each frame: nonlinear static pushover analysis (NSP) and incremental dynamic analysis (IDA). All structural analyses were conducted using Perform-3D (CSI, 2006). A planar model consisting of one of the two perimeter frames (E-W direction), which are parallel to the design ground motion, was used.

Nonlinear Static Pushover Analysis

Figure 5 displays the nonlinear static pushover curves with highlighted target displacements, first significant yields and the design base shear for both of the designs. Both models were pushed up to 4% reference drift, which is twice the drift limit of ASCE 7-05.

First significant yield is the level of force that causes the formation of the first plastic hinge in the structure, and the design base shear is $V = C_s W$, where C_s is the seismic response coefficient and W is the weight of the structure. The reason for the difference among the design base shear, first significant yield and actual strength of the structure is the overstrength. The overstrength factor is the ratio of the apparent strength to the design strength. As can be seen from the pushover curves, the overstrength factor was about 2 for the stability-controlled design and about 1.85 for the strength-controlled design. The reasons for the overstrength are the sequence of yielding of critical regions, load factors on the gravity system, strain hardening, capacity reduction (ϕ) factors and member selections (strong column–weak beam). Note that the system overstrength factor for special moment frame, Ω_0, is 3 in ASCE 7-05. Also, Ω_0 is not a true overstrength but an upper bound used for proportioning vulnerable components. Thus, Ω_0 is not used to assess the true system overstrength.

Both pushover curves reach negative stiffness due to the P-delta effects. Because the strong column–weak beam rule is satisfied in both of the designs, the only plastic hinges that formed in the columns formed at the bottom of the first story, when the structures were pushed up to the target displacement. Thus, weak-story mechanisms did not occur up to the target displacement level of pushover analyses.

The target displacement, which is intended to represent the maximum displacement likely to be experienced during the design earthquake, was found using the procedures outlined in ASCE 41-06 (2006b). If the stability ratios of the stories are more than the limit stipulated in ASCE 7-05, it is advisable to check the post-yield slope of the pushover curve at the target displacement and determine whether or not that slope is positive or negative. Note from Figure 5 that the tangent stiffness of the pushover curve is positive at the target displacement for the stability-controlled design, whereas the tangent stiffness of the strength-controlled design becomes negative prior to reaching the target displacement. This is an early warning for the possible collapses of the strength-controlled design without added dampers.

Incremental Dynamic Analysis

In this study, incremental dynamic analysis (Vamvatsikos, 2002) was conducted by using 10 different earthquake records with intensities of 0.2 to 2.0 times the ground motion scaled to match the design basis earthquake. Thus, the scale factor of 1.0 corresponds to the design basis earthquake (DBE), and the scale factor of 1.5 corresponds to the maximum considered earthquake (MCE). The ground motions were initially scaled to match the ASCE 7-05 spectrum at the structure's fundamental period. This scaling procedure was recommended for IDA analysis by Shome et al. (1998). The ground motions used in the analysis were the same as those used in the original SAC research (FEMA, 2000),

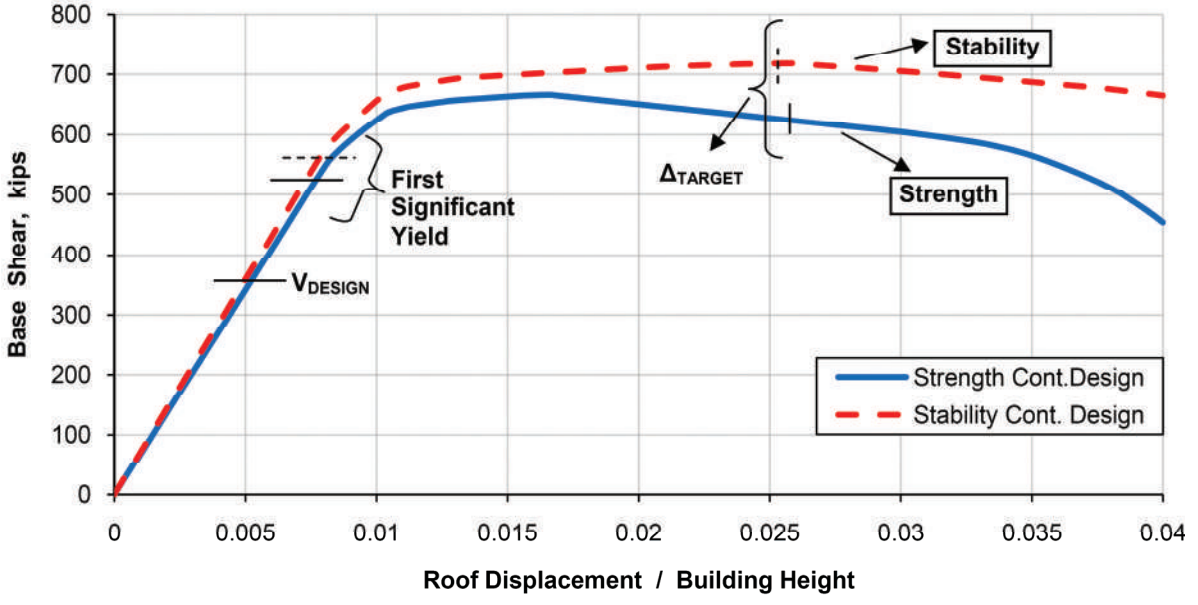

Fig. 5. Nonlinear static pushover curves for strength and stability controlled designs.

Table 5. Ground Motions							
Earthquake No.	SAC Name	Earthquake Name	Magnitude	Duration (s)	Time Step (s)	PGA (g)	Integration Time Step (s)
EQ00	SE 21	Mendocino, 1992	7.1	59.980	0.020	0.771	0.005
EQ01	SE 23	Erzincan, 1992	6.7	20.775	0.005	0.476	0.005
EQ02	SE 25	Olympia, 1949	6.5	79.980	0.020	0.206	0.005
EQ03	SE 27	Seattle, 1965	7.1	81.820	0.020	0.175	0.001
EQ04	SE 29	Valparaiso 1, 1985	8.0	99.975	0.025	0.564	0.0025
EQ05	SE 31	Valparaiso 2, 1985	8.0	99.975	0.025	0.321	0.001
EQ06	SE 33	Deep Interplate	7.9	79.980	0.020	0.207	0.001
EQ07	SE 36	Miyagi-oki, 1978	7.4	79.980	0.020	0.440	0.001
EQ08	SE 37	Shallow Interplate 1	7.9	79.980	0.020	0.599	0.005
EQ09	SE 40	Shallow Interplate 2	7.9	79.980	0.020	0.503	0.001

which are shown in Table 5. Bracketed duration, the time interval between the first and the last occurrence of an acceleration of 0.05 g, was calculated for each ground motion and used to establish the computation time of the analyses.

To prevent the numerical errors and fictitious dynamic instability, Newmark integration time steps were checked for each ground motion. The roof displacement response history was checked with the ground motions that have a scale factor of two times the DBE. In other words, the response histories of the roof were evaluated with the largest scale factor that does not cause collapses in the IDA study, and the time step was decreased by half of the previous one until the responses converged. In addition, each time a collapse occurred, the reasons for dynamic instabilities were investigated explicitly to differentiate the real collapses from numerical errors.

For the IDA study, the scale factor of the ground motions was used as the intensity measure, and the interstory drift, base shear, maximum and residual roof displacements, and IDA dispersion were used as the damage measures.

Effect of Dampers on Drift

As discussed earlier, the elastic drift limits of ASCE 7-05 were satisfied for both of the inherently damped strength and stability designs. In addition to the elastic drift limit

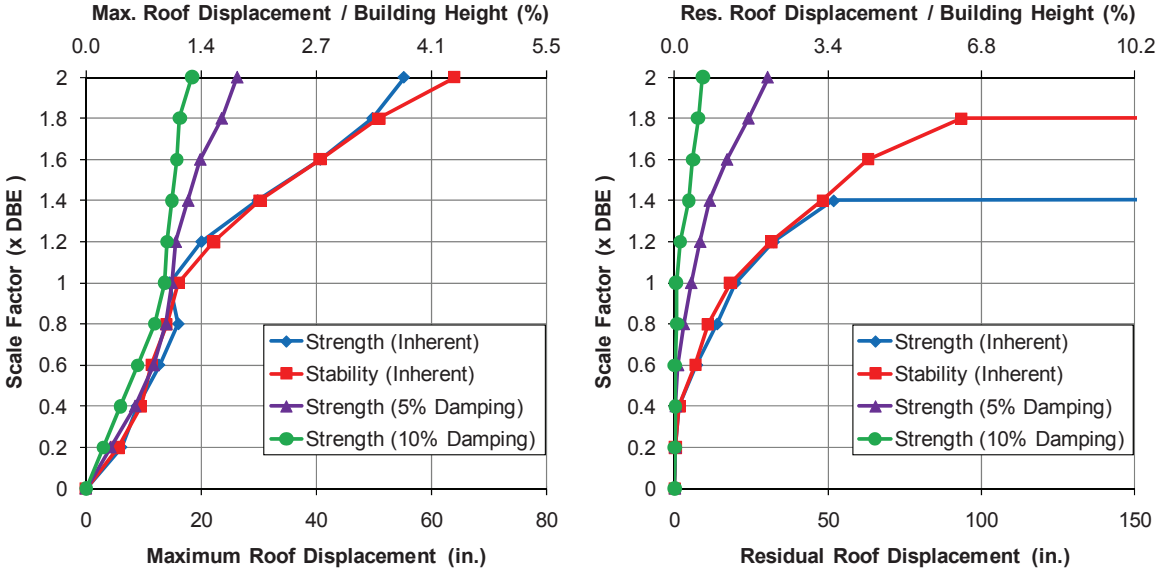

(a) *(b)*

Fig. 6. IDA plots for maximum and residual roof displacements using (a) Valpariso-1 and (b) Seattle ground motions.

Table 6. Maximum Drifts for Design Basis Miyagi-oki and Valparaiso-2 Earthquakes									
Level	Drift Limit (%125) (in.)	Miyagi-oki				Valparaiso-2			
		Strength Inherent Damping (in.)	Stability Inherent Damping (in.)	Strength 5% Damping (in.)	Strength 10% Damping (in.)	Strength Inherent Damping (in.)	Stability Inherent Damping (in.)	Strength 5% Damping (in.)	Strength 10% Damping (in.)
9th	3.90	3.13	3.37	1.94	1.02	**5.00**	**5.41**	2.21	1.04
8th	3.90	3.59	**4.16**	2.63	1.52	**6.64**	**7.61**	3.15	1.64
7th	3.90	**4.53**	**4.96**	2.97	1.99	**4.97**	**5.46**	3.37	1.98
6th	3.90	**4.46**	**4.81**	3.33	2.40	**4.06**	**5.28**	2.90	2.07
5th	3.90	**4.08**	**4.75**	3.37	2.69	**4.24**	**5.49**	2.73	2.02
4th	3.90	**4.36**	**4.74**	3.47	2.99	3.22	3.67	3.01	2.07
3rd	3.90	**4.64**	**4.63**	3.49	3.16	2.84	3.42	3.09	2.18
2nd	3.90	**4.30**	3.53	3.54	3.19	2.77	3.11	2.92	2.35
1st	5.40	**5.40**	4.04	4.12	3.69	4.63	4.37	3.56	3.01

check, according to Chapter 16 of ASCE 7-05, the results of nonlinear response history analysis (NRHA) shall not exceed 1.25 times the allowable drift limit (2% of story height in this study). However, the results of NRHA exceeded 1.25 times the allowable drift limit for both of the inherently damped designs for 6 out of 10 earthquakes used in this study. The added dampers play a crucial role here. Table 6 shows the maximum drift results of all the designs subject to two different ground motions at the design level. Note that the highlighted values exceed the limits.

For this study, the 5% totally damped strength controlled design satisfied the drift requirements under all 10 different earthquakes used. As expected, a further decrease in drift values occurred when the total damping increased to 10% of critical. Thus, a structure that satisfies the elastic drift limits of the code may not satisfy the drift limits by NRHA, but these limits can be met by using supplemental damping.

Figures 6a and 6b illustrate the maximum and residual roof displacement IDA plots by using the Valpariso-1 and Seattle earthquakes, respectively. All the designs resisted Valpariso-1 earthquake. However, the inherently damped strength design collapsed after the scale factor of 1.4 times the DBE, and the stability design collapsed after the scale factor of 1.8 times the DBE when frames are subjected to Seattle earthquake. Note that horizontal lines in IDA curves indicate collapses (see Figure 6b). The frames with added

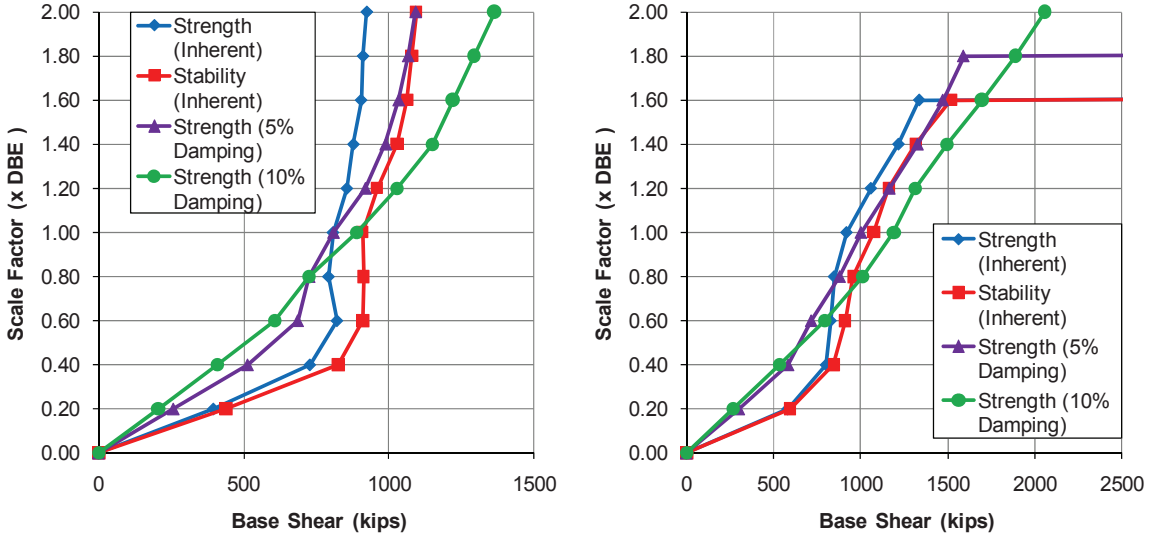

(a) *(b)*

Fig. 7. Base shear IDA plots for (a) Erzincan and (b) Miyagi-oki earthquakes.

dampers resisted the collapses for Seattle earthquake and reduced the maximum and residual roof displacements significantly.

Effect of Dampers on Base Shear

Figures 7a and 7b display base shear IDA plots for the Erzincan and Miyagi-oki earthquakes. At low-scale factors, where the structure behaves elastically, base shear decreases as damping increases. The IDA curves generally intersect before displaying an increase in terms of base shear with increased damping in the nonlinear region. The 5% damped strength-controlled design and the inherently damped stability-controlled design behaved very similar in base shear IDA responses after the structures yield. This is particularly true at ground-motion levels approaching the design and maximum considered earthquakes (scale factors 1.00 and 1.50, respectively). The same behavior was observed for the other eight earthquakes used in this study as well. Note that the difference between the base shear IDA plots of stability and 5% damped strength designs (at scale factors more than 1.60) in Figure 7b was due to collapses. The inherently damped stability design collapsed when the

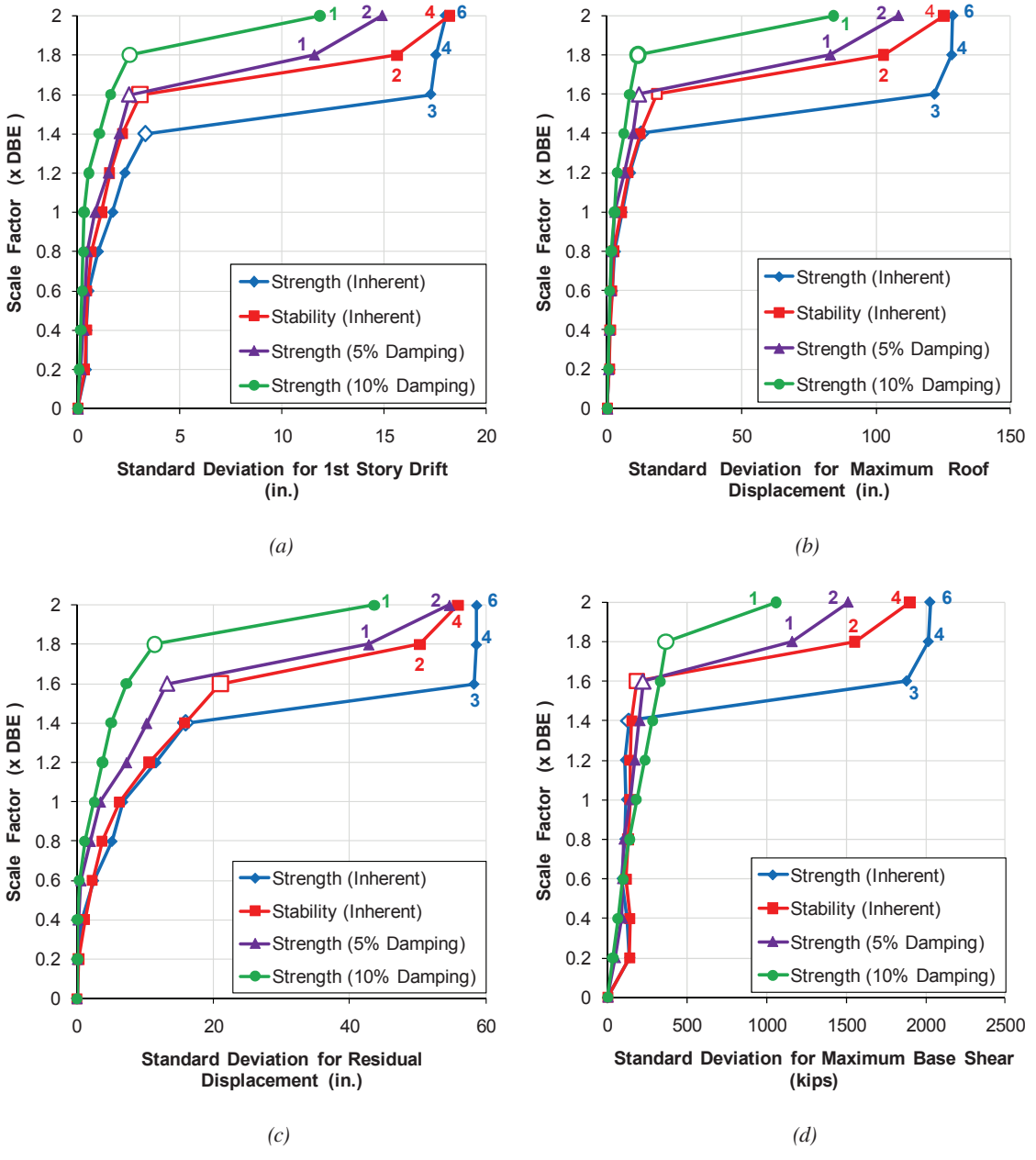

Fig. 8. Standard deviation IDA plots for different damage measures.

scale factor reached 1.80; however, the 5% damped strength design resisted the scale factor 1.80 and collapsed at a factor of 2.00 when the frames were subjected to Miyagi-oki earthquake.

The main drawback of linear viscous dampers is the high base shears in the inelastic region of the IDA plots. This study concludes that 5% damping with linear viscous dampers does not cause base shear problems. The 10% total damping increases the base shear between 10 and 30%, depending on the earthquake. As discussed earlier, the use of nonlinear viscous dampers, with the velocity exponent of about 0.4, would likely reduce the increase in base shear associated with added viscous damping, but this was not investigated in this study.

Effect of Dampers on IDA Dispersion

The dispersion of IDA curves can be used to see the effect of dampers in terms of giving a reliable estimate of the performance of the buildings. To measure the IDA dispersion, the standard deviation of the responses, produced at each intensity level of 10 different earthquakes, was calculated for each structure with different amounts of damping. The standard deviation increases as the amount of dispersion increases. When the standard deviation IDA curves for the different levels of damping are displayed together, the curve that has the steepest slope will correspond to the system that is best at reducing the IDA dispersion.

Figures 8a through 8d illustrate the IDA dispersion for different damage parameters. While the building response is elastic, there was not a significant dispersion. As the earthquake intensity increased, dispersion increased as well, and when the buildings collapse, dispersion increased because of the collapse measures used for the dispersion study. In all of the dispersion plots, the horizontal lines occurring at high-intensity measures indicate the collapses. The number of earthquakes that caused collapse is also labeled at the corresponding scale factors. Note that the final scale factors that resisted the collapses of all earthquakes are shown with an unfilled (empty) data point in Figure 8. When IDA dispersion plots are analyzed, it can be concluded that the 10% total damped strength-controlled design had a drastically improved performance when compared to the other designs. The 10% damped strength design gave higher dispersion or uncertainty than the other designs only for the base shear damage measure between scale factors of 0.8 and 1.6 (see Figure 8d). This was an expected result if the drawback of the linear viscous dampers at high damping ratios was considered. Above the scale factor of 1.6, the 10% damped strength design gave better results in terms of base shear IDA dispersion as well, because the other designs collapsed at high earthquake intensities and the use of collapse measures increased the dispersion.

Effect of Dampers on Energy Dissipation

Dampers reduce the damage in the structure by dissipating energy. Figures 9, 10 and 11 respectively illustrate the

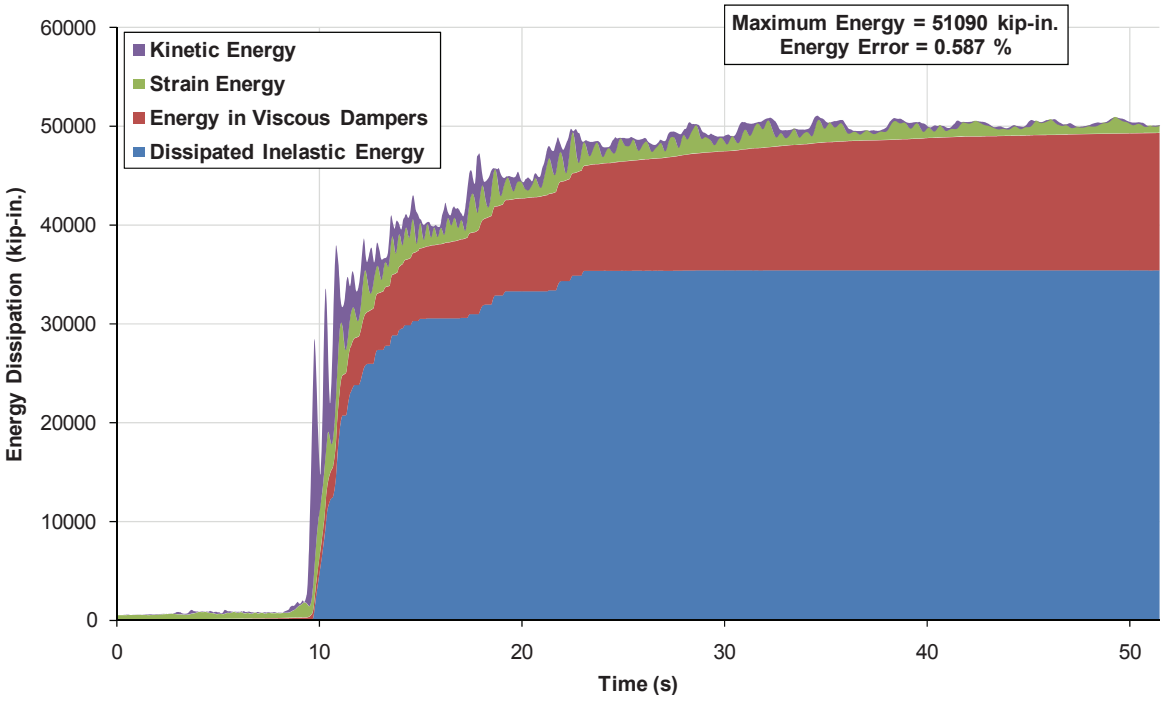

Fig. 9. Energy balance plot for inherently damped strength design frame under EQ07 (DBE).

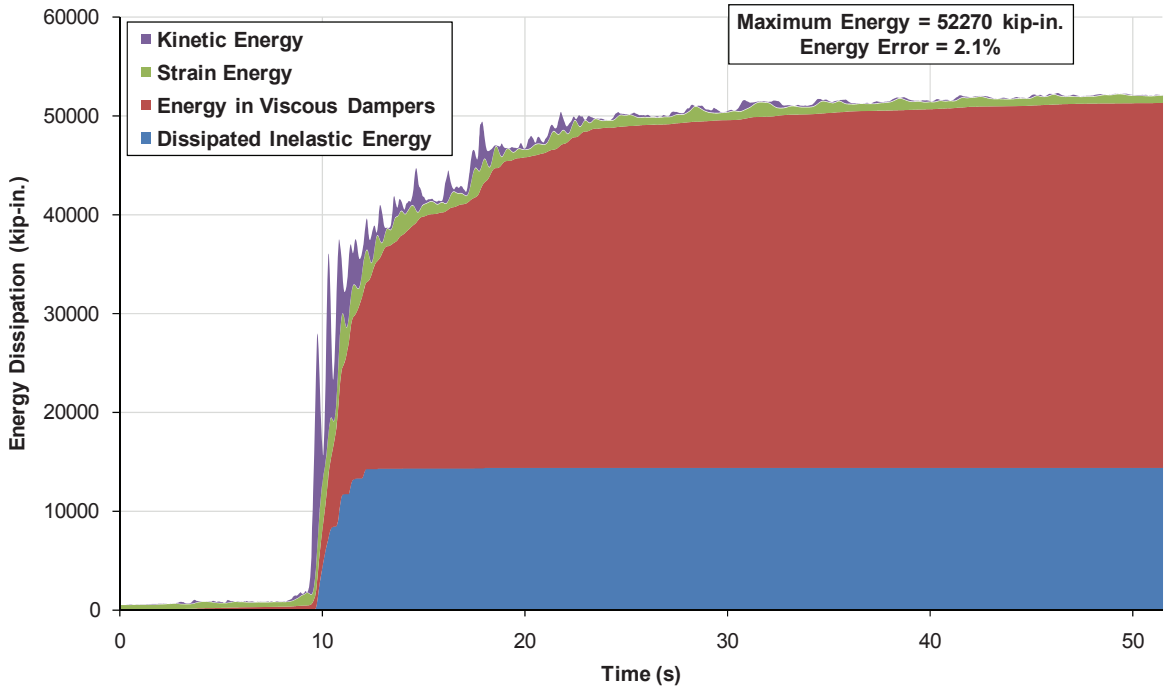

Fig. 10. Energy balance plot for 5% total damped strength design frame under EQ07 (DBE).

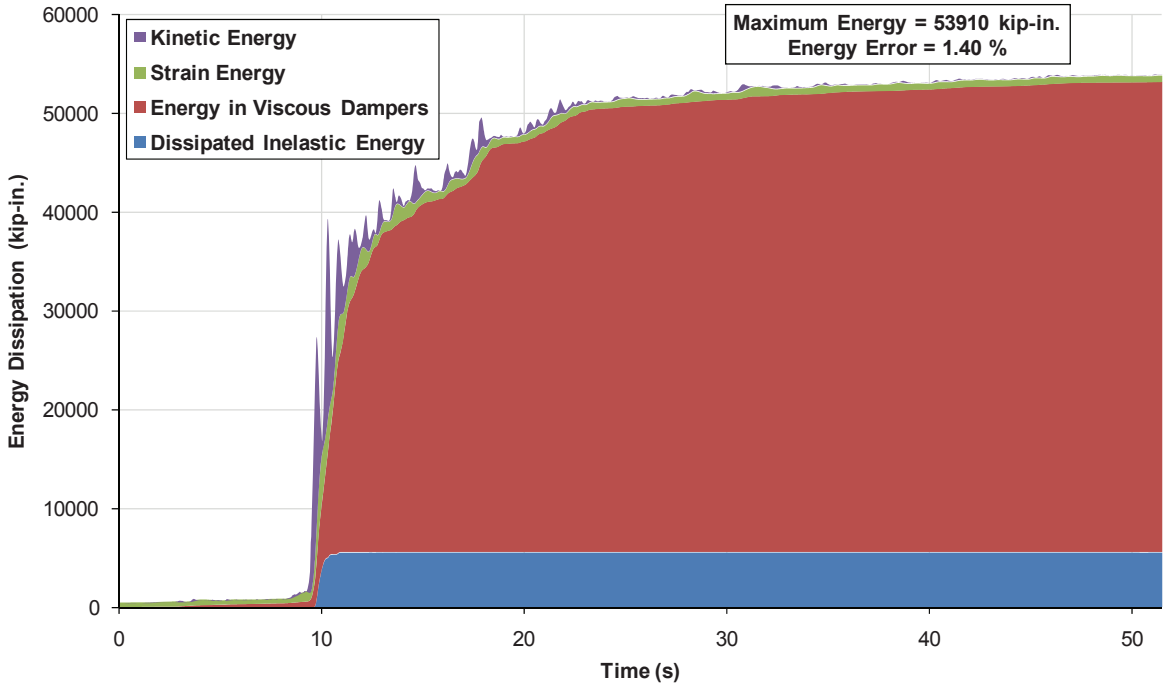

Fig. 11. Energy balance plot for 10% total damped strength design frame under EQ07 (DBE).

Table 7. Collapse Check for Selected Earthquakes							
Design	**Scale Factor**	**Seattle**	**Valparaiso-2**	**Deep Interpolate**	**Miyagi-oki**	**Shallow Interpolate-1**	**Shallow Interpolate-2**
Strength-controlled design with inherent damping	1.0	√	√	√	√	√	√
	1.2	√	√	√	√	√	√
	1.4	√	√	√	√	√	√
	1.6	Collapse	Collapse	√	√	√	Collapse
	1.8	Collapse	Collapse	√	Collapse	√	Collapse
	2.0	Collapse	Collapse	Collapse	Collapse	Collapse	Collapse
Stability-controlled design with inherent damping	1.0	√	√	√	√	√	√
	1.2	√	√	√	√	√	√
	1.4	√	√	√	√	√	√
	1.6	√	√	√	√	√	√
	1.8	√	√	√	Collapse	√	Collapse
	2.0	Collapse	Collapse	√	Collapse	√	Collapse
Strength-controlled design with 5% total damping	1.0	√	√	√	√	√	√
	1.2	√	√	√	√	√	√
	1.4	√	√	√	√	√	√
	1.6	√	√	√	√	√	√
	1.8	√	√	√	√	√	Collapse
	2.0	√	√	√	Collapse	√	Collapse
Strength-controlled design with 10% total damping	1.0	√	√	√	√	√	√
	1.2	√	√	√	√	√	√
	1.4	√	√	√	√	√	√
	1.6	√	√	√	√	√	√
	1.8	√	√	√	√	√	√
	2.0	√	√	√	√	√	Collapse

energy plots when the inherently 5% and 10% damped strength designs were subjected to Miyagi-oki earthquake (EQ07). These plots show how the ground-motion input energy is dissipated and absorbed by the structural system. In the energy plots, the X-axis is time and the Y-axis is the amount of different energy types in the system at the given time. As can be seen from the energy plots, as the damping increased (moving from Figure 9 to Figure 10 to Figure 11), the energy dissipated by viscous damping (inherent plus added damping) increased, and the dissipated inelastic energy decreased. Thus, structural damage decreased because this damage is related directly to dissipated inelastic energy. Strain and kinetic energy ratios are also shown in the energy plots. The energy errors shown in the plots are a measure of the accuracy of the structural analysis. The maximum error of 2.1 percent shown in Figure 10 is somewhat higher than desired but is acceptable for the purposes of this study.

Effect of Dampers on Dynamic Instability

One of the main purposes of this study was to investigate the effect of added dampers on dynamic instability (collapses). Table 7 shows the collapse check of the four structures subject to six earthquakes, from scale factors 1.0 to 2.0, which caused collapses in the IDA studies. Both the strength- and the stability-controlled designs did not collapse until the MCE. However, the strength design collapsed just after the MCE for three earthquakes, when the IDA scale factor reached 1.6. The main collapse mechanism was the intermediate-story mechanisms occurring at the bottom three stories due to P-delta effects.

The effect of damping on dynamic instability was obviously significant. Five percent damping prevented the collapses of four out of six earthquakes that occurred in the strength-controlled design. The 10% total damped structure resisted all the earthquakes except EQ09 with scale factor

of 2.0. The amount of damping necessary to prevent the collapse was dependent on the design of the structure. Regarding the strength-controlled design investigated in this study, 10% total damping was conservatively adequate for providing dynamic stability.

Note that the stability-controlled design (inherently damped) eliminated half of the collapses that occurred for the inherently damped strength-controlled design. This is consistent with the results of nonlinear pushover analyses. Because strength-controlled design reached negative stiffness before target drift on the pushover curve, story mechanisms and then collapses occurred at MCE level of shaking, which is almost the same level as a 1.6 scale factor in IDA studies.

CONCLUSIONS

The supplemental dampers have a remarkable effect on reducing the inelastic response of the elements of steel moment frames. The effects of added dampers were studied through incremental dynamic analysis by using various damage measures. After adding the linear viscous dampers to the strength designed frame, a significant performance improvement was achieved. The IDA responses of the roof displacement, residual displacement and interstory drifts decreased drastically as a result of added dampers. Although the inherently damped strength design satisfied the elastic drift requirements of ASCE 7-05, it did not meet the drift requirements for the nonlinear response history procedure where the allowable drift limits were increased by 25%. However, after adding the dampers, 5% total damping was adequate to meet the drift criteria of ASCE 7-05.

A collapse check study and an IDA dispersion study were implemented to investigate the effect of damping on dynamic instability. Regarding the optimum level of damping, 5% total damping was almost always adequate to prevent collapse at the MCE level. As the damping increased, the IDA dispersion plots got steeper, which indicates a more reliable performance of the structure under various earthquakes. The 10% total damped strength design gave the best results, followed by 5% damped strength and stability designs, in terms of IDA dispersion.

If the overall performance of the building under different damage measures used in IDA study is considered, the strength-controlled design with 10% damping is concluded to be efficient for the nine-story SMF building in Seattle, Washington. The required level of total system damping might vary for different type of steel frames at other locations; however, it is foreseen that the design approach discussed in this paper is worth consideration in addition to the conventional design methods for moment frame structures in highly seismic regions.

REFERENCES

AISC (2005), *Seismic Provisions for Structural Steel Buildings*, ANSI/AISC 341-05, American Institute of Steel Construction, Chicago, IL.

ASCE (2006a), *Minimum Design Loads for Buildings and Other Structures*, ASCE/SEI 7-05, American Society of Civil Engineers, Reston, VA.

ASCE (2006b), *Seismic Rehabilitation of Existing Buildings*, ASCE/SEI 41-06, American Society of Civil Engineers, Reston, VA.

Atlayan, O. (2008), "Effect of Viscous Fluid Dampers on Steel Moment Frames Designed for Strength, and Hybrid Steel Moment Frame Design," M.S. Thesis, Department of Civil Engineering, Virginia Tech, Blacksburg, VA, http://scholar.lib.vt.edu/theses/available/etd-05072008-110653/.

Charney, F.A. (2008), "Unintended Consequences of Modeling Damping in Structures," *Journal of Structural Engineering*, ASCE, Vol. 134, pp. 581–592.

Charney, F.A. and Barngrover, B. (2006), *NONLIN-Pro Base Program Description and User's Guide*, Advanced Structural Concepts Inc., Blacksburg, VA.

Charney, F.A. and Marshall, J.D. (2006), "A Comparison of the Krawinkler and Scissors Models for Including Beam-Column Joint Deformations in the Analysis of Steel Frames," *Engineering Journal*, AISC, Vol. 43, No. 1, pp. 31–48.

CSI (2006), *Perform-3D User's Guide*, Nonlinear Analysis and Performance Assessment of Structures, Computers and Structures Inc., Berkeley, CA.

FEMA (2000), *State of the Art Report on Systems Performance*, FEMA-355C, Federal Emergency Management Agency, Washington, DC.

Hwang, J.S. (2002), "Seismic Design of Structures with Viscous Dampers," International Training Program for Seismic Design of Building Structures, National Center for Research on Earthquake Engineering of Taiwan, http://www.ncree.gov.tw/itp2002/.

Kelly, T.E. (2001), *In Structure Damping and Energy Dissipation*, Design Guidelines, Holmes Consulting Group Ltd, Wellington, New Zealand.

Lee, D. and Taylor, D.P. (2001), "Viscous Damper Development and Future Trends," *The Structural Design of Tall Buildings*, Vol.10, No. 5, pp. 311–320.

Miyamoto, H.K. and Gilani, A. (2008), "Design of a New Steel-Framed Building Using ASCE 7 Damper Provisions," *Proc. 2008 Structures Congress,* Vancouver, BC, Canada, pp. 1–10.

Miyamoto, H.K. and Singh, J.P. (2002), "Performance of Structures with Passive Energy Dissipators," *Earthquake Spectra*, Vol. 18, No. 1, pp. 105–119.

Ruiz-Garcia, J. and Miranda, E. (2006), "Evaluation of Residual Drift Demands in Regular Multi-Story Frames for Performance Based Seismic Assessment," *Earthquake Engineering and Structural Dynamics*, Vol. 35, No. 13, pp. 1609–1629.

Shome, N., Cornell, C.A., Bazzurro, P. and Carballo, J.E. (1998), "Earthquakes, Records and Nonlinear Responses," *Earthquake Spectra*, Vol. 14, pp. 469–500.

Symans, M.D., Charney F.A., Whittaker A.S., Constantinou M.C., Kircher C.A., Johnson M.W. and McNamara R.J. (2008). "Energy Dissipation Systems for Seismic Applications: Current Practice and Recent Developments," *Journal of Structural Engineering*, ASCE, Vol. 134, pp. 3–21.

Taylor, D.P. (2003), "Mega Brace Seismic Dampers for the Torre Mayor Project at Mexico City," Taylor Devices Inc., NY, http://www.taylordevices.eu/case-studies.php.

Vamvatsikos, D. (2002), "Seismic Performance, Capacity, and Reliability of Structures as Seen Through Incremental Dynamic Analysis," Ph.D. Thesis, Department of Civil Engineering, Stanford University, Stanford, CA.

Wongprasert, N. and Symans, M.D. (2004), "Application of a Genetic Algorithm for Optimal Damper Distribution within the Nonlinear Seismic Benchmark Building," *Journal of Engineering Mechanics*, ASCE, Vol. 130, No. 4, pp. 401–406.

Design of Steel Buildings for Earthquake and Stability by Application of ASCE 7 and AISC 360

R. SHANKAR NAIR, JAMES O. MALLEY and JOHN D. HOOPER

Abstract

Design of steel buildings in the United States typically combines application of ASCE/SEI 7, *Minimum Design Loads for Buildings and Other Structures,* and ANSI/AISC 360, *Specification for Structural Steel Buildings*. For buildings designed for seismic effects, ANSI/AISC 341, *Seismic Provisions for Structural Steel Buildings,* may also be applicable. The ASCE 7 *Minimum Design Loads* standard includes specific design provisions related to stability under seismic loading which overlap and, in some instances, appear to conflict with the stability design requirements of the AISC *Specification*. This paper explores the areas of overlap and apparent conflict between ASCE 7 and AISC 360 and offers practical recommendations for seismic design incorporating the provisions of both.

Keywords: design loads, seismic design, structural stability.

Design of steel buildings in the United States typically combines application of ASCE/SEI 7, *Minimum Design Loads for Buildings and Other Structures* (ASCE, 2005), and ANSI/AISC 360, *Specification for Structural Steel Buildings* (AISC, 2005a; AISC, 2010). For buildings designed for seismic effects, ANSI/AISC 341, *Seismic Provisions for Structural Steel Buildings* (AISC, 2005b), may be applicable in conjunction with the *Specification*.

ASCE 7 is used, either directly or by reference from a building code, to define the loads for which the structure must be designed; AISC 360 and 341 are used to design the steel structure for those loads.

The ASCE 7 *Minimum Design Loads* standard, though generally focused on loads and not on design or the response of the structure to those loads, includes specific design provisions related to stability under seismic loading. These provisions overlap and, in some instances, appear to conflict with the stability design requirements of the AISC *Specification*. (The AISC *Seismic Provisions* do not include stability design requirements.)

This paper explores the areas of overlap and apparent conflict between ASCE 7 and AISC 360 and offers practical recommendations for seismic design incorporating the provisions of both.

R. Shankar Nair, Ph.D., P.E., S.E., Senior Vice President, Teng & Associates, Inc., Chicago, IL (corresponding). E-mail: nairrs@teng.com

James O. Malley, P.E., S.E., Senior Principal, Degenkolb Engineers, San Francisco, CA. E-mail: malley@degenkolb.com

John D. Hooper, P.E., S.E., Principal and Director of Earthquake Engineering, Magnusson Klemencic Associates, Seattle, WA. E-mail: jhooper@mka.com

The paper does not attempt to correlate design with expected actual behavior beyond the degree of correlation implied by compliance with ASCE 7 and AISC 360. This is an important limitation. It is generally recognized that actual displacements in an earthquake could be much larger than the elastic displacements due to code-specified design loads, and the resulting second-order effects could be quite different from those predicted by specification-compliant analysis; exploration of this issue is beyond the scope of this paper.

STABILITY DESIGN BY AISC 360

The Direct Analysis Method of design for stability was introduced in the 2005 edition of the AISC *Specification*. The 2010 edition makes that method the primary means of design; alternative approaches have been moved to an appendix. The discussion in this paper will be limited to the Direct Analysis Method and its application in seismic design in conjunction with ASCE 7; other stability design methods permitted in the AISC *Specification* are not considered.

The rational basis of the Direct Analysis Method is explained in AISC-SSRC (2003); a simple introduction to the practical application of the method is provided in Nair (2009a). Notes on the modeling of structures for design by the Direct Analysis Method are provided in Nair (2009b).

Design for stability by the Direct Analysis Method involves a second-order analysis, use of reduced stiffness in the analysis, consideration of initial imperfections (either by direct modeling of the imperfections or by application of notional loads in the analysis) under certain circumstances, and strength check of components using an effective length factor, K, of unity for members subject to compression.

Second-Order Analysis

The analysis of the structure must be a second-order analysis that, in the most general case, includes both P-Δ effects, which are the effects of loads acting on the displaced locations of joints or nodes in the structure, and P-δ effects, which are the effects of loads acting on the deformed shapes of members. In tiered buildings, P-Δ effects are the effects of loads acting on the laterally displaced locations of floors and roofs.

The 2010 AISC *Specification* exempts most buildings from the need to consider P-δ effects in the analysis of the overall structure; a P-Δ–only analysis is sufficient in almost all cases. This is an important simplification relative to the 2005 *Specification,* which does require inclusion of P-δ effects in the analysis of most moment-frame buildings. Regardless of whether P-δ effects need to be considered in the analysis of the overall structure, the P-δ effects on individual beam-columns must always be considered in the strength check of those members.

The second-order analysis required by the Direct Analysis Method of design may be performed using a computer program formulated to provide a second-order solution. Alternatively, a second-order solution may be obtained by manipulating the results of a linear or first-order analysis to account for second-order effects by application of the B_1 and B_2 multipliers defined in the *Specification*.

In the B_1 and B_2 procedure, B_2 alters the results of a first-order analysis to account for P-Δ effects; the B_2 multiplier also accounts, in an approximate way (by application of the factor R_M in the calculation of B_2), for the overall softening of the structure's response due to P-δ effects in individual members. For a given vertical loading, there will be a single value of B_2 for each story and each direction of lateral translation, applicable to the forces and moments caused by lateral loading in all members and connections in that story. In the unusual case where gravity load causes lateral translation, B_2 is also applicable to the forces and moments caused by the side-sway component of gravity load. While B_2 is a story parameter, B_1 is a member parameter; a B_1 multiplier is applied to the moments in each beam-column to account for P-δ effects in that member.

Another approach, usable in the typical case where P-δ effects do not need to be considered in the analysis of the overall structure, is to obtain a P-Δ–only second-order solution from a computer program and then to apply B_1 multipliers to account for P-δ effects in individual members.

Given that in second-order analysis the effect of a load is not proportional to its magnitude (and the principle of superposition of loads does not apply), the second-order analysis must be performed at the Load and Resistance Factor Design (LRFD) load level: For design by LRFD, LRFD load combinations must be applied in the analysis; for design by Allowable Strength Design (ASD), ASD load combinations increased by a factor of 1.6 must be applied in the analysis and the results must be divided by 1.6 to get the forces and moments for proportioning of members and connections.

Reduced Stiffness

In the second-order analysis, all stiffnesses in the modeling of the structure must be reduced by applying a factor of 0.8. An additional reduction factor, τ_b, must be applied to the flexural stiffnesses of all members whose flexural stiffnesses are considered to contribute to the lateral stability of the building. Factor τ_b is unity when the LRFD-level required compression strength of the member is less than half the yield strength.

When the compression is high and τ_b is not unity, the designer may still avoid the complication of calculating and applying τ_b by applying, instead, a small notional lateral load (0.001 times the LRFD-level gravity load applied at each floor) in the analysis. This notional load will typically be so much smaller than seismic loads that it may reasonably be neglected when seismic loads are present. Thus, it should be possible to take τ_b as unity in all cases in seismic design; what remains is the 0.8 factor, applied to all stiffnesses.

Initial Imperfections

The effect of initial imperfections must be considered in the analysis, either by direct inclusion of the imperfections in the analysis model or by application of notional loads, if either (1) the load combination being considered is a gravity-only loading with no applied lateral load or (2) the ratio of second-order drift to first-order drift in any story of the building is more than 1.7.

For seismic design, there will always be applied lateral load and condition 1 will not apply; condition 2 will also typically not apply for buildings that satisfy the limits on stability coefficient, θ, specified in ASCE 7. Therefore, it will not typically be necessary in seismic design to consider initial imperfections, either explicitly or by application of notional loads.

Component Strength Check

For design by the Direct Analysis Method, once the appropriate analysis has been performed, members and connections are checked for strength with no further consideration of overall structure stability. The effective length factor, K, for members subject to compression is taken as unity (unless a lower value is justified by rational analysis).

SEISMIC DESIGN STABILITY PROVISIONS IN ASCE 7

Background and commentary on the seismic design provisions of the ASCE 7 *Minimum Design Loads* standard may

be found in FEMA (2009). Specific requirements for stability in conjunction with seismic design are presented in the ASCE standard in a section titled "P-Delta Effects" (Section 12.8.7)*; these requirements are included as part of the "Equivalent Lateral Force Procedure" for seismic analysis (Section 12.8).

The P-Delta Effects section of ASCE 7 defines a stability coefficient, indicates when P-delta effects must be considered, places limits on the stability coefficient and specifies methods of accounting for P-delta effects.

Stability Coefficient, θ

The stability coefficient, θ, is approximately the ratio of the actual vertical force on a story of a building to the vertical force that would cause elastic lateral buckling of the story. An equation† is provided for the coefficient; the coefficient is calculated with nominal, unreduced stiffnesses and for load combinations with no individual load factor exceeding unity.

When Must P-delta Effects Be Considered?

Under ASCE 7, P-delta effects need be considered only when the stability coefficient, θ, is more than 0.10. This is roughly equivalent to an AISC B_2 multiplier (ratio of second-order story drift to first-order story drift) of 1.2, after accounting for the fact that θ is calculated with nominal stiffnesses and for load combinations with no individual load factor exceeding unity, while B_2 is calculated with reduced stiffnesses and for LRFD-level load combinations.

Limit on Stability Coefficient

The stability coefficient, θ, must never be higher than θ_{max}, which is variable (a function of β, the ratio of shear demand to shear capacity of the story, and of C_d, the deflection amplification factor), but never higher than 0.25. A θ of 0.25 is roughly equivalent to an AISC B_2 multiplier of 1.7 after correction for the different stiffnesses and loadings in the θ and B_2 calculations.

Method of Analysis for P-delta Effects

ASCE 7 specifies that when P-delta effects are required to be considered (i.e., when the stability coefficient, θ, exceeds 0.10), "the incremental factor related to P-delta effects on displacements and member forces shall be determined by rational analysis." Two types of rational analysis are envisioned: (1) nonlinear static (pushover) analysis and (2) nonlinear response history analysis, both of which require extensive, additional effort.

As an alternative to the rational analysis, "it is permitted to multiply the displacements and member forces by $1.0/(1 - \theta)$." This is analogous to application of the AISC B_2 multiplier with $R_M = 1$ in the equation for B_2, which amounts to neglecting P-δ effects in the analysis. However, given that θ is calculated with nominal stiffnesses and for load combinations with no individual load factor exceeding unity, while B_2 is calculated with reduced stiffnesses and at LRFD-level load combinations, the AISC approach will indicate significantly higher second-order displacements and forces.

Use of an analysis that included P-Δ effects (but not P-δ effects), and subsequent application of AISC B_1 multipliers to individual beam columns to account for P-δ effects, would also satisfy the requirement of ASCE 7.

Seismic Design by Modal Response Spectrum Analysis

The preceding discussion of stability-related requirements in the seismic design provisions of ASCE 7 was based on use of the Equivalent Lateral Force procedure. An alternative seismic analysis procedure prescribed in ASCE 7 (Section 12.9) is the Modal Response Spectrum Analysis approach. Design by Modal Response Spectrum Analysis is applicable to all structures of all Seismic Design Categories; the Equivalent Lateral Force procedure is not permitted for certain structures in Seismic Design Categories D through F.

Stability requirements are not presented independently in the Modal Response Spectrum Analysis section; the same P-delta requirements prescribed for the Equivalent Lateral Force procedure are incorporated by reference in the Modal Analysis section. There is an obvious complication here in that the Modal Analysis approach involves combining the results of analyses for different modes, but second-order analyses (i.e., analyses incorporating P-delta effects) cannot normally be combined. A means of overcoming this difficulty is suggested in the following section.

COMPARISON AND RECOMMENDATIONS

Selected features of the Direct Analysis Method of design for stability in the AISC *Specification* and provisions related to seismic design and stability in the ASCE 7 *Minimum Design Loads* standard, as discussed in the preceding sections, are summarized in Table 1. Clearly, there are areas of divergence between the two sets of requirements. Nonetheless, as outlined in the following, steel buildings may be designed for seismic effects and stability in general conformance with both the AISC *Specification* and ASCE 7.

---

* ASCE 7 does not explicitly differentiate between the P-Δ effects and P-δ effects recognized by the AISC *Specification*; the "P-delta" effects addressed in ASCE 7 are the P-Δ effects of AISC.

† There is an error in Equation 12.8-16, the equation for stability coefficient, θ, in ASCE 7-05. There should be I (for importance factor) in the numerator on the right-hand side of the equation. This has been corrected in ASCE 7-10.

Table 1. Comparison of Analysis and Stability Provisions in ASCE 7 and AISC 360			
Subject	**ASCE 7 Equivalent Lateral Force Procedure[a]**	**AISC 360 Direct Analysis Method**	**Recommendation for Seismic Design**
Limit on *P*-Δ effect	Stability coefficient θ must not exceed θ_{max}.	No limit.	Observe ASCE limit, which corresponds to *P*-Δ multiplier of 1.33 or less.[b]
Must *P*-Δ effects be considered?	Only when θ is greater than 0.1.	Yes; in all cases.	Always consider *P*-Δ effects.
P-Δ effects by rational analysis?	Permitted.	Permitted.	Rational analysis may be used.
P-Δ effects by approximate analysis?	Permitted. [Multiply lateral load effects by $1/(1-\theta)$.]	Permitted. [Multiply lateral load effects by B_2.]	The AISC method may be used; note that $1/(1-\theta) \approx B_2$.
Must *P*-δ effects be considered in the analysis?	Not specified.	Generally yes in 2005; generally no in 2010.	Observe AISC 2010.[c]
Load in the stability analysis	Not specified for rational analysis. Load factor not greater than 1.0 for θ calculation.	LRFD load combinations for LRFD; 1.6 times ASD combinations for ASD.	Observe AISC: LRFD load combinations for LRFD; 1.6 times ASD load combinations for ASD.
Structure stiffness in the stability analysis	Not specified.	Apply factor of 0.8 τ_b to *EI*; 0.8 to all other stiffnesses.	Apply factor of 0.8 (no τ_b) to all stiffnesses.
Must initial imperfections be considered?	Not specified.	Yes, with exceptions; either model directly or apply notional loads.	Need not consider initial imperfections (neither direct modeling nor notional loads).
Analysis to assess conformance to drift limits	Elastic stiffness; same type of analysis as for strength.	Not specified.	Use of same analysis as for strength is permissible but may be too conservative; see text.
Analysis to determine period	Not specified, although upper limits are defined.	Not specified.	Use linear analysis (no *P*-Δ effects) with nominal, unreduced stiffnesses.

[a] See text for additional considerations for Modal Response Spectrum Analysis procedure.
[b] The stability coefficient, θ, is calculated at lower load than used in AISC stability analyses; therefore, *P*-Δ multipliers corresponding to the ASCE 7 thresholds are not strictly comparable to AISC 360 parameters.
[c] Regardless of whether it is considered in the analysis of the overall structure, *P*-δ must always be considered in the strength check of individual beam-columns.

General recommendations:

1. Observe the ASCE 7 limit on stability coefficient; θ must not exceed θ_{max}. The nominal (unreduced) stiffness of the structure and the ASCE 7 vertical load (with no individual load factor greater than 1.0) may be used in the calculation of coefficient θ.
2. In the analysis for assessing strengths, consider *P*-Δ effects in the analysis for all structures; also consider *P*-δ effects in the analysis where required by the AISC *Specification*. (Do not observe the ASCE 7 provision that exempts from P-delta considerations all buildings with a stability coefficient, θ, less than 0.10.)

Recommendations specific to seismic design by the Equivalent Lateral Force procedure:

1. Determine the fundamental period of the building either by analysis or by use of the approximate methods prescribed in ASCE 7. If determined by analysis, use first-order analysis (no second-order effects), with nominal (unreduced) stiffnesses.
2. Consider second-order effects either by second-order

analysis or by application of the AISC B_1 and B_2 multipliers to the results of first-order analysis. The options are:

a. Complete second-order analysis that considers both P-Δ and P-δ effects.

b. P-Δ–only second-order analysis, followed by application of B_1 to individual beam columns (not permissible in the unusual cases where inclusion of P-δ effects in the overall analysis is required by the AISC *Specification*).

c. First-order analysis, followed by application of B_2 and B_1 multipliers.

3. Perform the second-order analysis and/or calculate the B_1 and B_2 multipliers at LRFD-level loads; that is, use LRFD load combinations if design is by LRFD, use 1.6 times ASD load combinations if design is by ASD. (After second-order analysis under ASD, divide the analysis results by 1.6 for member and connection strength checks.)

4. Apply a factor of 0.8 to all stiffnesses in the second-order analyses and in the calculation of B_1 and B_2 multipliers. For load combinations that include seismic load, the additional stiffness reduction factor τ_b need not be applied.

5. In the analysis for load combinations that include seismic load, it is not necessary to model initial imperfections or to apply notional loads to account for the imperfections.

6. Perform strength checks in accordance with the AISC *Specification*, using an effective length factor, K, of unity for members subject to compression (unless a lower value is justified by rational analysis).

7. Conformance to ASCE 7 seismic drift limits may be checked using the same analysis used for strength checks (analysis at reduced stiffness, second-order analysis, second-order effects determined at LRFD-level loads). This may be excessively conservative, however, and it is permissible to base drift checks on an analysis using the full unreduced stiffness of the structure, with second-order effects determined at the lower loads specified by ASCE 7 for calculation of the stability coefficient, θ. The deflection amplification factor, C_d, should be applied in either case.

Recommendations specific to seismic design by the Modal Response Spectrum Analysis approach:

1. Determine modes and frequencies using first-order analysis, with nominal (unreduced) stiffnesses.

2. Determine member forces and moments due to gravity load by first-order analysis, with a factor of 0.8 applied to all stiffnesses.

3. Use the properties of each mode and the ASCE 7 design response spectrum to determine a set of lateral forces for that mode; using these lateral forces, perform a first-order analysis, with a factor of 0.8 applied to all stiffnesses, to determine member forces and moments. Repeat for all modes considered.

4. Calculate a single B_2 multiplier, applicable to all modes,‡ for each story and each direction of lateral translation, based on reduced stiffness (0.8 factor) and the full LRFD-level vertical load on the story.§

5. Combine first-order modal results (item 3) as specified in ASCE 7 Section 12.9.3. Apply B_2 multipliers to the combined results (member forces and moments caused by lateral loading). Then scale the combined results as specified in ASCE 7 Section 12.9.4. Algebraic signs will typically be lost in modal combinations; the member forces and moments due to seismic effects should, therefore, be considered reversible (i.e., use absolute values of forces and moments in the modal combinations and then consider the resulting overall forces and moments due to seismic effects to be fully reversible).

6. Combine the member forces and moment due to seismic effects (item 5) with the member forces and moments due to gravity load (item 2), with load factors as specified in ASCE 7.

7. Apply B_1 multipliers to the moments in beam-columns. The B_1 multiplier should be based on the full LRFD-level axial force in the member, including axial forces due to lateral loading, but need be applied only to that part of the moment in the beam-column that is caused by gravity loading. (Designers may use the conservative approximation of applying B_1 to the full moment to avoid the obvious bookkeeping difficulties involved in this calculation.)

8. Perform strength checks in accordance with the AISC *Specification*, using an effective length factor, K, of unity for members subject to compression (unless a lower value is justified by rational analysis).

---

‡ This is an approximation. If the B_2 calculations for all stories are based on story shears and drifts due to lateral load applied at the roof alone, the resulting B_2 values should be reasonably accurate or conservative (high) for all modes.

§ It should also be possible (as an alternative to the B_2 multiplier procedure used herein) to adapt the modified geometric stiffness approach for use with design by Modal Response Spectrum Analysis.

9. As in the Equivalent Lateral Force procedure, conformance to ASCE 7 seismic drift limits may be checked using either the same analysis used for strength checks (convenient, but potentially very conservative) or an analysis using the full unreduced stiffness of the structure, with second-order effects (B_1 and B_2 multipliers) determined at the lower loads specified by ASCE 7 for calculation of the stability coefficient, θ.

SUMMARY AND CONCLUSIONS

Provisions related to seismic design and stability in ASCE/SEI 7, *Minimum Design Loads for Buildings and Other Structures* (ASCE, 2005), and features of the Direct Analysis Method of design for stability in ANSI/AISC 360, *Specification for Structural Steel Buildings* (AISC, 2005a; AISC, 2010), have been explored and compared. While there are inconsistencies between the two sets of provisions, they are not fundamentally incompatible. Recommendations are offered for the design of steel buildings for seismic effects and stability in general conformance with both the AISC *Specification* and the ASCE 7 standard.

REFERENCES

AISC (2005a), *Specification for Structural Steel Buildings*, ANSI/AISC 360, American Institute of Steel Construction, Chicago, IL.

AISC (2005b), *Seismic Provisions for Structural Steel Buildings*, ANSI/AISC 341, American Institute of Steel Construction, Chicago, IL.

AISC (2010), *Specification for Structural Steel Buildings*, ANSI/AISC 360, American Institute of Steel Construction, Chicago, IL.

AISC-SSRC (2003), "Background and Illustrative Examples on Proposed Direct Analysis Method for Stability Design of Moment Frames," *Technical White Paper*, AISC Technical Committee 10, AISC-SSRC Ad Hoc Committee on Frame Stability, American Institute of Steel Construction, Chicago, IL.

ASCE (2005), *Minimum Design Loads for Buildings and Other Structures*, ASCE/SEI 7-05, American Society of Civil Engineers, Washington, DC.

FEMA (2009), *NEHRP Recommended Seismic Provisions for New Buildings and Other Structures*, FEMA P-750, Federal Emergency Management Agency, Washington, DC.

Nair, R.S. (2009a), "Simple and Direct," *Modern Steel Construction*, AISC, January.

Nair, R.S. (2009b), "A Model Specification for Stability Design by Direct Analysis," *Engineering Journal*, AISC, Vol. 46, No. 1, pp. 29–37.

Seismic Design and Response of Crane-Supporting and Heavy Industrial Steel Structures

JULIEN RICHARD, SANDA KOBOEVIĆ and ROBERT TREMBLAY

ABSTRACT

This paper presents an analytical study of the seismic behavior of two different types of industrial buildings; a regular mill-type crane-supporting steel structure and an irregular heavy industrial building housing a vertical mechanical process. For both structures, the seismic response is examined through elastic time-history dynamic analyses in order to validate the predictions from the equivalent static force procedure and the response spectrum analysis method prescribed in current building codes. The analyses also serve to assess the inelastic demand in crane-supporting structure. For the crane-supporting structure, analyses are performed for sites in Montreal and Vancouver in Canada and in Seattle in the United States. The results show that the median horizontal displacement and acceleration from the time-history analyses are generally well predicted by the code analysis methods. Inelastic response in these buildings is likely to develop in the form of buckling of the lower column segment, a failure mode that exhibits limited ductility. For the tall irregular building, the analyses are performed for the Montreal site only. The results show the equivalent static method provides fair displacements estimate, but may lead to unconservative predictions of column and brace forces. Response spectrum analysis method, as prescribed in design codes, appears to provide appropriate prediction of the seismic response of such highly irregular structures. For both building types, a good prediction from response spectrum and time-history analysis methods is possible only when a sufficient number of modes are used.

Keywords: seismic design, crane structures, industrial buildings.

Industrial buildings house a wide variety of manufacturing, assembly, refining, mining or material handling processes, covering a broad range of products. They can also be part of critical facilities such as power plants and communication systems. Adequate seismic behavior is critical for these structures in order to shorten downtime periods that can cause substantial loss of revenues, unemployment or shortage of goods, electrical power and communication services. Industrial buildings may also serve for the production or storage of hazardous materials, and the unsatisfactory seismic structural response causing the leakage or malfunction can pose a major risk.

Steel-framed industrial buildings generally exhibited good overall structural performance in recent earthquakes. However, the reported structural damage to individual components or connections has resulted in disruption of operations in most of the industrial structures examined. Typical damage observed after the 1999 Kocaeli earthquake in Turkey included bolt shearing at column to roof truss connections in automotive plants, buckled and fractured braces, stretching and fracture of anchor bolts in moment-resisting frames, and shearing of anchor bolts (Bendimerad et al., 1999; Rahnama and Morrow, 2000; Sezen et al., 2000; Johnson et al., 2000). The 1994 Northridge earthquake caused yielding and failure of anchor bolts in an asphalt rock plant and brace buckling in a brewing facility (Tremblay et al., 1995). Failure of welds at brace connections was observed after the 1988 Spitak, Armenia, earthquake (Yanev, 1989). One steel-framed warehouse collapsed in the 1991 Costa Rica earthquake, but the cause was attributed to the overturning of the heavy building content against the steel columns (Swan and Hamburger, 1992). In the 1985 Chile earthquake (Thiel, 1986) and the 1989 Loma Prieta earthquake (Swan et al., 1990), buckling of braces and brace connection failures (sheared bolts, gusset plate buckling, and weld failures) occurred in various steel frames supporting equipments such as elevated tanks, cooling units and reactors.

Current code seismic design provisions in Canada and the United States have been essentially developed for conventional office or residential buildings that usually have regular and well-defined seismic force-resisting systems. The application of these provisions to industrial buildings that are typically characterized by complex and irregular geometries, uneven mass and/or stiffness distribution, and a large variety of dynamic properties is not straightforward for practicing engineers (Rolfes and MacCrimmon, 2007; Daali, 2004). In particular, there exist uncertainties regarding

Julien Richard, Structural Engineer, Hatch Engineering, Montreal, Quebec, Canada (corresponding author). E-mail: jrichard@hatch.ca

Sanda Koboević, Ph.D., Assistant Professor, Department of Civil, Geological and Mining Engineering, École Polytechnique, Montreal, QC, Canada. E-mail: sanda.koboevic@polymtl.ca

Robert Tremblay, Ph.D., Professor and Canada Research Chair in Earthquake Engineering, Department of Civil, Geological and Mining Engineering, École Polytechnique, Montreal, QC, Canada. E-mail: robert.tremblay@polymtl.ca

the amplitude and distribution of the seismic force and deformation demand on industrial structures. Furthermore, the highly ductile seismic force-resisting systems that have been introduced in codes in the last decades are not well suited for industrial applications. In order to achieve good inelastic performance and high energy dissipation capacity, these highly ductile systems rely on a carefully tailored lateral load path with balanced strength hierarchy, a condition that can hardly be maintained when mass or structural modifications are imposed over the years due to evolving production processes (e.g., addition of equipment or removal of braces or columns). Thus, for the sake of simplicity and flexibility, engineers typically prefer selecting conventional steel design and construction techniques, trading the simpler design and detailing for higher design seismic loads.

Both the National Building Code of Canada (NBCC) (NRCC, 2005) and the ASCE 7-05 code (ASCE, 2005) in the United States propose steel seismic force-resisting systems for which only limited or no special seismic detailing or capacity design verifications are required. Recognizing the inherent ductility of steel, it is permitted to design those simpler systems for seismic loads that are lower than the expected seismic elastic force level, i.e., using seismic force modification factors greater than 1.0: $R_d = 1.5$ in Canada, for the conventional construction category, and R between 3.0 and 3.5 in the United States, depending on the system used. Although these factors are much lower than those specified for the highly ductile systems (up to $R_d = 5.0$ in Canada and $R = 8.0$ in the United States), the solution may still be attractive in view of the lesser complexity in design and detailing and the greater flexibility for future modifications.

In moderate and high-seismicity zones, however, severe restrictions apply to buildings framed with these low-ductility systems. In Canada, the height of buildings designed with $R_d = 1.5$ is limited to 15 m (50 ft), recognizing the greater likelihood of localized high-ductility demand in taller structures subjected to seismic ground motions. In the United States, systems not specifically detailed for seismic resistance ($R = 3.0$) are not permitted in moderate and high seismic active zones, and only single-story structures with light roof dead loads are permitted up to 18.3 m (60 ft) if built with an ordinary braced steel frame ($R = 3.25$) or up to 20 m (65 ft) if ordinary moment-resisting frames ($R = 3.5$) are used. Typical industrial buildings often exceed these height limits, forcing the selection of highly ductile systems.

Exemptions or alternative design routes may apply to specific projects. For instance, the Commentary on NBCC (NRCC, 2005) specifies that the 15-m height restriction for $R_d = 1.5$ systems is intended to maintain the traditional three-story height limit imposed in previous NBCC editions and need not apply to single-story steel industrial structures such as steel mills, thus allowing low-ductility solutions to be adopted for these structures, regardless of their height. According to ASCE 7-05, relaxation of height limits is possible for ordinary braced frames and moment-resisting frames if the structure is designed as a nonbuilding structure, in accordance with requirements provided in Chapter 15. Unfortunately, it is not always clear in ASCE 7-05 under which circumstances an industrial building can be classified as a nonbuilding structure. Yet, this avenue may represent the only available option for tall industrial structures to be erected in moderate and high seismic zones.

Although the preceding limitations and exemptions generally make sense, there is very limited data on the seismic demand on industrial building steel structures under strong ground motions. Current system restrictions in codes have been essentially established from studies of the seismic performance of conventional office or residential buildings. It is, therefore, of the upmost importance to (1) gain a better knowledge of the seismic response of industrial buildings, (2) critically review existing design procedures, and (3) introduce seismic design provisions so that the intended performance can be achieved for these structures. The first step is necessary to support future actions, and the need for such data is becoming more pressing because changes are currently taking place in codes that will likely motivate the use of low-ductility systems for industrial buildings. In the upcoming 2010 edition of NBCC (Humar et al., 2010; Tremblay et al., 2010), it is proposed to increase the 15-m height limit for low-ductility steel frames, provided that minimum additional seismic requirements are implemented. In ASCE 7-10 (ASCE, 2010), precisions have been made in the definition of nonbuilding structures that allow for buildings housing equipment—with occupants involved only in the maintenance or monitoring of that equipment—to be considered as nonbuilding structures.

This paper describes the initial phase of an ongoing study investigating the seismic response of industrial buildings. The objective was to determine (1) if the analysis methods proposed in codes can adequately predict the actual force and deformation demand under seismic loads and (2) the location, extent and nature of the inelastic demand anticipated under strong ground motions from earthquakes. The study was carried out on selected industrial buildings designed according to the current building code provisions. Two building types were considered: (1) a regular crane-supporting steel structure typical of buildings found in the mill industry and (2) an irregular heavy industrial building housing a vertical mechanical process representative of mining and metal refining industry. In both cases, low-ductility seismic force resistant systems were assumed, even if that category was not permitted in current building codes, the intent being to obtain data that could be used to evaluate the relevance of current code restrictions. For the mill-type building, three different cities in North America (Montreal, Quebec; Vancouver, British Columbia; and Seattle, Washington) were

considered to examine the influence of seismic hazard and ground motion characteristics on the structural response. For the Vancouver site, two different soil conditions were investigated. For the irregular heavy industrial building, the study was carried out for the Montreal site only. In all cases, elastic dynamic time-history analyses were conducted for selected acceleration records compatible with the design spectra at the site, and the results are were compared to those obtained from the static equivalent force procedure and the response spectrum analysis method prescribed in codes. For the irregular heavy industrial building, for which three-dimensional analysis was employed, attention is also given to the appropriate number of modes to use in response spectrum analysis and to the possible impact of the direction of seismic loading on member force demand.

DESIGN AND SEISMIC RESPONSE OF CRANE-SUPPORTING BUILDINGS

Building Geometry

A three-dimensional view of the crane-supporting structure studied is shown in Figure 1. The structure has a clear span of 25 m (82.0 ft) and consists of transverse moment-resisting frames that are regularly spaced 10 m (32.8 ft) on center to form a single crane aisle. Each frame includes a roof truss and simple columns that extend from fixed-base laced columns supporting both the roof and the crane runway girders (Figure 2). The truss-to-column connections are moment-resistant. The structure supports two 40-t (44-T) capacity overhead cranes. Horizontal loads acting along the longitudinal direction are resisted by horizontal X-bracing located at the roof level and by vertical X-bracing below and above the crane girders along the exterior walls. Typical steel siding supported on girts and purlins is used for the walls and the roof.

In this study, the seismic response of the transverse moment-resisting frames is examined, with particular attention directed to the crane-supporting columns. In view of the exploratory nature of the study, it was assumed for simplicity that lateral loads were resisted individually by each of the frames, thus omitting the possibility that part of the inertia loads induced by the crane weight be distributed to adjacent frames through the horizontal roof bracing. A two-dimensional numerical model of one transverse frame was therefore adopted for the design and analysis. For consistency with this assumption, a redundancy factor of 1.3 should have been considered in the seismic load calculation for the Seattle site, according to ASCE 7. This increase in seismic design loads was, however, ignored in this study to assess the actual seismic demand-to-capacity ratio without the bias introduced by the additional resistance required in ASCE 7 to compensate for the lack of redundancy. It was also assumed that the frame was located in the middle part of the aisle and was not a part of the longitudinal bracing system.

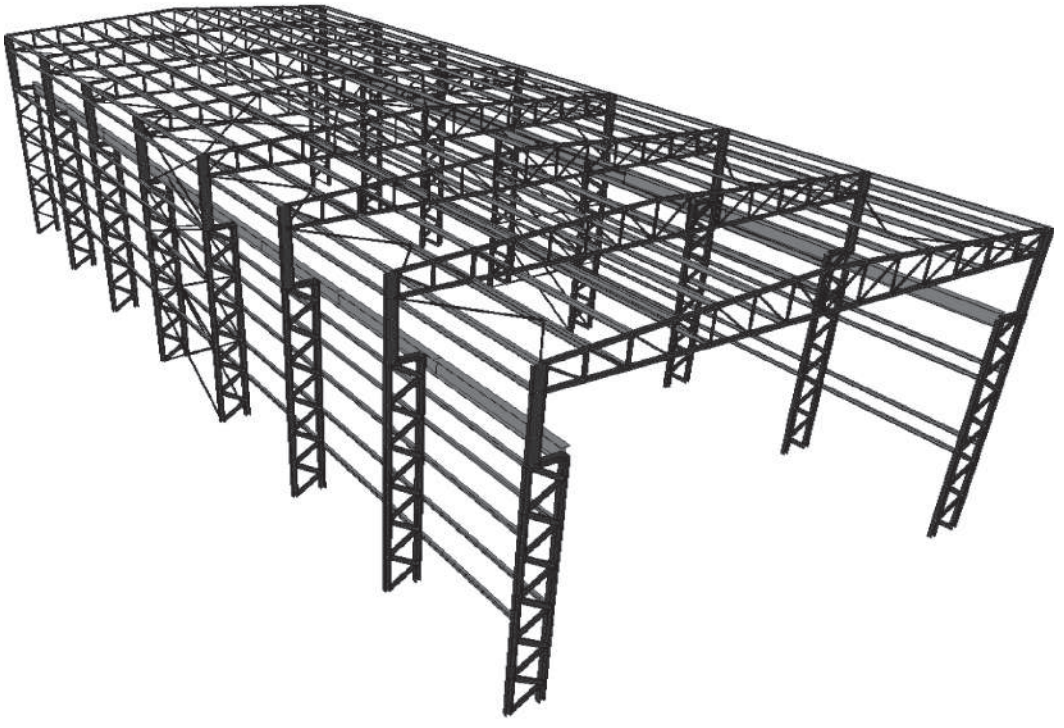

Fig. 1. Three-dimensional view of the crane-supporting building.

Table 1. Properties of the Crane-Supporting Structures (per frame)				
Parameter/Site	**MTL-C**	**VAN-C**	**VAN-E**	**SEA-E**
Total roof gravity load (S or L), kN (kips)	574 (129)	375 (84)	375 (84)	281 (63)
Total horizontal wind load, kN (kips)	211 (47)	256 (58)	256 (58)	187 (42)
T_1, s	1.34	1.25	1.20	1.21
T_2, s	0.21	0.23	0.26	0.21
T_3, s	0.10	0.10	0.10	0.10
M_1/M, %	89.0	87.5	87.3	87.5
M_2/M, %	2.6	2.9	3.0	3.1
M_3/M, %	4.5	5.4	5.5	5.2
W, kN (kips)	1230 (277)	1180 (265)	1190 (268)	1060 (238)
V, kN (kips)	71 (16)	176 (40)	333 (75)	146 (33)
V/W, %	5.8	14.9	28.0	13.8
V_t, kN (kips)	62 (14)	155 (35)	290 (65)	128 (29)
V_t/V	0.87	0.88	0.87	0.88
Steel tonnage, t	11.8	11.5	11.9	10.5

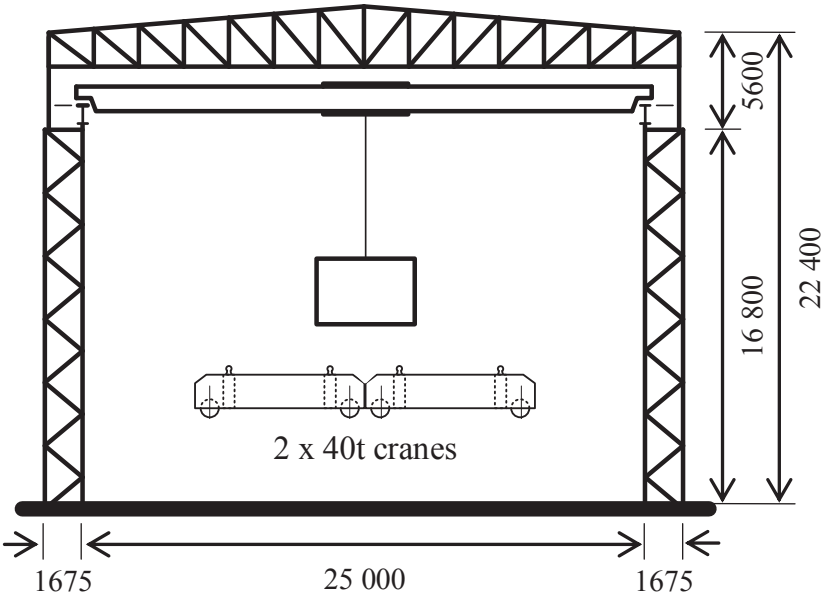

Fig. 2. Two-dimensional view of the frame studied (dimensions in mm).

Building Design

The structure was designed for four different sites: class C site in Montreal (MTL-C), class C and E sites in Vancouver (VAN-C and VAN-E), and class D site in Seattle (SEA-D). The designs were performed according to the applicable building codes at the sites: the 2005 National Building Code of Canada (NBCC) (NRCC, 2005) and the CAN/CSA-S16 (CSA, 2001) steel design standard for the Canadian locations and the ASCE 7-05 (ASCE, 2005) and the AISC *Specification* (AISC, 2005) for Seattle. All relevant loads and load combinations specified in codes were considered in the design. Roof snow loads of 1.96 kPa (40.9 psf) and 1.28 kPa (26.7 psf) were used for Montreal and Vancouver, respectively. In Seattle, the minimum roof live load of 0.96 kPa (20.0 psf) governed. The design guide for crane-supporting structures by MacCrimmon (2004) was consulted for the load combinations including crane induced loads as well as for the design of the runway girders. Deflection criteria were established according to AISE (2003) and Fisher (2004). Lateral deflections at the crane level under nonseismic loads were limited to the lesser of 50 mm (2.0 in) and $h/240$ (= 16,800 mm/240 = 70 mm = 2.8 in). Under seismic loads, the limit on total lateral deflections, including inelastic effects, at the crane and roof levels was taken as 2.5% of the respective heights, as recommended in buildings codes. Drift limits did not govern the design of any of the structures.

The design loads are summarized in Table 1. As required by NBCC, $1.0D + 0.25S$ (D = dead load, S = roof snow load) was included both in the calculation of seismic weight of the structure, W, and in the load combinations involving seismic loads. Vertical ground motion effects were not considered, as prescribed by NBCC. For the Seattle site, the seismic weight included dead load only, while $1.4D$ plus 50% of the roof live load was considered in the seismic load combinations. The factor 1.4 includes the ASCE 7 load factor of 1.2 and vertical acceleration effects (0.2). At all sites, the dead load of the two cranes, without lifted loads, was included in the seismic weight (or mass) as well as in the seismic load combinations. In this calculation, the two cranes were positioned longitudinally in the building to produce the most critical condition for the frame studied. Lateral loads from cranes were equally distributed to each side assuming double flanged wheels.

The elastic spectrum used for the seismic design at each site is shown in Figure 3. The fundamental periods obtained from modal analysis, T_1, are given in Table 1. For all cases, the T_1 value is close to or shorter than the upper limits on periods prescribed in codes for steel moment-resisting frames (in NBCC: $T \le 1.5\ T_a = 1.5 \times 0.085h^{0.75} = 1.31$ s, with h expressed in meters; in ASCE 7: $T \le C_u T_a = 1.4 \times 0.028h^{0.8} = 1.22$ s with h expressed in feet; where $h = 22.4$ m = 73.5 ft) and thus T_1 was used to determine the elastic spectral ordinates. The structures in Canada were assumed to be of the conventional construction (type CC) category. The total design lateral earthquake load or base shear, V, was obtained by dividing the elastic base shear, V_e, by R_dR_o, where R_d and R_o are the ductility- and overstrength-related force modification factors, respectively, with $R_d = 1.5$ and $R_o = 1.3$ ($R_dR_o = 1.95$). The base shear, V_e, is equal to $S(T_a)M_vIW$, where $S(T)$ is the design spectral acceleration at the period T, based on 2% probability of exceedance in 50 years, M_v is the higher mode adjustment factor, I is the importance factor, and W is the seismic weight. The design base shear V need not exceed two-thirds of the value of V

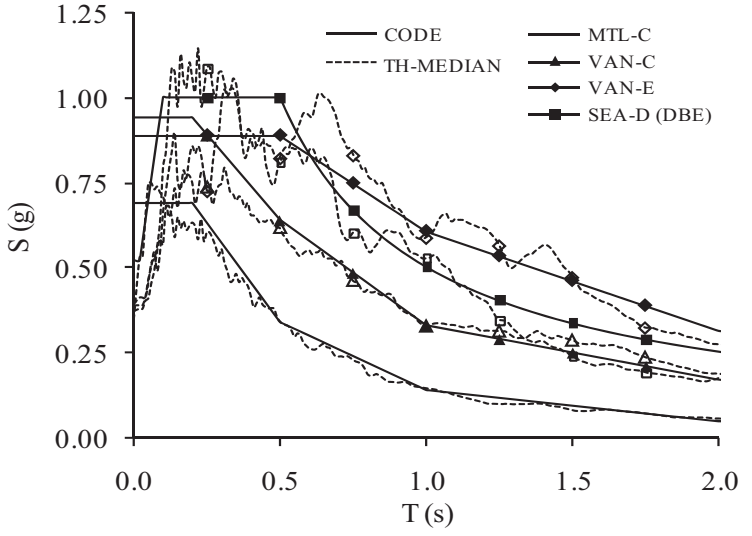

Fig. 3. Code design response spectra and median 5% damped acceleration spectra for the ground motion ensembles.

determined with $T = 0.2$ s. For Seattle, the design base shear $V = C_S W$, where $C_S = S_{D1}/T(R/I) < S_{DS}/(R/I)$ for the period range of the building studied. In the expression for C_S, S_{DS} and S_{D1} are the design spectral accelerations at short (0.2 s) and 1.0 s periods, respectively, and R is the force modification factor. The structure was designed as a building structure with $R = 3.0$ applicable to structures not explicitly detailed for seismic resistance. An importance factor $I = 1.0$ was adopted for all structures. The resulting values of V are presented in Table 1. Note that the building height exceeds the current 15-m (50-ft) limit prescribed for type CC systems in Canada, and an $R = 3.0$ system is not permitted for Seattle according to ASCE 7. As previously discussed, these code system restrictions were purposely ignored to examine their relevance.

Member forces and deflections for seismic design were determined using the modal response spectrum analysis method, and the modal contributions were combined using the complete quadratic combination (CQC) method, assuming 5% of critical damping in each mode. Member forces and deflections were also determined with the equivalent static force method for comparison purposes. In both methods, the total seismic weight (or mass) was distributed to every node of the structural model according to their tributary seismic weight (or mass). In the equivalent static method, the seismic lateral load V was distributed among the nodes based on the node heights and seismic weights in accordance with the applicable code vertical distribution procedure. For the response spectrum analysis, the results were divided by $R_d R_o$ or R, as applicable, and the resulting base shear force V_t was determined. The ratios V_t/V are presented in Table 1; the values are very consistent (0.87–0.88) and are all less than 1.0. Building codes require that the results from response spectrum analysis be scaled to avoid seismic forces much lower than the forces associated to the design earthquake force V. For the structures in Montreal and Vancouver, the response analysis results were scaled by the ratio V/V_t, as required in NBCC for irregular structures. For Seattle, V_t exceeds 0.85 V, and no calibration was required as per ASCE 7. Deflections from both analysis methods were multiplied by $R_o R_d = 1.95$, for the Canadian sites, and by the deflection amplification factor $C_d = 3.0$, for Seattle, to obtain deflection estimates including inelastic response effects.

Such a difference between V and V_t for a single-story building may seem counter-intuitive at first. It can be attributed to the fact that only two modes were considered in the modal combination to include up to 90% of the total structure mass, as prescribed in building codes. Table 1 gives the periods T_i and fraction of participating masses (M_i/M in %) for the first three lateral modes of vibration. The corresponding mode shapes are illustrated in Figure 4 for the MTL-C building. Higher modes with complex deformed shapes and substantial participating mass levels still exist in the structures, essentially because significant seismic weight is present at both the roof and crane levels (essentially the dead load of the cranes for the latter). Including a larger number of modes in the response spectrum analysis improves the prediction of the total seismic force. For instance, the base shear increases from 0.87 to 0.92 V for the MTL-C building when the contribution of the third mode of vibration is added, resulting in 96% total mass participation. Including additional modes has no further impact on the results, and the remaining difference between the static and response spectrum base shears arises from the inherent simplifying assumptions behind the equivalent static method. This effect is less pronounced when the cranes are not present in the frame bay studied, but this situation is less critical because the total seismic weight is reduced and the seismic loads are lower (by 30% and 15% on average, respectively, for the four buildings). Note that the response spectrum analysis results obtained for the case with the cranes present and considering only the first two modes of vibration, as prescribed in codes, are used herein for the discussion.

The columns are critical components of the seismic force-resisting system for these structures. For out-of-plane buckling, effective lengths were taken equal to the vertical distance between braced points, i.e., at third points between the base and the crane girder level for the laced column segment (at location of horizontal struts) and between the crane girder level and the truss bottom chord for the upper column segment. For in-plane buckling, the approach proposed by Schmidt (2001) was adopted. For each load combination,

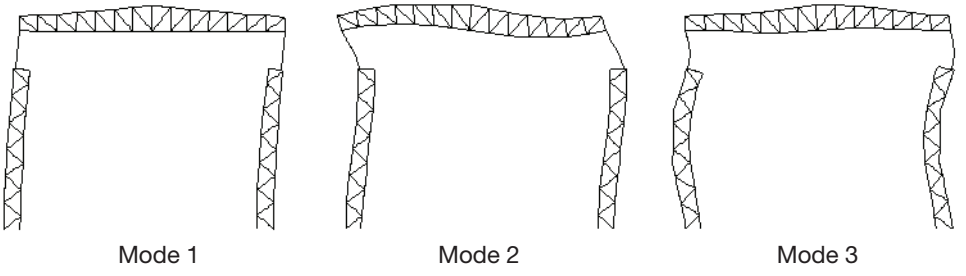

Fig. 4. First three lateral vibration modes for the MTL-C building (cranes not shown, but crane seismic weight included in analysis).

second-order analysis was performed, and horizontal notional loads equal to 0.5% of the gravity loads and acting in the same direction as the lateral loads were applied at the location where gravity loads were applied. For the seismic load combinations, second-order effects of gravity loads acting on the laterally displaced structure were determined by multiplying the first-order analysis results by the amplification factors given in CSA-S16 standard and ASCE 7 provisions. The notional loads account for the effects of initial out-of-plumbness and inelasticity and an effective length equal to the total column height (22.4 m = 73.5 ft) was adopted for both the upper and lower column segments. A K factor of 1.0 was used for bracing members, for both in-plane and out-of-plane buckling, as commonly done in design practice.

The upper column was oriented such that strong axis bending is in the plane of the frame. For that column segment, out-of-plane buckling about weak axis was critical in design. For the laced column segment, the interior and exterior columns were oriented such that in-plane buckling of the individual members occurs about the weak axis and the lacing members were assumed to be welded to the columns. The strength of the individual column members was determined using an equivalent slenderness accounting for the interaction between global and individual buckling modes, as specified in steel design standards. In-plane buckling of the individual column members at the column base governed the design of the interior and exterior columns.

After completion of the design, elastic buckling analysis was carried out for the VAN-C building to verify the effective slenderness ratios assumed in design for in-plane buckling of individual members. The verification was performed for different buckling modes and load combinations, and the cases where buckling mainly develops in the critical column members were identified. For these cases, the effective slenderness ratio of the member, KL/r, were obtained from the elastic buckling load equation: $(KL/r)^2 = \pi^2 EA/P_{cr}$, where $E = 200{,}000$ MPa (29,000 ksi), A is the cross-sectional area of the member and P_{cr} is the axial load carried by the member at buckling. In general, the slenderness ratios from analysis were smaller than the design values for the upper column segment and close to the design values for the individual column members at the base of the laced column segment. Figure 5a shows the frame global lateral buckling mode under dead, crane and wind loads. For this particular case, the KL/r value for the upper column is 73 from buckling analysis, compared to 105 assumed in design. Interaction between global and local buckling of the individual exterior column member at the base under the combination of dead, wind and snow loads is illustrated in Figure 5b. In this case, KL/r from analysis is 59 versus 63 in design. The slenderness ratios assumed in design were used later to evaluate the capacity of the members.

The required steel tonnage per frame is given in Table 1. Due to the relative importance of the crane loads, the final designs at the different sites were quite similar in spite of the differences between wind and seismic loads. In fact, for the Canadian sites, the seismic loads only governed the design of the upper column segment as well as the exterior column and lacing members of the laced column segment of the VAN-E frame. For Seattle, seismic load combinations were also critical for the upper column segment and the exterior column of the laced column segment, even if a higher force modification factor was used. This is partly due to the consideration of vertical seismic acceleration effects in design. In all other cases, crane or wind loads were critical except for the upper column segment of the frame in Montreal that was governed by roof snow load.

Validation of the Seismic Analysis Methods Used in Design

Elastic dynamic time-history analyses were carried out under sets of ground motions compatible with the design spectra to evaluate how successful the design procedures were in predicting the seismic-induced frame deformations and the distribution of seismic member forces. For each site, historical and simulated ground-motion time histories were selected based on magnitude–hypocentral distance scenarios that dominate the seismic hazard. A total of 14 records were

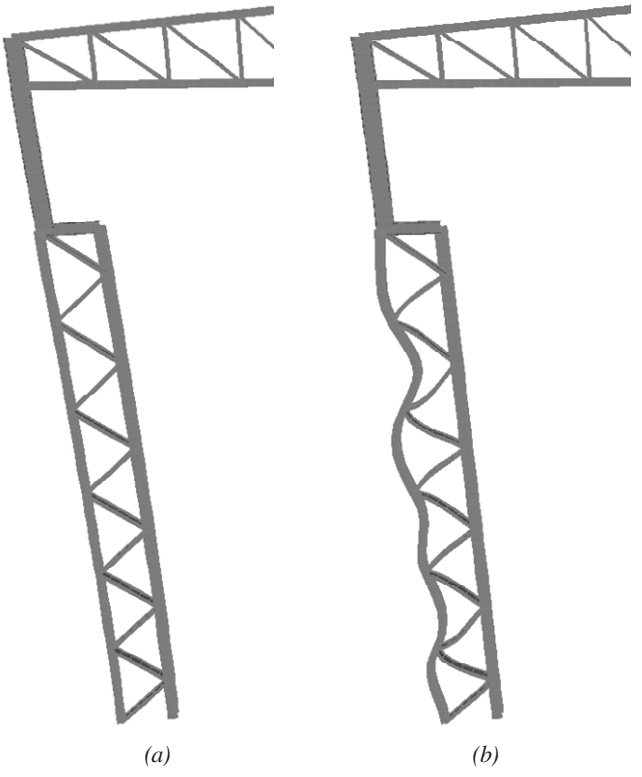

Fig. 5. In-plane buckling modes of the frame: (a) global lateral buckling; (b) interaction between global lateral and individual exterior column buckling.

chosen for MTL-C, 24 for VAN-C, 12 for VAN-E and 20 for SEA-D. The records were scaled to represent the level of seismic loads considered in design. For Canadian locations, the calibration was done by matching the spectral intensities of the record and design spectrum at studied locations over the range of periods determined on basis of the best visual fit between the two spectra. For Seattle, the records available from the SAC database for that location were already calibrated for the appropriate site class and level of seismic hazard, and no additional scaling was needed. Detail of the ground motion selection and scaling can be found in Richard (2009). In Figure 3, the resulting median acceleration response spectra obtained for the four sites are compared to the corresponding design spectra. Time-history dynamic analysis was performed assuming 5% Rayleigh damping in the first two modes and the same seismic nodal masses as those used in design to ensure a consistent comparison.

The time-history analysis results are compared to the predictions from both the equivalent static force and response spectrum analysis methods. The response parameters examined are the peak lateral displacements and peak horizontal accelerations at the crane and roof levels, as well as the stress ratios for the upper column segment and for the individual exterior column member at the base of the laced column. These two column members were identified in design as the most critical under seismic load combinations, which was subsequently confirmed in the time-history analysis. For the column stress ratios, the force demand from time-history analysis was divided by $R_d R_o$ or R, as applicable, and then combined with gravity load effects. The calculations were done using factored member resistances calculated with $\phi = 0.9$ and the nominal steel yield strength. The most critical results obtained from code interaction equations for the different possible failure modes (cross-section strength, in-plane flexural buckling and lateral-torsional buckling) were retained and compared to the corresponding stress ratios calculated for the seismic demand obtained from static and response analysis methods. For all response parameters, the peak values were first determined for each individual record, and the 50th and 84th percentile values were calculated for each ground-motion ensemble. Design procedures were evaluated on the basis of the median results, while the 84th percentile results are commented on to illustrate dispersion.

The total anticipated drift at the crane and roof levels, Δ_c and Δ_r, respectively, normalized by the height measured from the column base to each of the two locations, are shown in Figure 6. In all cases, displacement estimates obtained from the static and response spectrum analysis methods are similar, although the static values are generally slightly higher. The median values from time-history analysis are the smallest but still compare well with those obtained from static and response spectrum analyses. This similarity suggests that the first vibration mode dominated the displacement response. For the Vancouver frames, the 84th percentile values from time-history analysis exceed static analysis predictions, with the difference being more pronounced for Vancouver frame on soft soil (approximately 50%). The median displacements are all well below the limits adopted for seismic design. Note that ASCE 7-05 does not impose drift limits for single-story structures with flexible cladding, such as the structures examined in this study. However, with the exception of the Montreal site, the computed drifts do exceed the 50 mm (2.0 in) (0.30% h) limit that was considered in design for nonseismic load combinations to guard against the possible damage to the lifting equipment. In view of the importance of operational requirements for industrial buildings, it would be appropriate to include the limits on drifts computed at the crane level under seismic loads to prevent damage to the lifting equipment due to earthquakes.

In Figure 7, the results obtained for peak accelerations from response spectrum and time-history analysis are compared. With the exception of the VAN-E site, the median peak acceleration values from time-history analysis are equal or slightly smaller than those obtained from response spectrum analysis. For all cases, the difference between the 84th percentile and median values is less than 40%. For the Montreal frame, the computed accelerations at the crane level are larger than at the roof level, suggesting that higher modes were relatively more excited due to the high-frequency components of the ground motions in eastern North America.

For all sites studied, the column stress ratios predicted by static and response spectrum methods compare very well

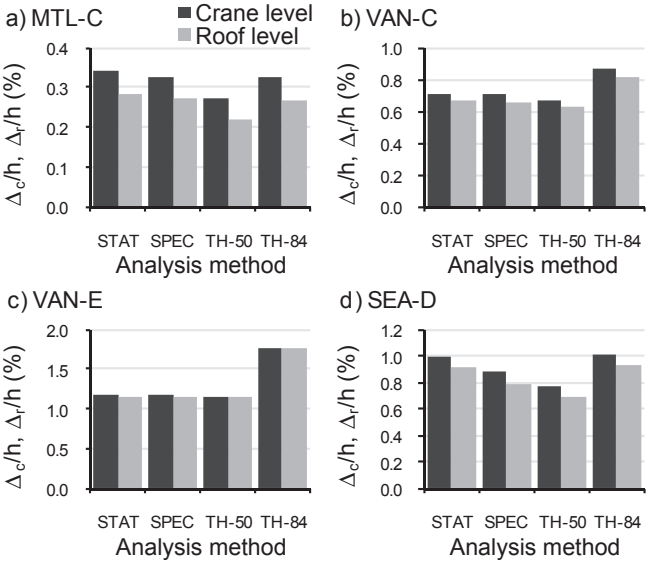

Fig. 6. Peak horizontal displacements from equivalent static (STAT), response spectrum (SPEC) and time-history (TH-med and TH-84th) analysis methods.

with the median values obtained from time-history analysis (Figure 8). The only noticeable difference is observed for the exterior base column in the Seattle frame (about 15% overprediction). The variability of earthquake records has a more pronounced effect on the response of the Vancouver frames, as can be seen from the 84th percentile results. The high stress ratio values in Figure 8 under the seismic effects reduced by force modification factors $R_dR_o = 1.95$ or $R = 3.0$ suggest that the demand from design-level earthquakes will, in fact, exceed the column capacities. This in itself is not a major concern as long as the level of ductility implicitly assumed in design can be effectively provided. This aspect is examined further next.

Assessment of Inelastic Demand

No explicit ductility capacity or strength hierarchy checks were performed in design because the structural systems selected are of the low-ductility category. For these systems, it is expected that the lower seismic force modification factors considered in design would translate into limited and uniformly distributed inelastic demand. It was thus of interest to examine the amplitude and distribution of the expected inelastic response and evaluate the potential for nonductile member failure modes that can detrimentally affect the structural integrity. For this purpose, the peak seismic force demands on the columns from the elastic dynamic time-history analyses described earlier were combined with the member forces from gravity loads. The stress ratios were computed at the expected strength level, i.e., with member resistances determined with a resistance factor of 1.0 and expected steel yield strength, R_yF_y, equal to 1.1 times the nominal value. Note that the forces from time-history analysis are not divided by the force modification factors, as was done previously, such that the seismic force demand corresponds to the design earthquake level.

The computed median and 84th percentile stress ratio values are illustrated in Figures 9, 10 and 11 for the two Vancouver sites and Seattle, respectively. The stress ratios for the Montreal building were less than 1.0 (the columns would remain elastic), and the results for this structure are not discussed further. The values presented are the maximum values obtained for the different limit states and for both sides of the buildings. For the Vancouver frame on firm ground (VAN-C, Figure 9), the columns are expected to remain elastic at the median demand level, but the capacity of three members is exceeded under the 84th percentile force demand. The base of the exterior column was identified as the most critical location (26% overload). The situation is more critical for the VAN-E case: the base of the exterior column (29% overload), the upper column segment (31% overload) and diagonal members in the upper part of the laced column are expected to sustain inelastic demand under the 50th percentile seismic demand. These results are not surprising because the seismic load combinations governed the design of the same members for that structure and system ductility was accounted for in design. For this site, nearly all column members are overstressed under the 84th percentile force level, and the maximum demand-to-strength ratio (252%) is observed at the base of the exterior column. In Figure 11, the results for the Seattle site are similar to the ones obtained

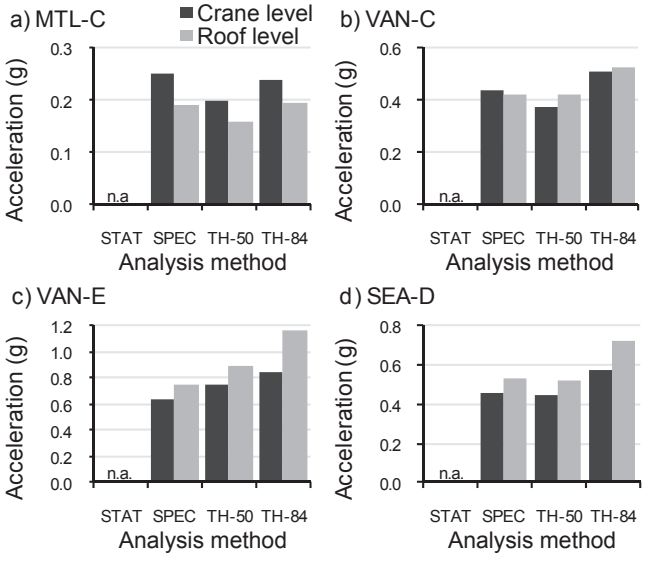

Fig. 7. Peak horizontal accelerations from equivalent static (STAT), response spectrum (SPEC) and time-history (TH-med and TH-84th) analysis methods.

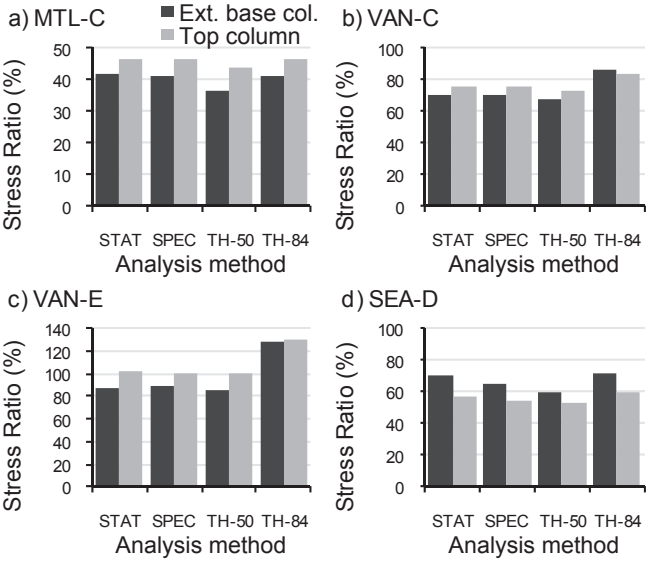

Fig. 8. Peak column stress ratios from static (STAT), response spectrum (SPEC) and time-history (TH-med and TH-84th) analysis methods.

for the VAN-C site at the base of the laced column. However, the demand on the upper column segment is reduced. It is noted that that the time-history analysis for Seattle was performed under the design-level ground motions. Higher demand would be expected under the maximum credible earthquake (MCE) level typically used for assessing seismic performance (1.5 times higher).

The ductility capacity associated with column failure depends on whether bending moments or axial loads dominate the seismic force demand. Figure 12a illustrates the axial load-bending moment demand at the base of the exterior column for the VAN-C case under a ground motion recorded during the 1989 Loma Prieta earthquake. The interaction equations for cross-section strength and in-plane buckling are illustrated in the figures. Both interactions are based on expected member strength with $\phi = 1.0$ and $R_yF_y = 1.1F_y$. As shown, the seismic demand is highly dominated by axial load due to the cantilevered truss action that develops under lateral loads, and column instability failure is predicted, regardless of whether single or double curvature ($\kappa = -1$ or +1) is assumed in the interaction equations. The same response was observed in all other cases studied, suggesting that column buckling, a failure mode that exhibits limited ductility, is likely to occur at the base of the laced columns in these structures. Conversely, the building seismic response induces highly variable in-plane bending moments in the upper column segment while the axial load remains nearly constant (Figure 12b). Verification of the interaction equations at every time step indicates that failure will likely develop on the form of lateral-torsional buckling, rather than by in-plane flexural yielding, suggesting limited ductility capacity. Ductile in-plane flexural hinging response of the upper column segment could be achieved by adding lateral bracing.

SEISMIC DESIGN AND RESPONSE OF THE IRREGULAR BUILDING

Building Studied and the Analysis Model

A three-dimensional view of the heavy industrial building selected for this study is shown in Figure 13a. It is an existing structure located near Montreal, Canada, that houses a vertical mechanical titanium refinement process. The geometry, mass and stiffness distribution are highly irregular. The layout of the columns at the base of the building is illustrated in Figure 13b. The main portion of the building has 37-m by 59-m (121-ft by 194-ft) plan dimensions and is 43 m (141 ft) high. An 8-m (26-ft) tall penthouse is located in the southwest part of the structure. The building also includes two extensions, one in the northwest corner (5 m by 6 m [16 ft by 20 ft]; 18 m [59 ft] high) and one in the southeast corner (24 m by 8 m [79 ft by 26 ft]; 6 m [20 ft] high). Figure 13a shows a recent addition to the south of column line 11. That addition is not illustrated in subsequent figures and was not considered in the study. Several platforms supporting different equipments are concentrated in the south and

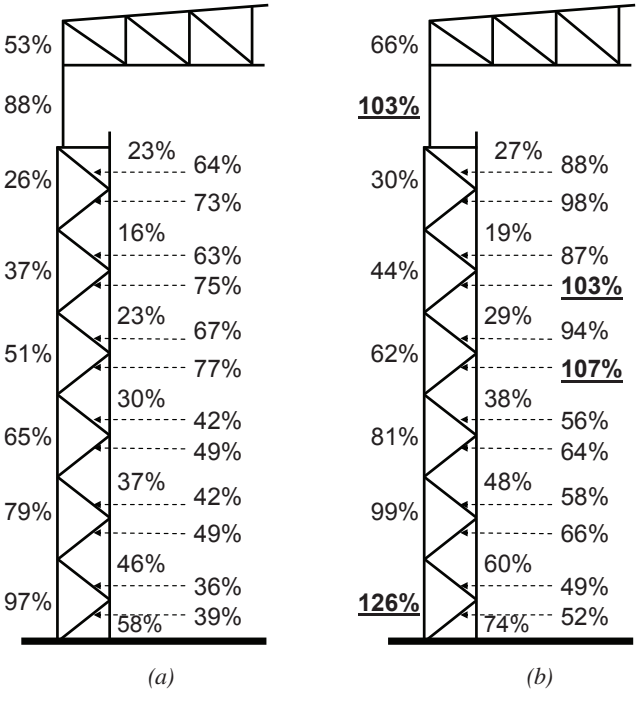

Fig. 9. Stress ratios for the VAN-C frame using expected member resistance: (a) median values; (b) 84th percentile values.

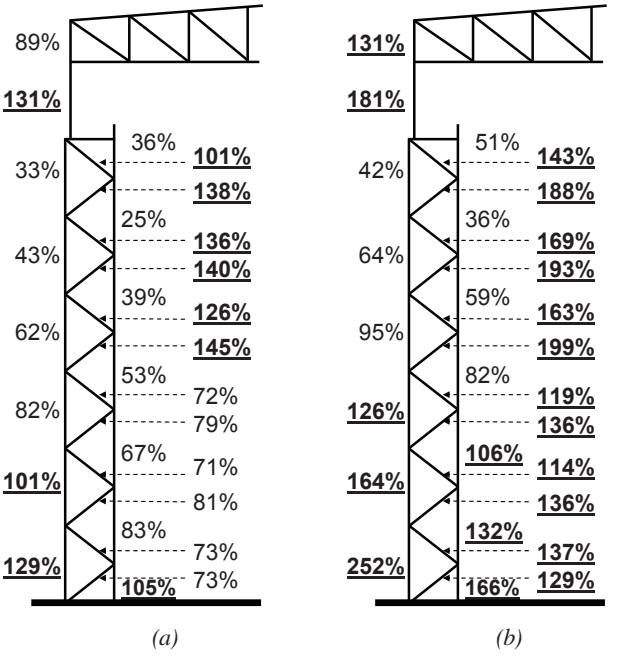

Fig. 10. Stress ratios for the VAN-E frame using expected member resistance: (a) median values; (b) 84th percentile values.

north portions of the building, leaving a large open space in the center that extends almost throughout the whole building height. The building also houses two large-capacity silos (750 t and 1200 t [830 T and 1300 T]) between lines 1 and 4, as well as other smaller pieces of equipment located throughout the structure. Lateral loads are primarily resisted by concentrically braced steel frames located at the perimeter of the building. Additional braced frames are provided in the vicinity of the heavy equipment and large openings.

The existing design served as a start-off point to build the three-dimensional numerical model shown in Figure 14. Some simplifications were made to obtain results that could be indicative of the behavior of similar buildings of this type and not only of the particular building studied. The model was created using the program STAAD.Pro (Bentley, 2008) and includes columns, beams, horizontal bracing and vertical braced frames. The members providing support for the main equipments were also included. Although all

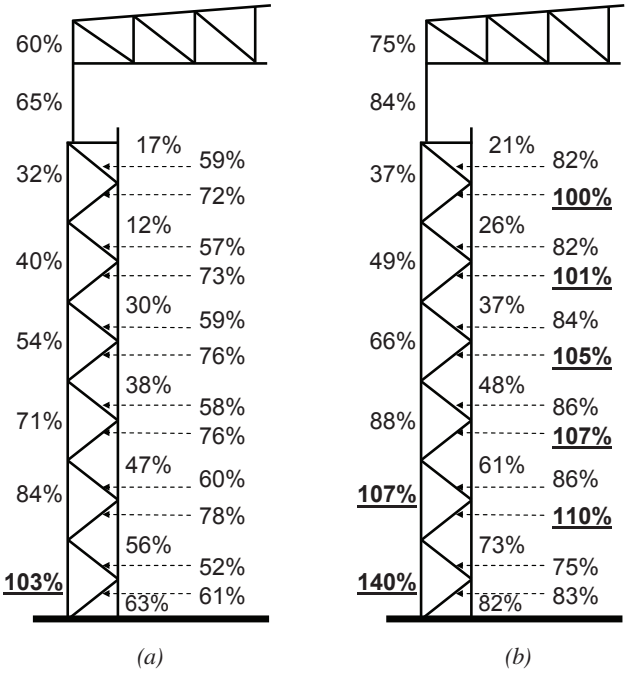

Fig. 11. Stress ratios for the SEA-D frame using expected member resistance: (a) median values; (b) 84th percentile values.

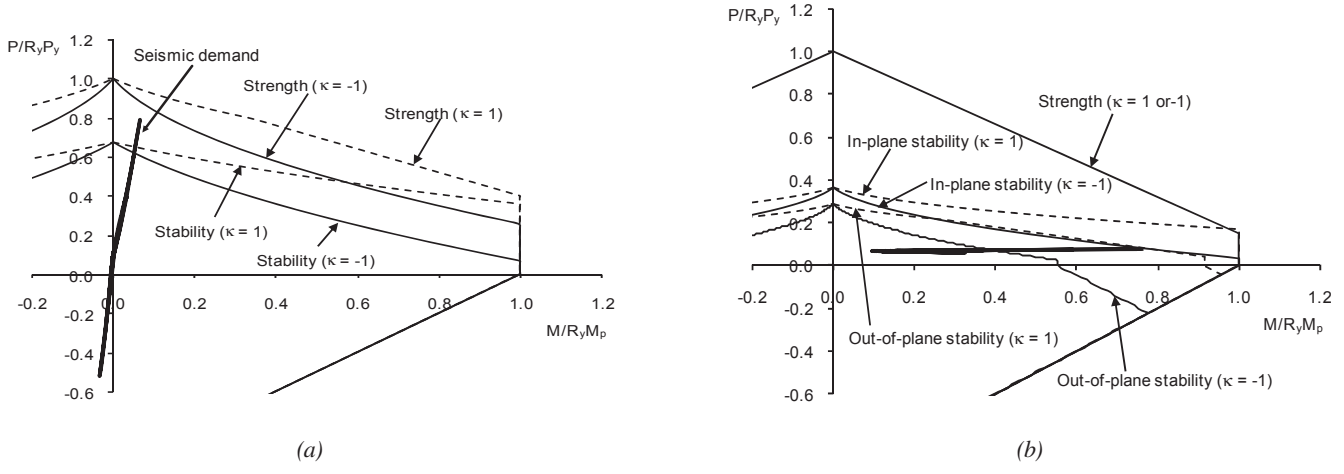

Fig. 12. Axial load-bending moment seismic demand under the Loma Prieta ground motion record versus expected member resistance of the exterior column of the VAN-C building: (a) at the base of the lower column segment; (b) at the base of the upper column segment (axial compression is positive in the graph).

the platforms were included in the model, rigid diaphragm properties were considered only for the floors with a concrete slab. The floor arrangement is illustrated in Figure 14a; the four perimeter braced frames that will be examined later are illustrated in Figure 14b.

The total seismic weight of the structure (W = 74,200 kN = 16,700 kips) was determined in accordance with NBCC 2005 and includes the weight of the structural members, 25% of the roof snow load and the weight of the main pieces of equipment in the fully loaded condition. As in the crane-supporting structure, the seismic weight was distributed at every node of the structure model. In view of their importance and nonuniform distribution, the masses of the major equipments were assigned to additional nodes positioned at the center of gravity of the equipment and linked to the rest of the structure with very stiff members. By doing so, local overturning moments due to the horizontal inertia forces acting above the base of the equipments could be incorporated in the analyses. The masses of the remaining equipment were assigned to the supporting columns at each floor in proportion to their tributary areas.

Validation of Seismic Analysis Methods Used in Design

Seismic load effects were first determined using the equivalent static and response spectrum analysis methods. Selected response parameters were then compared to values obtained from elastic time-history analysis to validate the application of current seismic design procedures to irregular industrial buildings. According to NBCC 2005, dynamic analysis, either spectral or time history, is mandatory for such a highly irregular building. Nevertheless, the equivalent static method is also considered; it is much simpler to use at the preliminarily design phase and is commonly employed by practicing engineers for this purpose. The study was done for the class C site in Montreal for consistency with the existing design. The elastic design spectrum shown in Figure 3 and the ensemble of 14 synthetic accelerograms previously described for the crane-supporting building at the MTL-C site were then applied again herein. In the static and response spectrum analysis methods, the force modification factors R_dR_o were set equal to 1.0 for direct comparison with time-history analysis. For simplicity, accidental torsion was ignored in the calculations, and gravity loads were not included in the model. Consequently, P-delta effects were neglected in the analyses.

The fundamental periods were computed first using the Rayleigh method: 1.29 and 1.28 s in the E-W and N-S directions, respectively. Modal analysis was then performed for verification and the results are presented in Table 2. The analysis confirmed that the two principal modes of the building were in the orthogonal directions, with periods equal to 1.38 and 1.32 s in the E-W and N-S directions, respectively. Both directions had strong torsional components. Period estimates from the NBCC empirical formula for braced frames, $T_a = 0.025\ h$, with h in meters, are also in good agreement with the Rayleigh and modal periods: T_a = 1.08 s when h = 43 m (141 ft) is used and T_a = 1.28 s with h = 51 m (167 ft) at the penthouse location. The NBCC allows

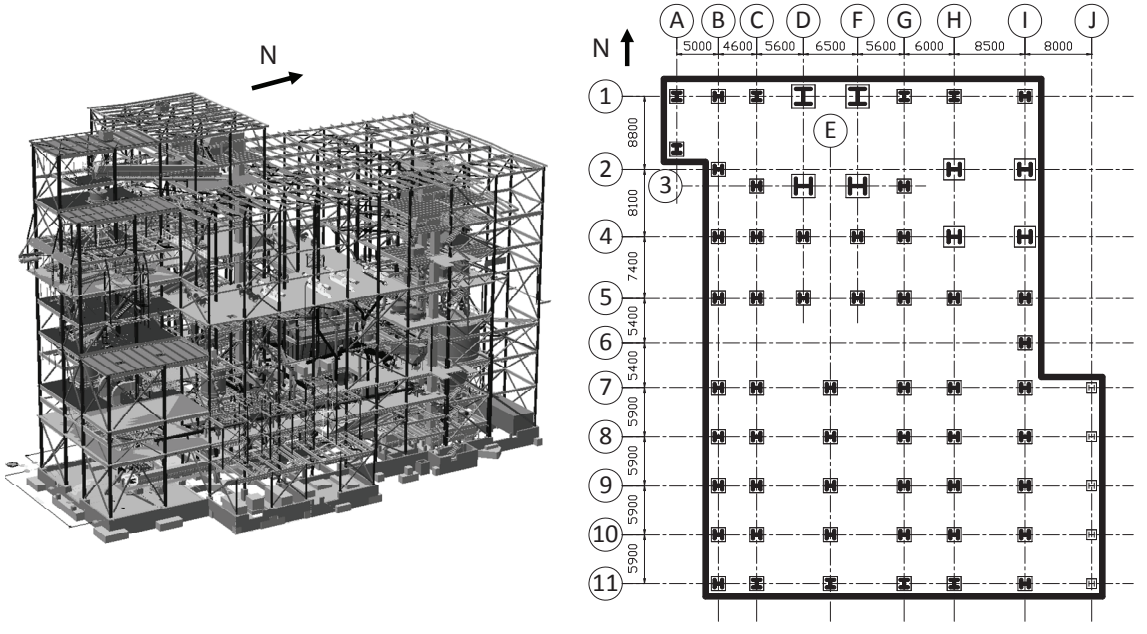

(a) *(b)*

Fig. 13. Irregular building studied: (a) three-dimensional view; (b) column layout at the base.

periods up to 2.0 times T_a when justified by modal analysis.

Elastic values of the base shear forces from the equivalent static method, V, were determined using the periods from the Rayleigh method: 8900 kN (2000 kips) and 9000 kN (2025 kips) along the E-W and N-S directions, respectively. As shown in Table 2, the masses associated with these two fundamental modes only correspond to 53 and 63% of the total mass. In comparison, the mass associated with higher modes is small (less than approximately 7% each). For the response spectrum analysis, a total of 70 modes had to be considered for the E-W direction and 95 modes for the N-S direction in order to obtain the 90% mass participation required by codes (see Table 2). The resulting base shear forces V_t are equal to 5690 kN (1280 kips) and 6460 kN (1450 kips) in the E-W and N-S directions, respectively, i.e., corresponding to only 64 and 72% of the equivalent static method values, respectively. As was the case for the mill-type building, the equivalent static method is found to provide conservative estimates of the force demand. By including up to 126 modes, the combined mass participation increases to 97 and 96% in each of the two directions (see Table 2) and the two associated base shear forces increase to 71 and 79% V, respectively. Similarly to the mill-type building, further increasing the number of modes did not lead to any further enhancement of the response spectrum analysis base shears, and the remaining differences between V_t and V could be attributed to the inability of the static method to adequately represent the dynamic response of complex structures. In this context, the need to scale response spectrum analysis results to values obtained by equivalent static method could be questioned when the number of modes used in the spectral analysis is sufficient to reach convergence; however, this would necessitate further investigation. Herein, the results of the first response spectrum analysis based on 90% participating mass were scaled by the V/V_t ratio, as required in NBCC 2005 provisions, and then used for the comparison with other methods. The force demand from the equivalent static method was obtained from two seismic load profiles in order to assess the approach for inclusion of higher modes: (1) the linear distribution with concentrated force at the top of the structure prescribed in NBCC 2005 and (2) the parabolic distribution as defined in ASCE 7-05.

Three-dimensional dynamic time-history analysis was carried out using the modal superposition routine available in the program STAAD.Pro. Damping equal to 5% of the critical value was assigned in all modes. Preliminary analyses were performed to determine the appropriate number of modes required to adequately predict the seismic base shear, story displacements and maximum brace forces. The number of modes was gradually increased to achieve 90% (70 modes in E-W direction, 95 modes in N-S direction), 97% (126 modes) and ±100% (500 modes) participating mass. Increasing the participating mass from 90 to 97% resulted in peak base shear forces increasing by as much as 25%; however, no further base shear increase was observed beyond 126 modes. Similarly, brace maximum forces changed significantly until 126 modes were included, and the results remained constant when additional modes were considered. Story displacements were the least sensitive to the number of modes selected; however, for specific building levels, it was necessary to solicitate 97% of the mass to avoid changes in the results. Based on these three observations, 126 modes were selected for all time-history analyses. In view of the number of selected accelerograms, median results from time-history analysis can be considered as representative, but 84th percentile values were also tracked to illustrate

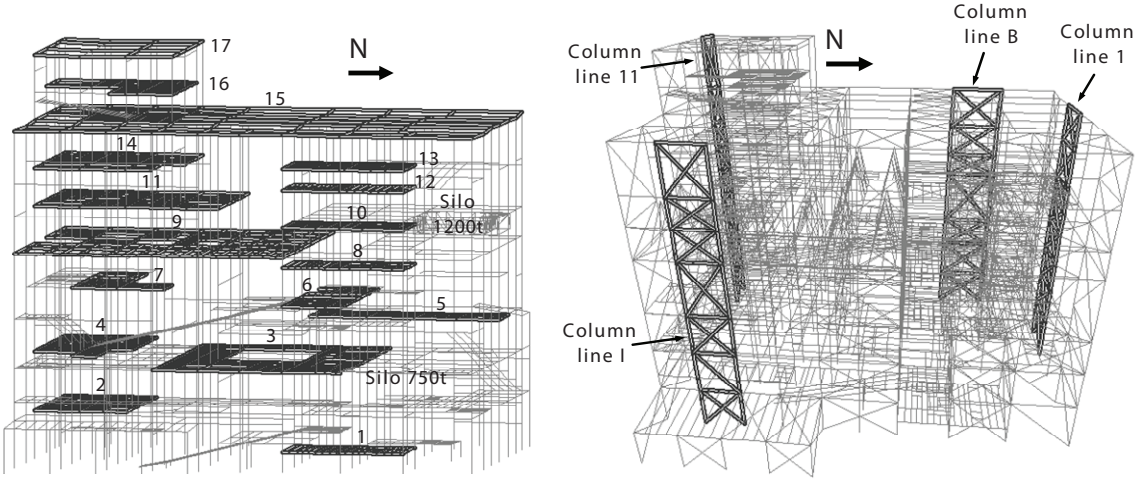

(a) *(b)*

Fig. 14. Building floors and braced frames studied: (a) location of floors; (b) elevation of the braced frames studied.

Table 2. Modal Properties of the Irregular Building Along the Building Orthogonal Directions					
Mode	T_i s	E-W		N-S	
		M_i %	$\Sigma M_i/M$	M_i %	$\Sigma M_i/M$
1	1.46	0.0	0.0	0.2	0.2
2	1.38	53.2	53.2	2.1	2.1
3	1.32	1.5	54.7	63.4	65.7
4	1.11	0.2	54.8	0.2	65.9
5	1.07	7.1	62.0	0.0	65.9
6	1.05	4.2	66.2	0.2	66.1
7	1.02	0.0	66.2	0.0	66.1
8	0.98	3.8	70.0	0.7	66.9
9	0.96	0.7	70.7	5.1	72.0
…	…	…	…	…	…
70	0.38	0.1	90.0	0.1	86.2
…	…	…	…	…	…
95	0.33	0.5	92.9	0.4	90.3
…	…	…	…	…	…
126	0.26	0.3	97.1	0.1	96.1

dispersion. The analyses were conducted for two sets of orthogonal axes: the principal axes of the building and the set of axes oriented at a 45° angle with respect to the principal axes. The latter set was selected to evaluate the impact that the direction of the analysis may have on the response. Three response parameters provided bases for comparison between the different analysis methods, namely, the seismic base shear, story displacements and the axial forces in columns and braces of the selected perimeter braced frames illustrated in Figure 14b. The results are presented in Figures 15, 16 and 17, respectively.

Figure 15 shows that similar base shear values were obtained in two principal building directions. This result was expected because the corresponding building periods in two directions are very close. Elastic design shears were approximately 40% higher compared to median values of time-history results, and even slightly exceeded the maximum values obtained from time-history analysis. Note that median results are in good agreement with results obtained from response spectrum analysis when no scaling of base shear is applied, confirming the conservatism of the static force demand based on fundamental mode response.

Figure 16 shows calculated peak displacements for loads and ground motions applied in the N-S direction. The displacements were normalized by the story height measured from ground. All employed methods predicted comparable displacement profiles. For the equivalent static method, very little difference was observed between the results obtained when using the NBCC 2005 and ASCE 7-05 load distributions. Spectral values were slightly smaller than those obtained for equivalent static load profiles in all but two locations and about 40% higher than the mean values from time-history analysis. Eighty-fourth percentile results were also below the predictions of the equivalent static and response spectrum methods. These observations are consistent with those made for the base shear.

Figure 17 compares column and brace axial load profiles in the selected braced frames for earthquake action along the N-S direction of the building. Results obtained for E-W load application showed similar trends. In general, for the columns and diagonals studied, all methods resulted in similar force profiles. The response spectrum analysis values are consistently higher compared to median time-history results and even exceed the 84th percentile time-history values for almost all elements studied. This is not surprising in view of the scaling procedure that was applied to the response spectrum analysis results. The results obtained with the static equivalent method are comparable to response spectrum values for the frames oriented in the direction of the analysis. For the frames in the perpendicular direction, however, the equivalent static method underpredicted the member forces by a large margin in some cases. This can be attributed to the inadequate inclusion of higher mode effects and the effects of torsion when equivalent static method is used for such an irregular structure.

It was of further interest to see if the direction of the application of the load can affect response forces. Figure 18 summarizes results obtained for four directions of load

application: along the two principal directions of the building and along the two orthogonal axes oriented at a 45° angle with respect to the building principal axes. Force envelopes obtained from the response spectrum analysis are also shown for comparison. The reader is reminded that column lines B and I run in the N-S direction, while column lines 1 and 11 are in the E-W direction. It would normally be expected that the highest forces in columns and braces are induced when the load is applied in the direction of the braced frame. In Figure 18, this is indeed the case for the braces of all frames studied. However, in the upper columns of the frames along the E-W direction, up to 30% higher forces are observed when the ground motion is applied in directions other than the direction parallel to the frames, including loading at 45°. This is attributed to the fact that these columns are also part of other braced frames (not studied herein) acting in the perpendicular direction. This situation is not unusual in industrial buildings of this type, and the results indicated that caution should be exercised when selecting the direction of the seismic loading. For such columns, NBCC requires that forces from members framing into the columns from all directions be considered in design. In ASCE 7, columns that form part of two intersecting systems must be designed for ground motions applied in any directions, but only if the structure is assigned to Seismic Design Categories D or E. In all cases studied, the member forces obtained from response spectrum analysis were the highest and would thus provide conservative estimates of design forces.

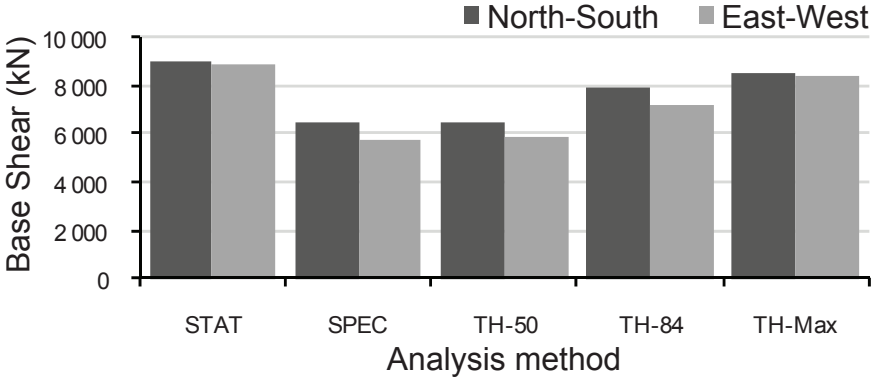

Fig. 15. Peak base shear from equivalent static (STAT), response spectrum (SPEC) and time-history (TH-med and TH-84th) analysis methods (1 kip = 4.45 kN).

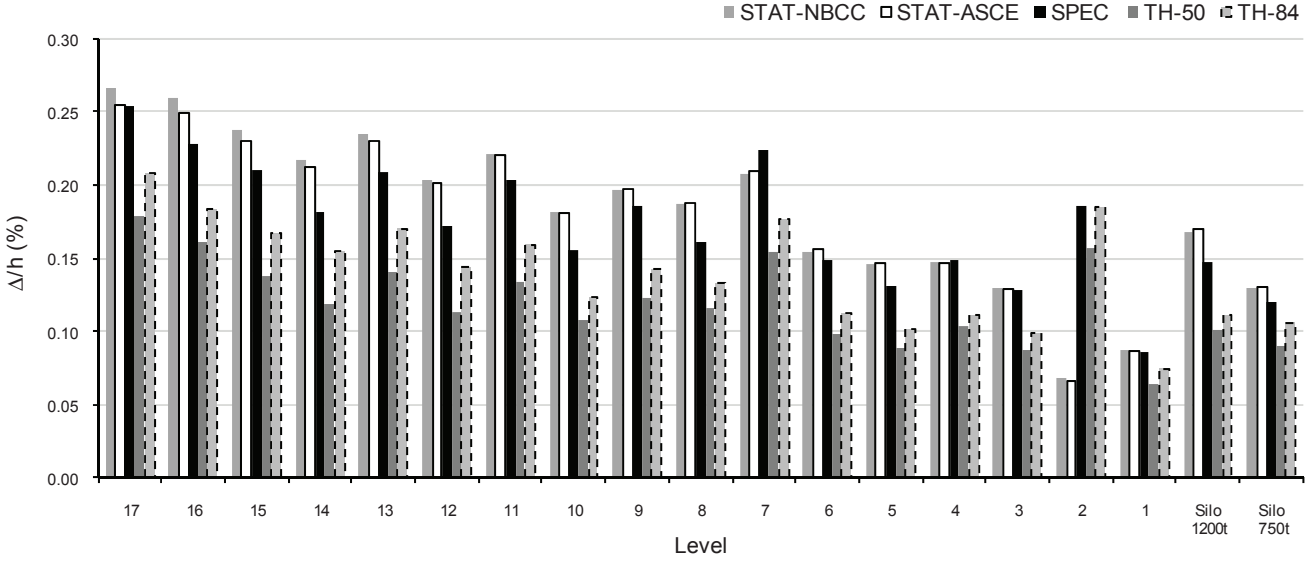

Fig. 16. Peak drift from equivalent static (STAT), response spectrum (SPEC) and time-history (TH-med and TH-84th) analysis methods and for earthquake action along the N-S direction.

CONCLUSIONS AND FINAL COMMENTS

Elastic time-history dynamic analyses were performed for two different types of industrial buildings to validate the predictions from the equivalent static force procedure and the response spectrum analysis method prescribed in current building codes. The first building studied was a typical crane-supporting, mill-type building. The study was carried out for four different sites representative of typical eastern and western North American seismic conditions. The second building is an existing tall structure that is highly irregular in geometry, mass and stiffness distribution. Its seismic response was studied only for the Montreal site for consistency with the original design. The structures as designed do not meet the restrictions imposed in current (2005) building codes; the height of the buildings exceed the 15-m (50-ft) limit imposed in the National Building Code of Canada for steel seismic force-resisting systems of the conventional construction category, and $R = 3.0$ as used for the design of the building in Seattle is not permitted for building structures according to ASCE 7.

For both structures, the fundamental periods of vibrations from code empirical formulas compared well with

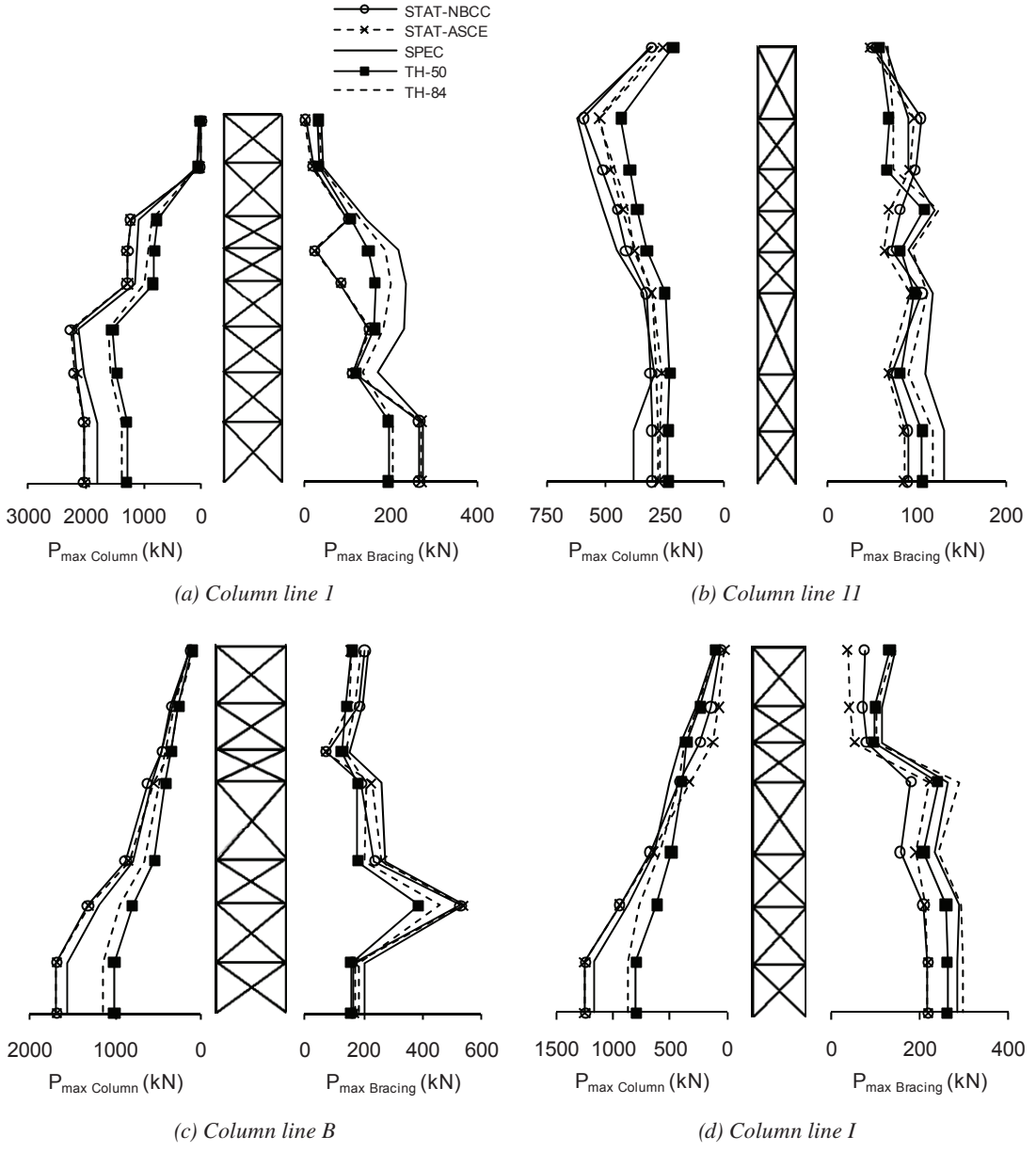

(a) Column line 1 *(b) Column line 11*

(c) Column line B *(d) Column line I*

Fig. 17. Peak axial load in columns and bracing members from equivalent static (STAT), response spectrum (SPEC) and time-history (TH-med and TH-84th) analysis methods for earthquake action along the N-S direction (1 kip = 4.45 kN).

the periods obtained from modal analysis. For the irregular structure, good period match was also obtained when using the Rayleigh method. The equivalent static force procedure static method consistently gave higher values of the total earthquake force, or base shear, compared to the response spectrum analysis method when the number of modes considered in the latter was set to obtain 90% combined mass participation, as prescribed in codes. This effect on the global seismic demand is corrected when applying the scaling procedures prescribed in codes. For the structures studied, no further significant change in the base shear obtained by response spectrum analysis was observed when the number of modes considered increased beyond the one required to obtain in the order of 96 to 97% participating mass. Therefore, it is recommended to adopt a tighter criterion in response spectrum analysis, prior to scaling to equivalent static values, to better represent the complex dynamic response of these structures, especially for tall and irregular buildings such as the one examined herein.

For the crane-supporting building, the horizontal displacements from both code analysis methods are similar and agree well with the median demand from seismic ground motions. Except for the Montreal site, the drifts at the crane level exceeded the limit recommended to prevent damage

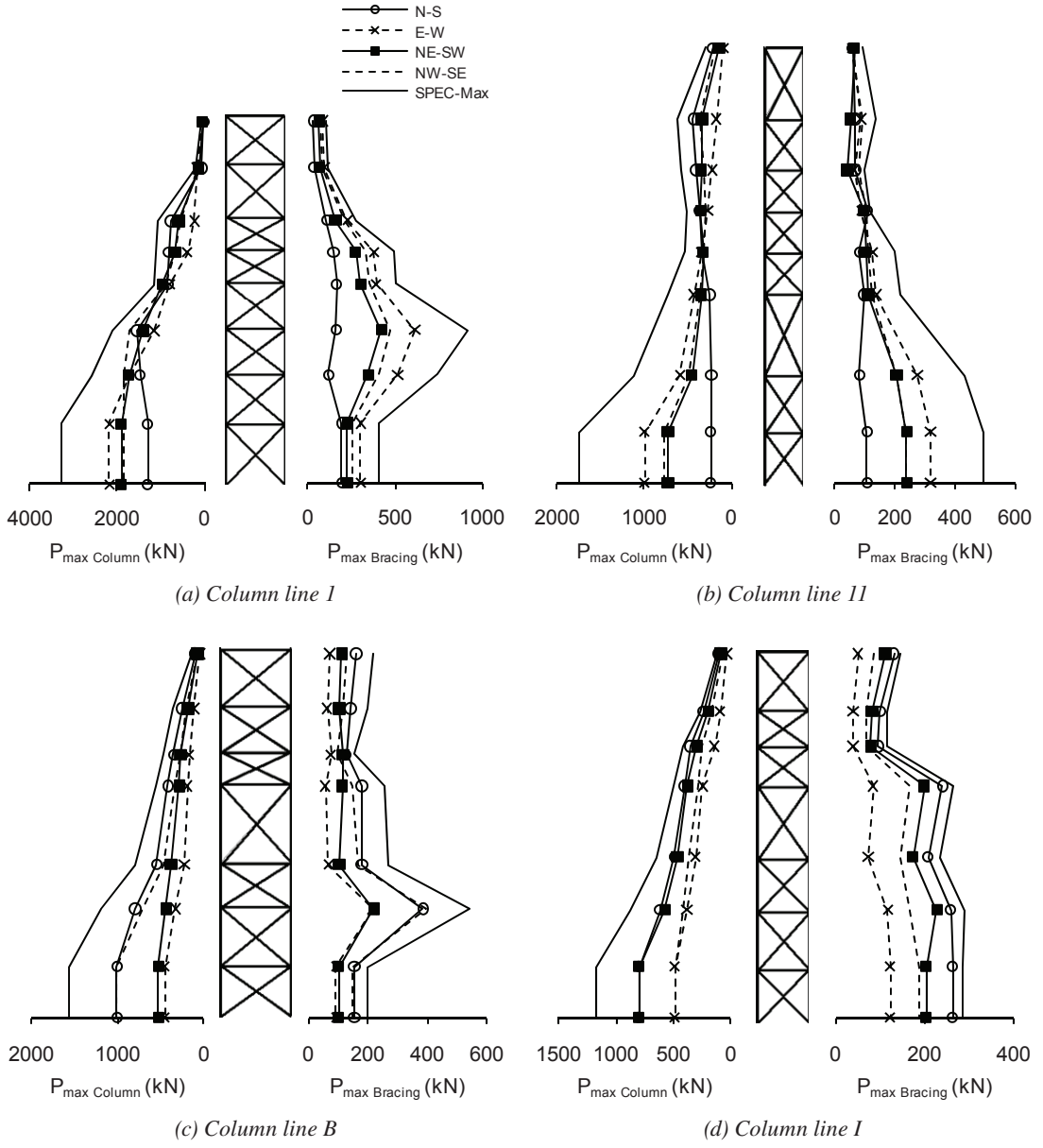

(a) Column line 1

(b) Column line 11

(c) Column line B

(d) Column line I

Fig. 18. Peak axial load in columns and bracing members from time-history and response spectrum analysis methods (1 kip = 4.45 kN).

to the lifting equipment in this building type. Median peak horizontal accelerations from dynamic analysis are well predicted by response spectrum analysis. Seismic force demand governed the design of the upper column segment, individual column members at the base of the laced column segment and lacing members. For the column members, the static and response spectrum analysis methods predicted well the median force demand obtained from time-history analyses. That force demand was found to exceed the expected member strengths, at both the 50th and 84th percentile levels, indicating that inelastic column behavior may occur in these structures. This response is a consequence of the force modification factors used in design and was expected. However, the study also showed that stability limit states would govern the inelastic column response. The ductility capacity associated with such inelastic behavior can be limited, and can possibly be less than that implicitly assumed in design, with potential detrimental impact on the structural integrity in case of strong earthquakes.

The study of the irregular building showed that the equivalent static method can be used to estimate displacements, but may lead to unconservative predictions of column and brace forces. In all cases studied, regardless of the direction of the analysis, response spectrum analysis also resulted in higher force demand compared to elastic time-history analysis. Scaling requirements prescribed in codes likely contributed to this conservatism. Nevertheless, the method appears to be very appropriate to predict the seismic response of such highly irregular structures. If dynamic time-history analysis is performed using a modal superposition technique, as was done in this study, the results showed that element forces are sensitive to the number of modes considered and can be significantly underestimated if an insufficient number is selected. For the building studied, the number of modes for obtaining 97% global mass participation was needed to adequately predict the base shear force demand. The study also showed that the selection of the direction in time-history analysis should be done with care, because the maximum forces in elements that are part of two orthogonal-braced frames are not always induced by seismic loads acting in the direction parallel to the bracing systems.

The results presented in this paper were obtained for a limited number of structures and cannot be fully generalized. Further studies on additional structures should be performed to validate the findings of this research. However, the results provide insight into possible limitations of current seismic design procedures and possible directions for future investigation. For instance, one could study the need for scaling the results from response spectrum analysis to the equivalent static values when a sufficient number of modes are considered in the response spectrum analysis. Modal superposition time-history analyses, with constant damping ratios in all modes, were performed in this study, which may result in conservative predictions of the higher-mode effects. Comparison should be made with direct integration techniques and Rayleigh damping models. Nonlinear time-history analyses should be carried out to better assess the inelastic demand imposed on critical members and connections of industrial buildings and evaluate the effects of this inelastic response. Physical testing should be conducted to assess the ductility capacity associated with the governing limit states that are predicted by analysis. For mill-type buildings, this study suggests that column buckling is a possibility: out-of-plane of the frame for the upper column segment and in-plane for the base columns. In case the available ductility is found to be inadequate, techniques should be examined to enhance the inelastic seismic column response (e.g., minimum bracing requirements to prevent out-of-plane buckling of the upper columns or ductile fuse systems to control the axial force demand in the base column members).

ACKNOWLEDGMENTS

This project was funded by the Natural Sciences and Engineering Research Council (NSERC) of Canada and Hatch Ltd. (Consulting Engineering). The authors express their appreciation to Robert A. MacCrimmon of Hatch Energy, Niagara Falls, Canada, for his most valuable input in the selection and design of the structures studied.

REFERENCES

AISC (2005), *ANSI/AISC 360-05, Specification for Structural Steel Buildings,* American Institute of Steel Construction, Chicago, IL.

AISE (2003), *Guide for the Design and Construction of Mill Buildings*, *AISE Technical Report No. 13,* Association for Iron and Steel Technology, Pittsburgh, PA.

ASCE (2005), *ASCE/SEI 7-05, Including Supplement No. 1, Minimum Design Loads for Buildings and Other Structures,* American Society of Civil Engineers, Reston, VA.

ASCE (2010), *ASCE/SEI 7-10, Minimum Design Loads for Buildings and Other Structures,* American Society of Civil Engineers, Reston, VA.

Bendimerad, F., Johnson, L., Coburn, A., Rahnama, M. and Morrow, G. (1999), *Kocaeli, Turkey Earthquake*—Event Report, Risk Management Solutions, Inc., Menlo Park, CA.

Bentley (2008), *STAAD.Pro. Version 20.07.03.16.* Bentley Systems, Inc., Yorba Linda, CA.

CSA (2001), *CAN/CSA-S16-01 Limits States Design of Steel Structures*, *Including CSA-S16S1-05 Supplement No. 1,* Canadian Standards Association, Willowdale, ON, Canada.

Daali, M. (2004), "Industrial Facilities and Earthquake Engineering," *Proc., 13th World Conference on Earthquake Engineering,* Vancouver, BC, Canada, Paper No. 330.

Fisher, J.M. (2004), *Design Guide 7 Industrial Buildings, Roofs to Anchors Rods*, 2nd ed., American Institute of Steel Construction, Chicago, IL.

Humar, J., Adams, J., Tremblay, R., Rogers, C. and Halchuk, S. (2010), "Proposals for the Seismic Design Provisions of 2010 National Building Code of Canada," *Proc. 9th US National and 10th Canadian Conference on Earthquake Engineering*, Toronto, ON, Canada, Paper No. 1387.

Johnson, G.S., Ascheim, A. and Sezen, M. (2000), "Industrial Facilities," *Earthquake Spectra*, Vol. 16, No. S1, pp. 311–350.

NRCC (2005), *NBCC 2005.* National Building Code of Canada. National Research Council of Canada, Ottawa, ON, Canada.

MacCrimmon, R.A. (2004), *Guide for the Design of Crane-Supporting Steel Structures,* Canadian Institute of Steel Construction, Toronto. ON, Canada.

Rahnama, M. & Morrow, G. (2000), "Performance of Industrial Facilities in the August 17, 1999, Izmit Earthquake," *Proc. 12th World Conference on Earthquake Engineering,* Auckland, New Zealand.

Richard, J. (2009), Étude du comportement sismique de bâtiments industriels avec systèmes de contreventement de faible ductilité, M.Sc. Thesis, École Polytechnique, Montréal, QC, Canada (in French).

Rolfes, J.A. & MacCrimmon, R.A. (2007), "Industrial Building Design—Seismic Issues," *Iron and Steel Technology,* Vol. 4, No. 5, pp. 282–298.

Schmidt, J.A. (2001), "Design of Mill Building Columns Using Notional Loads," *Engineering Journal*, AISC, Vol. 39, No. 2, pp. 90–99.

Sezen, H., Elwood, K.J., Whittaker, A.S., Mosalam, K.M., Wallace, J.W. and Stanton, J.F. (2000), "Structural Engineering Reconnaissance of the August 17, 1999, Kocaeli (Izmit), Turkey, Earthquake," PEER Report No. 2000/09, PEER Center, University of California, Berkeley, CA.

Swan, S.W. and Hamburger, R. O. (1991), "Industrial Facilities," *Earthquake Spectra*, Vol. 7, No. S2, pp. 49–58.

Swan, S.W., Wesselink, L., Bachman, R.E., Malik, L., Eli, M. and Porush, A. (1990), "Industrial Facilities," *Earthquake Spectra*, Vol. 6, No. S1, pp. 189–238.

Thiel, C. (Ed.) (1986), "The Chile Earthquake of March 3, 1985—Industrial Facilities," *Earthquake Spectra*, Vol. 2, No. 2, pp. 373–409.

Tremblay, R. Timler, P., Bruneau, M. and Filiatrault, A. (1995), "Performance of Steel Structures During the 1994 Northridge Earthquake," *Canadian Journal of Civil Engineering,* Vol. 22, No. 1, pp. 338–360.

Tremblay, R., Bruneau, M., Driver, R., Metten, A., Montgomery, C.J. and Rogers, C. (2010), "Seismic Design of Steel Structures in Accordance with CSA-S16-09," *Proc. 9th US National and 10th Canadian Conference on Earthquake Engineering*, Toronto, ON, Canada, Paper No. 1768.

Yanev, P. (1989), "Performance of Industrial Facilities," *Earthquake Spectra*, Vol. 5, No. S1, pp. 101–113.

Design of Braced Frames in Open Buildings for Wind Loading

W. LEE SHOEMAKER, GREGORY A. KOPP, and JON GALSWORTHY

Abstract

Open-frame buildings are often used to provide a measure of weather protection over equipment or other sheltered storage on industrial sites. These shelters have a roof covering and minimal wall cladding, if any. ASCE 7 provides no guidance on the wind loads acting perpendicular to the frames that would control the design of the longitudinal braces. This paper summarizes wind tunnel tests that were performed on open-frame, low-rise buildings with a roof covering to determine the base shear and bracing loads parallel to the ridge. Two examples are provided to illustrate how the results of this study may be used to obtain the forces in longitudinal bracing.

Keywords: open-frame buildings, wind bracing.

A common application, particularly on industrial sites, is the utilization of an open-frame building to provide a measure of weather protection over equipment or other sheltered storage, as shown in Figures 1 and 2. These shelters have a roof covering, but there is usually minimal, or no wall cladding. ASCE 7-05 (ASCE, 2005) provides no guidance on the wind loads acting perpendicular to the frames that would control the design of the longitudinal braces. This paper will summarize the wind tunnel tests that were performed on open-frame, low-rise buildings with a roof covering to determine the drag (base shear) and bracing loads in the longitudinal direction, i.e., parallel to the ridge. Two examples are provided to illustrate how the results of this wind tunnel study can be used to obtain the forces to design the longitudinal bracing.

Prior to the latest research conducted at the University of Western Ontario (UWO), as discussed in this paper, the only available method to determine these longitudinal drag loads utilized data from studies of open lattice structures (Georgiou and Vickery, 1979; Georgiou et. al., 1981; MBMA, 2006). The new UWO study addresses the concern that the use of wind loads derived for open lattice structures may lead to inappropriate loads for low-rise buildings. That is, the presence of both a roof and the ground would be expected to play a significant role on the flow speeds and directions through the open building, perhaps leading to quite different loads, when compared to open-lattice structures. Specifically, shielding factors may be different for low-rise building frames compared to lattice tower frames.

W. Lee Shoemaker, Ph.D., P.E., Director of Research & Engineering, Metal Building Manufacturers Association, Cleveland, OH (corresponding author). E-mail: lshoemaker@mbma.com

Gregory A. Kopp, Ph.D., P.Eng., Professor and Canada Research Chair in Wind Engineering, University of Western Ontario, London, ON, Canada. E-mail: gak@blwtl.uwo.ca

Jon Galsworthy, Ph.D., P.Eng., Principal, Rowan Williams Davies & Irwin, Inc., Guelph, ON, Canada. E-mail: jon.galsworthy@rwdi.com

WIND TUNNEL STUDY

The details of the wind tunnel study are documented in both the final report (Kopp et al., 2008) and a recent paper (Kopp et al., 2010). A brief summary will be provided here as a basis for the proposed design method.

There is a wide range of parameters to be considered for these open buildings; therefore, many test configurations were required to account for practical building applications. Three different combinations of frame widths, B, and eave heights, H, were used:

1. $B = 40$ ft and $H = 12$ ft
2. $B = 70$ ft and $H = 20$ ft
3. $B = 100$ ft and $H = 30$ ft

The roof slope was 2 on 12 (9.46°) for all combinations. Building models consisting of three, six and nine frames (see Figures 3 through 5) were evaluated, along with four different solidity ratios, because this is an important parameter with regard to wind flow through the open building. The solidity ratio refers to a ratio of the blocked area, A_O, to the total area enclosed by the end frame, A_E. The lowest value of solidity was based on a bare-end frame, while larger solidities either represented deeper end frame members, partial end wall cladding (gable in-fill) or full end wall cladding as shown in Figures 6 and 7. In total, 18 configurations were tested, as listed in Table 1.

Table 1. Wind Tunnel Test Configurations							
Case	Description	Number of Frames	Frame Width, W (ft)	Eave Height, H (ft)	End Wall Area, A_E (ft^2)	Blocked Area, A_o (ft^2)	Solidity Ratio, A_o/A_E
1	Nominally open	3	40	12	547	88	0.161
2	Nominally open	6	40	12	547	88	0.161
3	Nominally open	9	40	12	547	88	0.161
4	Nominally open	9	100	30	3417	315	0.092
5	Nominally open	6	100	30	3417	315	0.092
6	Nominally open	3	100	30	3417	315	0.092
7	End wall members larger	3	70	20	1604	253	0.158
8	Nominally open	3	70	20	1604	154	0.096
9	Gable end filled in	3	70	20	1604	563	0.351
10	End wall filled in	3	70	20	1604	1604	1.00
11	End wall members larger	6	70	20	1604	253	0.158
12	Nominally open	6	70	20	1604	154	0.096
13	Gable end filled in	6	70	20	1604	563	0.351
14	End wall filled in	6	70	20	1604	1604	1.00
15	End wall members larger	9	70	20	1604	253	0.158
16	Nominally open	9	70	20	1604	154	0.096
17	Gable end filled in	9	70	20	1604	563	0.351
18	End wall filled in	9	70	20	1604	1604	1.00

The wind tunnel models (1:100 scale) were designed to determine both the total base shear (drag) as well as a reasonable estimate of the proportion of wind load going through the longitudinal brace as shown in Figure 3. The entire model was mounted to a plate that was positioned on a force balance to directly measure the overall base shear. The attachment of the frames to the base plate replicated pin connections. The longitudinal bracing was connected to the base plate through small load cells that measured the axial load in the bracing members. A typical model drawing is shown in Figure 8.

Fig. 2. Example of large open-building application.

Fig. 1. Example of small open-building application.

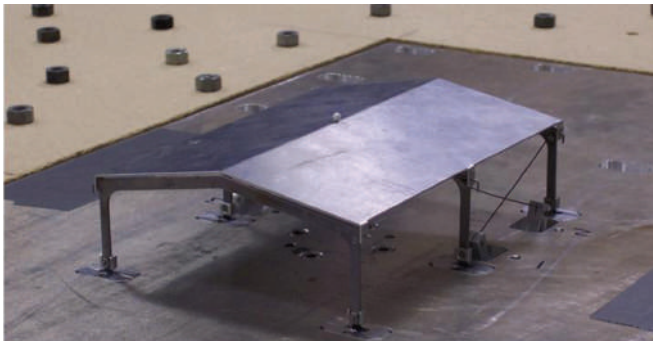

Fig. 3. Wind tunnel model with three frames, showing longitudinally braced bay.

Fig. 4. Wind tunnel model with six frames.

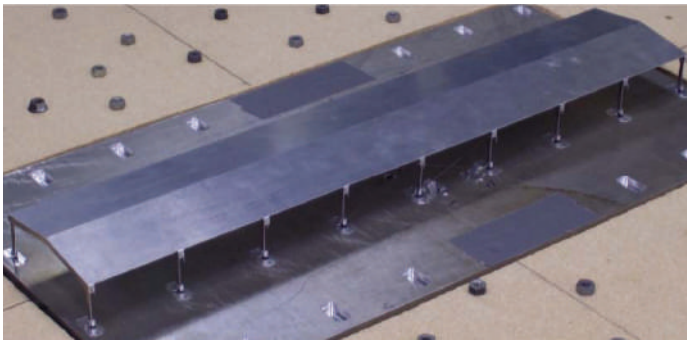

Fig. 5. Wind tunnel model with nine frames.

Fig. 6. Gable in-filled end wall (configuration 9, solidity ratio = 0.351).

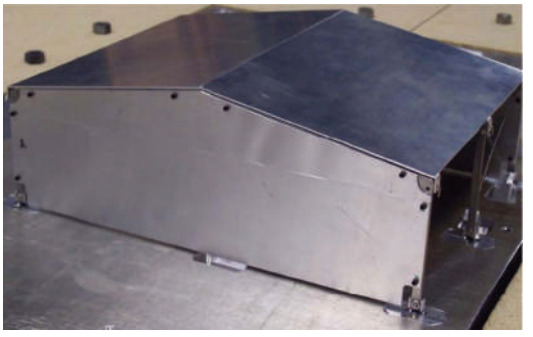

Fig. 7. End wall totally filled with cladding (configuration 10, solidity ratio = 1.00).

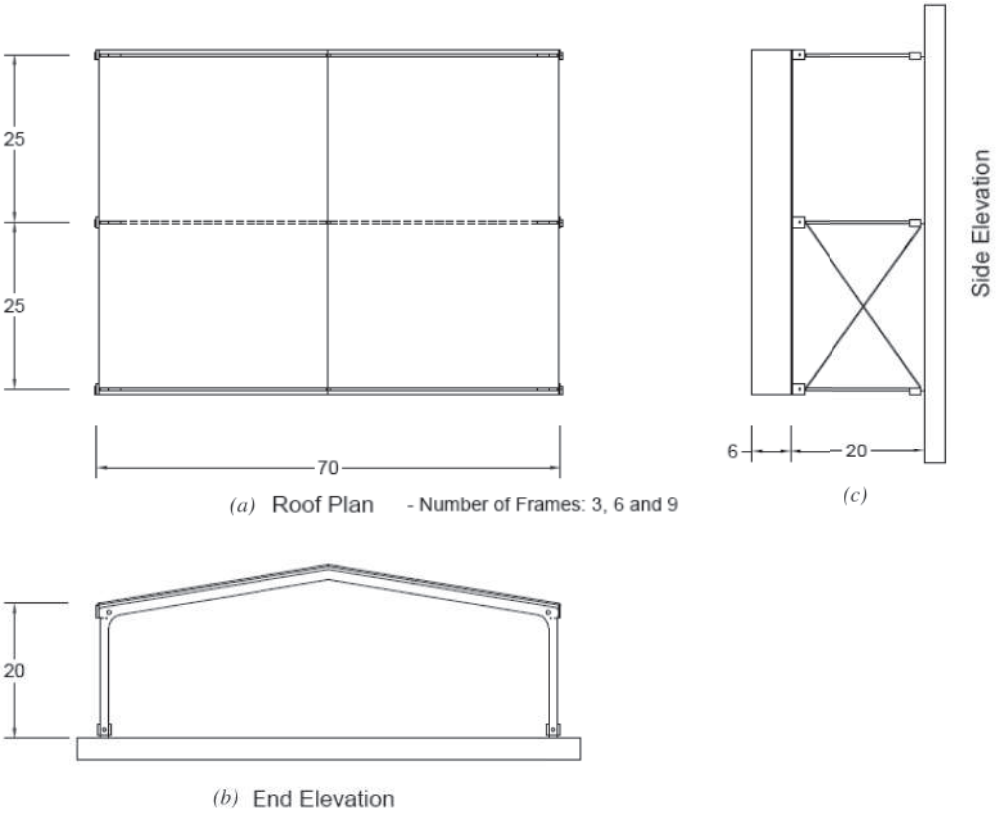

Fig. 8. Typical model drawing: (a) roof plan (three, six and nine frames); (b) end elevation showing transverse moment frame; (c) side elevation showing braced frame being evaluated.

No testing was done with obstructions underneath the building, i.e., from stored materials, etc. The worst case for the horizontal loads is expected with the building open to free unobstructed wind. It should be noted that this would not be the case for uplift on the roof, but that is not the subject considered in the current study. ASCE 7-05 does have provisions to determine the wind uplift on the roof of an open building such as evaluated in this study (Section 6.5.13.2 for MWFRS and Section 6.5.13.3 for Components and Cladding); the uplift is dependent on any obstructions to the wind flow that might be present.

Wind Tunnel Results

Load cell measurements were taken for 19 wind angles between 0° and 180°, where the minimum and maximum angles represent wind direction parallel to the ridge and 90° would be at an angle perpendicular to the ridge. Horizontal loads from the force balance (S_x and S_y) were measured along with horizontal component of the longitudinal bracing load, B_x.

The base shear coefficient can be defined as

$$C_{Sx} = \frac{s_x}{\frac{1}{2}\rho V_H^2 A_o} \tag{1}$$

where

ρ = density of air
V_H = mean hourly wind speed at the eave height
A_o = blocked area as listed in Table 1

The base shear coefficient could also be defined in terms of the total area of the end wall, if it were totally clad, A_E. This coefficient would be defined as, $C_{Sx}\varphi$, where φ is the solidity ratio A_o/A_E.

The horizontal component of the bracing force can be normalized in the same way such that

$$C_{Bx} = \frac{B_x}{\frac{1}{2}\rho V_H^2 A_o} \tag{2}$$

More relevant to design practice, these force coefficients can be converted to ASCE 7-05 format as follows:

$$(GC_p)_{eq} = \frac{q_H \hat{C}_{Sx} A_o}{q_{33,3S} K_{zt} K_h K_d I A_o} \tag{3}$$

where

$(GC_p)_{eq}$ = equivalent wind tunnel pressure coefficient
q_H = wind pressure at the eave height
$q_{33,3S}$ = basic wind pressure from ASCE 7-05 (3 s gust measured at 33 ft height)
K_{zt} = topographic factor
K_h = factor that converts wind pressure to eave height
K_d = directionality factor
I = importance factor
$\hat{C}_{Sx}$ = peak load coefficient, which is the sum of the mean coefficient and gust coefficient

The worst wind angle for each configuration was between 0° and 40°, with 20° to 30° typically yielding slightly higher load coefficients. For all frame sizes, the number of frames is an important factor because the load was observed to increase monotonically with the number of frames.

Empirical Model for Base Shear (Longitudinal Drag)

The UWO wind tunnel study (Kopp et al., 2008; Kopp et al., 2010) determined that the major parameters that affect the wind-induced base shear loads on low-rise open-frame buildings in the longitudinal direction are frame size (width and height), number of frames and solidity ratio. The analysis of the load coefficient variations—holding two of these parameters constant and varying the third—suggested that multiplicative factors accounting for the load effects of these parameters would be a reasonable model. The aerodynamic behavior and load magnitude also suggested that a model based on enclosed low-rise buildings rather than open lattice structures such as electrical power transmission towers would be more appropriate.

The ASCE 7-05 method for defining the pressure loads due to wind for enclosed low-rise buildings can be modified for open-frame buildings by introducing two multiplicative factors: K_B, which accounts for building width effects, and K_s, which accounts for both the solidity ratio and number of frames.

Therefore, Equation 6-18 of ASCE 7-05 is replaced with:

$$p = q_h (GC_{pf})(K_B K_S) \tag{4}$$

where

GC_{pf} = pressure coefficient from Figure 6-10, ASCE 7-05
q_h = velocity pressure at mean roof height as defined by Equation 6-15, ASCE 7-05

$$K_B = \begin{cases} 1.8 - 0.010B & \text{for } B < 100 \text{ ft} \\ 0.8 & \text{for } B \geq 100 \text{ ft} \end{cases} \tag{5}$$

$$K_S = 0.2 + 0.073(n-3) + 0.4e^{1.5\phi} \tag{6}$$

n = number of frames
ϕ = solidity ratio, A_o/A_E

Because the wind tunnel tests were run with three, six and nine frames, the applicability of the method for less than three frames and more than nine frames was evaluated. For solidity ratios that were due only to the transverse frames—i.e., no end wall cladding—the loads increased linearly with the number of frames in the range tested. This would likely continue for a larger number of frames, but not necessarily for fewer than three due to relative changes in shielding of the members. However, the data shows that three frames are sufficient for this asymptotic behavior to occur. On the other hand, there is no linear variation with end wall cladding in place, perhaps due to changes in the flow through the building because of large blockage at the ends. The data show that extrapolating beyond nine frames would be conservative. Therefore, Equation 6 is determined applicable to applications where the number of frames exceeds nine, but for less than three frames, use $n = 3$. Also, with regard to GC_{pf} from Figure 6-10 in ASCE 7-05 for the "longitudinal direction", building surfaces 1 and 1E would be used for the windward end wall, and building surfaces 4 and 4E would be used for the leeward end wall, with the coefficients from Figure 6-10 based on a flat roof ($\theta = 0°$).

The total wind force on the main wind force resisting system (MWFRS) in the longitudinal direction is given by:

$$F = q_h(GC_{pf})(K_B K_S)A_E \tag{7}$$

DESIGN EXAMPLE 1

Design the longitudinal cross bracing for the building shown in Figure 9 using ASCE 7-05 and the procedure outlined in this paper. The building is a storage facility located in Mobile, Alabama, in Open Country—Exposure Category C, and the basic wind speed is $V = 130$ mph. Building represents a low hazard to human life in the event of failure; therefore, Occupancy Category I is appropriate.

Determine velocity pressure q_h (Equation 6-15, ASCE 7-05):

$$q_h = 0.0256K_h K_{zt} K_d V^2 I$$

where

K_h = 0.90 From Table 6-3, ASCE 7-05, (note: h = eave height because roof slope < 10°)

K_{zt} = 1.0 (no topographic effects)

K_d = 0.85 From Table 6-4, ASCE 7-05

I = 0.77 From Table 6-1, ASCE 7-05

Therefore,

$$q_h = 0.00256(0.90)(1.0)(0.85)(130)^2(0.77) = 25.5 \text{ psf}$$

Blocked area, A_o:

Column area = [(8 + 24)/2](20/12) = 26.67 ft^2

Rafter area = [(24 + 12)/2](33/12) = 49.5 ft^2

A_o = 2(26.67 + 49.5) = 152 ft^2

Total area of end wall, A_E:

A_E = 2[(20 + 25.83)/2](35) = 1604 ft^2

Solidity ratio, ϕ:

$\phi = A_o/A_E = (152/1604) = 0.095$

Building width factor, K_B:

$K_B = 1.8 - 0.010(70) = 1.1$

Solidity factor, K_S:

$K_S = 0.2 + 0.073(5 - 3) + 0.4e^{1.5(0.095)} = 0.81$

Pressure coefficient, GC_{pf}:

First, determine the width ($2a$) of the edge zone—see Note 9 of Table 6-10 of ASCE 7-05.

a = 10% of the least horizontal dimension or $0.4h$, whichever is smaller, but not less than either 4% of the least horizontal dimension or 3 ft.

(1) Smaller of

a. 10% of 70 ft = 7 ft ⇐ **governs**

b. $0.4h = 0.4(20 \text{ ft}) = 8$ ft

Note: h is the mean roof height, but except the eave, height shall be used for $\theta \le 10°$.

(2) But not less than

a. 4% of 70 ft = 2.8 ft

b. 3 ft

End wall surface area in zones 1E (windward wall) and 4E (leeward wall) as depicted in Figure 10:

$$A_{1E} = A_{4E} = 2\left(\frac{20 + 22.33}{2}\right)(14) = 592.62 \text{ ft}^2$$

End wall surface area in zones 1 (windward wall) and 4 (leeward wall):

$$A_1 = A_4 = 2\left(\frac{22.33 + 25.83}{2}\right)(21) = 1011.36 \text{ ft}^2$$

GC_{pf} = 0.61 + 0.43 = 1.04 in zones 1E and 4E (From Table 6-10, ASCE 7-05)

GC_{pf} = 0.40 + 0.29 = 0.69 in zones 1 and 4 (From Table 6-10, ASCE 7-05)

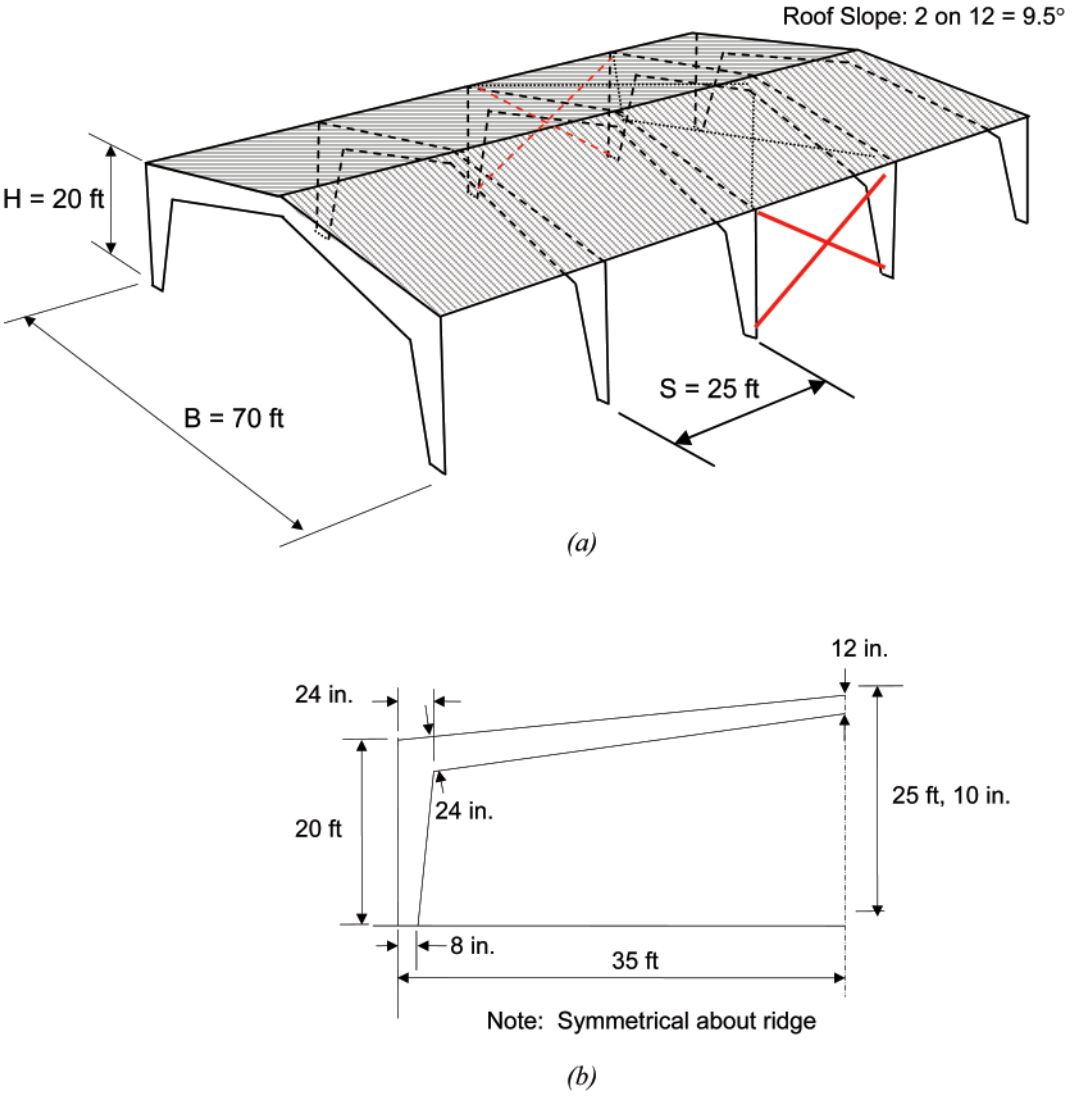

Fig. 9. Design example 1: (a) building layout; (b) typical frame dimensions.

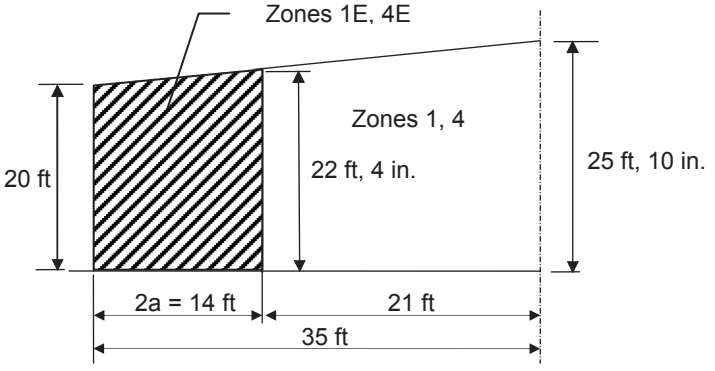

Fig. 10. End zone locations.

Total effective GC_{pf} for end wall:

$$GC_{pf} = \frac{1.04(592.62) + 0.69(1011.36)}{1604} = 0.819$$

Total longitudinal force:

$$F = q_h(GC_{pf})(K_B K_S)A_E =$$
$$= (25.5 \text{ psf})(0.819)(1.1)(0.81)(1604 \text{ ft}^2) = 29{,}847 \text{ lb}$$

The next step in designing the longitudinal cross bracing is to determine the portion of this total longitudinal load that is carried by the bracing and how much is carried directly through the columns to the foundation. The paper on the UWO research (Kopp et al., 2010) recommends that 75% of the total base shear (drag) be used to design the bracing members, based on the measurements taken on the wind tunnel models. However, this recommendation is limited to the construction and assumptions used in the wind tunnel models, so a rational analysis can alternately be done on the building with the longitudinal force applied to determine the force distribution to the bracing members.

The design wind forces for the braced bay, for each side of the building, are shown in Figure 11 as follows:

Using the 75% recommendation:

$F_H = 0.75\ F_{side} = 0.75(14{,}924 \text{ lb}) = 11{,}193 \text{ lb}$

$$\text{Required strength of brace} = \frac{11{,}193}{\cos(38.66)} = 14{,}334 \text{ lb}$$

As a comparison, the total longitudinal force can be calculated for this same design example using the method derived from open lattice structural research described in the *Metal Building Systems Manual* (MBMA, 2006).

Using the same solidity ratio ($\phi = 0.095$), the gust response factor for a single frame is calculated as:

$GC_p(0) = 1.71 - 4.10\phi = 1.32$ (see Figure A7.3.3(a); MBMA 2006)

Then, from Figure A7.3.3(b), the shielding coefficient (n_2) based on two frames is determined as:

$n_2 = 0.95$ (using $S/B = 25/70 = 0.357$)

From Figure A7.3.3(c), the shielding coefficient (n_N) for N frames is determined as:

$n_N / n_2 = 0.85$

Therefore, $n_N = 0.85 n_2 = 0.81$

Then, the total longitudinal force is:

$GC_p(0) q_h A_o[1 + (N - 1)n_N] = 1.32(25.5 \text{ psf})(152 \text{ ft}^2)[1 + 4(0.81)] = 21{,}693 \text{ lb}$

This is compared to 29,847 lb, determined earlier using the method outlined in this paper.

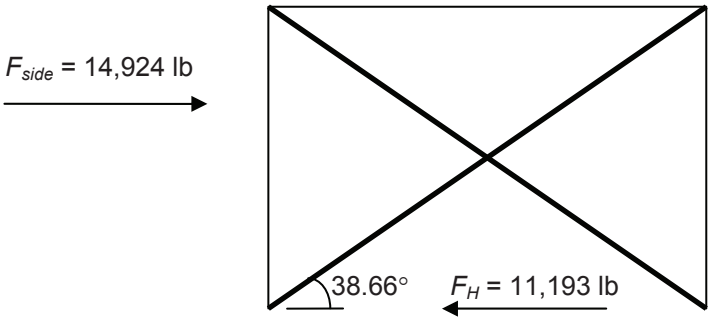

Fig. 11. Design example 1: horizontal force for bracing design.

DESIGN EXAMPLE 2

Same as design example 1, but add partial end wall cladding as shown in Figure 12. Note that this would be a similar configuration to the buildings shown in Figures 1 and 2.

Design the longitudinal cross bracing for the preceding building using ASCE 7-05 and the procedure outlined in this paper. The building is a storage facility located in Mobile, Alabama, in Open Country—Exposure Category C, and the basic wind speed is $V = 130$ mph. Building represents a low hazard to human life in the event of failure; therefore, Occupancy Category I is appropriate.

Note that the only changes from design example 1 are the calculation of the blocked area (A_o), the solidity ratio (ϕ) and the solidity factor (K_S).

Blocked area, A_o:

Column area = $[(8 + 16)/2](20/12) = 20$ ft^2

End wall clad area = $[(15.83 + 10)/2](35) = 452$ ft^2

$A_o = 2(20 + 452) = 944$ ft^2

Total area of end wall, A_E:

$A_E = 2[(20 + 25.83)/2](35) = 1604$ ft^2

Solidity ratio, ϕ:

$\phi = A_o/A_E = (944/1604) = 0.589$

Solidity factor, K_S:

$K_S = 0.2 + 0.073(5 - 3) + 0.4e^{1.5(0.589)} = 1.31$

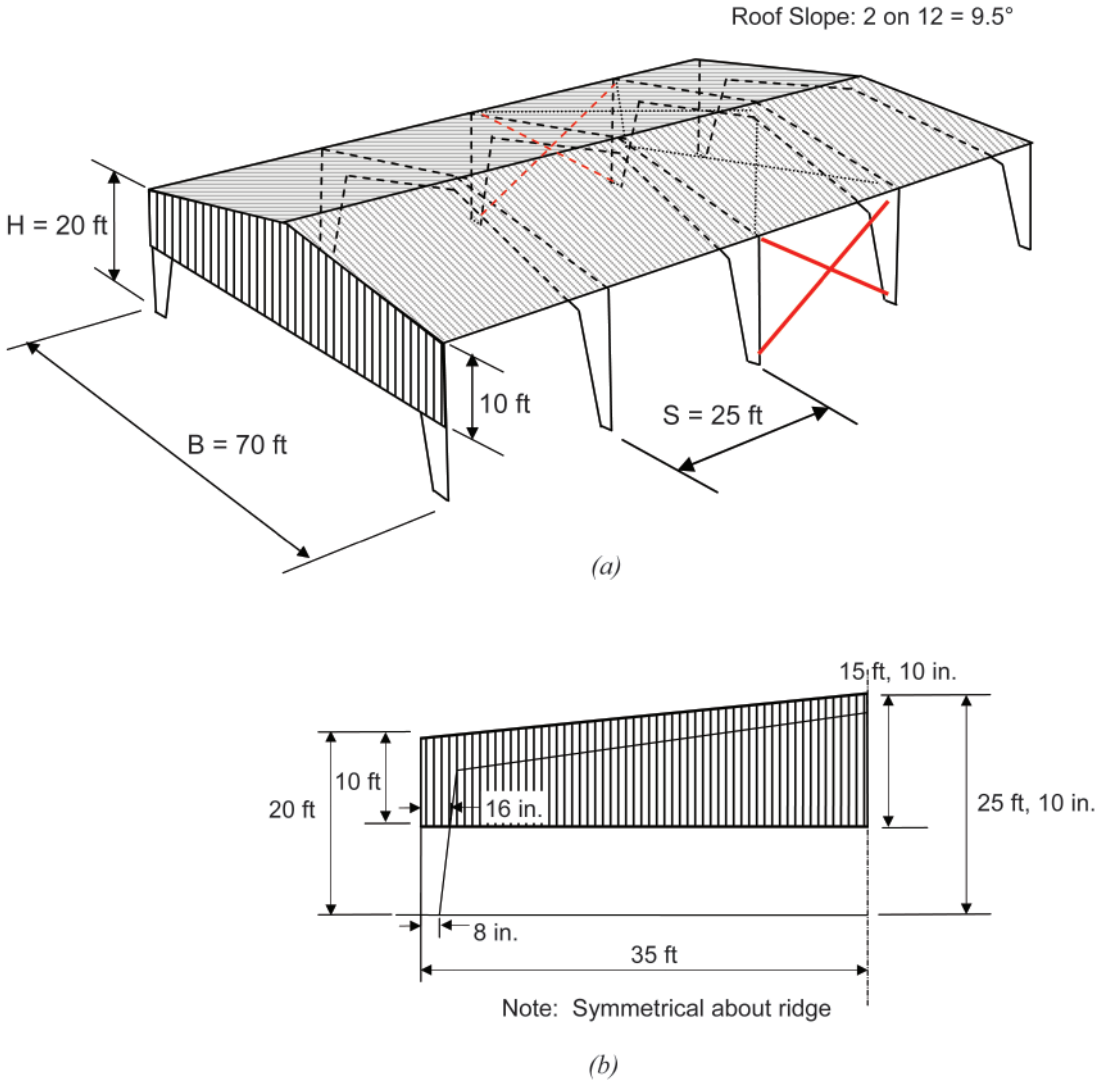

Fig. 12. Design example 2: (a) building layout; (b) end wall cladding.

Total longitudinal force:

$$F = q_h(GC_{pf})(K_B K_S)A_E$$
$$= (25.5 \text{ psf})(0.819)(1.1)(1.31)(1604 \text{ ft}^2) = 48{,}272 \text{ lb}$$

The design wind forces for the braced bay, for each side of the building, are shown in Figure 13 as follows:

Using the 75% recommendation: $F_H = 0.75\ F_{side} = 0.75(24{,}136 \text{ lb}) = 18{,}102$ lb

$$\text{Required strength of brace} = \frac{18{,}102}{\cos(38.66)} = 23{,}182 \text{ lb}$$

It is clear that in design example 2, more than one braced bay will likely be needed to economically carry the required brace force. The final sizing of the brace and connections will determine this.

CONCLUSIONS

This paper summarizes the wind tunnel tests that were performed on open-frame, low-rise buildings to determine the drag (base shear) and bracing loads in the longitudinal direction. Two examples are provided, illustrating how the results of this wind tunnel study can be used to design longitudinal bracing for this type of common open-frame building.

REFERENCES

ASCE (2005), *Minimum Design Loads for Buildings and Other Structures*, ASCE/SEI 7-05, American Society of Civil Engineers, Reston, VA.

Georgiou, P. and Vickery, B.J. (1979), "Wind Loads on Building Frames," *Proc. 5th International Conference on Wind Engineering*, Fort Collins, CO, July, pp. 421–433.

Georgiou, P., Vickery, B.J. and Church, R. (1981), "Wind Loading on Open Framed Structures," *Proc. 3rd Canadian Workshop on Wind Engineering*, Vancouver, BC, Canada, April.

Kopp, G., Galsworthy J. and Oh, J.H. (2008), "Wind Loads on Open-Frame Buildings," Boundary Layer Wind Tunnel Report, BLWT-SS4-2008, University of Western Ontario, London, ON, Canada.

Kopp, G., Galsworthy, J. and Oh, J.H. (2010), "Horizontal Wind Loads on Open-Frame, Low-Rise Buildings," *Journal of Structural Engineering*, ASCE, January.

MBMA (2006) *Metal Building Systems Manual,* 2006 edition, Metal Building Manufacturers Association, Cleveland, OH.

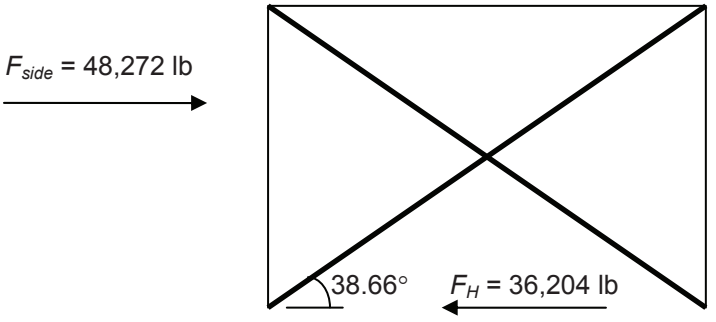

Fig. 13. Design example 2: horizontal force for bracing design.

Current Steel Structures Research
No. 27

REIDAR BJORHOVDE

This issue of "Current Steel Structures Research" for the *Engineering Journal* focuses on a selection of research projects at three of the leading universities in Europe. The descriptions will not discuss all of the current projects at the schools. Instead, selected studies provide a representative picture of the research efforts and demonstrate the importance of the schools to the home countries and indeed to the efforts of industry and the profession worldwide.

The universities and many of their structural steel researchers are very well known in the world of steel construction: University of Coimbra in Coimbra, Portugal; Karlsruhe Institute of Technology in Karlsruhe, Germany; and University of Naples, Federico II, in Naples, Italy. Other projects at some of these institutions have been discussed in previous research papers, but the studies that are presented in the following reflect major, long-time efforts in a number of areas of the construction industry of Europe. Much of the work is tied to the research programs of the European Union and its member countries, and the collaboration among universities in several countries for many of the projects is very impressive. All of the projects are multiyear efforts, emphasizing the need for careful planning and implementation of research needs and applications, including the education of graduate students and advanced researchers. Naturally, and as always intended in the United States as well, the outcomes of the studies focus on design standards and industry needs. The magnitude of the economic impact of the work cannot be overemphasized.

In true forward-looking fashion, the researchers at these institutions have been active for many years, as evidenced by their leading roles in the design standards development efforts of Europe, the well-known Eurocodes. Specifically, for steel construction, Eurocodes 3, 4 and 8 are reflected in the applications of the results, addressing the design of steel structures, composite structures and structures subjected to seismic effects, respectively. Large numbers of English-language technical papers and conference presentations have been published, contributing to a collection of studies that continue to offer solutions to complex problems for designers as well as fabricators and erectors. Not the least important, some of these efforts complement ongoing work in the United States and elsewhere. The broad sharing of knowledge that is taking place promises significant results, not the least because of issues of finances and the sheer cost of research.

References are provided throughout the paper, whenever such are available in the public domain. However, much of the work is still in progress, and in some cases reports or publications have not yet been prepared for public dissemination.

SOME CURRENT RESEARCH WORK AT THE UNIVERSITY OF COIMBRA IN COIMBRA, PORTUGAL

For many years the University of Coimbra has been one of the leaders in international academia, due to its being the fifth oldest university in the world. Its leadership role in structural engineering is, of course, of much more recent date, but the faculty has pursued an aggressive development of technical programs and research facilities. There have been numerous principal contributors, and the faculty of the Department of Civil Engineering of the university, with the leadership of Professor Luis Simões da Silva as chairman for several years, has been very active in the development of solutions to many technical problems. In particular, Professor da Silva and his colleagues have conducted extensive studies of the performance of steel and composite frames and bridges, connections for steel structures, response of steel structures to fire effects, strength and performance of wind towers for the energy industry, and extensive evaluations of sustainability.

In a development that is somewhat similar to the research centers of the National Science Foundation in the United States, the national research foundation of Portugal provided funding in 2007 for the establishment of the Institute for Sustainability and Innovation in Structural Engineering (ISISE), to be operated as a joint effort of the University of Coimbra and the University of Minho. Administratively, the institute was organized into three research areas: (1) steel and mixed construction technology, (2) structural concrete and (3) historical and masonry structures. With strong research groups in various areas, the University of Coimbra will focus on area 1, the University of Minho will focus on area 3 and area 2 will be shared by the two institutions. Researchers from related university areas will also participate, to the effect that support will be provided from architectural, mechanical and metallurgical engineering.

Reidar Bjorhovde, Dr.-Ing., Ph.D., P.E., Research Editor of the *Engineering Journal.* Tucson, AZ. Email: rbj@bjorhovde.com

For steel and composite construction at Coimbra, particular emphasis has been placed on behavior and strength of connections as well as members and structures, including fire and other extreme effects; and sustainability; life-cycle engineering; and monitoring and maintenance. Bridges, buildings and special areas of construction such as wind towers form the central activities. The research team includes 13 faculty members, 10 collaborators from other university departments and industry, 2 technicians and 28 doctoral graduate students. The physical testing facilities are excellent.

Economical and Safe Design of Steel Joints Subjected to Natural Fires: This three-year project (2009–2012) is sponsored by the European Commission, with a total budget of €1.7 million ($2.5 million), and is shared among the University of Coimbra as the lead institution, receiving €300,000 ($430,000); the University of Manchester, United Kingdom; the Technical University of Luleå, Sweden; the Technical University of Prague in the Czech Republic; and Corus Tubes, United Kingdom. The project director is Professor Luis da Silva.

The research work has focused on the development of component-based design methods for composite connections, in particular connections between composite beams and columns. Composite columns in European design practice are most commonly concrete-filled hollow structural sections (HSS) or partially encased open sections. The intent is that the connections will be designed to the same level of fire resistance as the frame, adhering to the requirements of Eurocode 3, Part 1-2 (CEN, 2005b; Franssen and Vila Real, 2010).

Numerical models have been developed, and fire tests have been conducted with components, individual connections, structural subassemblages and demonstration structures. As an example, Figure 1 shows the model for the assemblage of a steel beam and a concrete-filled HSS while subjected to the high temperatures of a natural fire (Carvalho Lopes et al., 2010).

Robustness of Car Parks against Localized Fire: This three-year project (2008–2011) is sponsored by the European Commission with a total budget of €1.3 million ($1.9 million), of which €250,000 ($360,000) is for Coimbra. The funding is shared among the University of Liège in Belgium as the lead institution; the University of Coimbra; Imperial College, London; ArcelorMittal, Luxembourg; CSTB and CTICM, France; and Greisch Ingenierie, Belgium.

It is interesting to note that steel has not been the construction material of choice for parking garages in Europe, which has been a recurring issue in the United States (although it is less of an issue than 40 years ago). In Europe the particular problem has been the response of garage structures to highly localized fires, which was the specific problem that led to the full scale fire test in a parking garage in Scranton, Pennsylvania, in 1972 (Gage-Babcock et al., 1973; Harris, 1979).

The project aims at developing a general philosophy for the design of robust structures for "exceptional" events, to include practical guidelines. Examples of the testing that is being done for composite structures are given in Figures 2

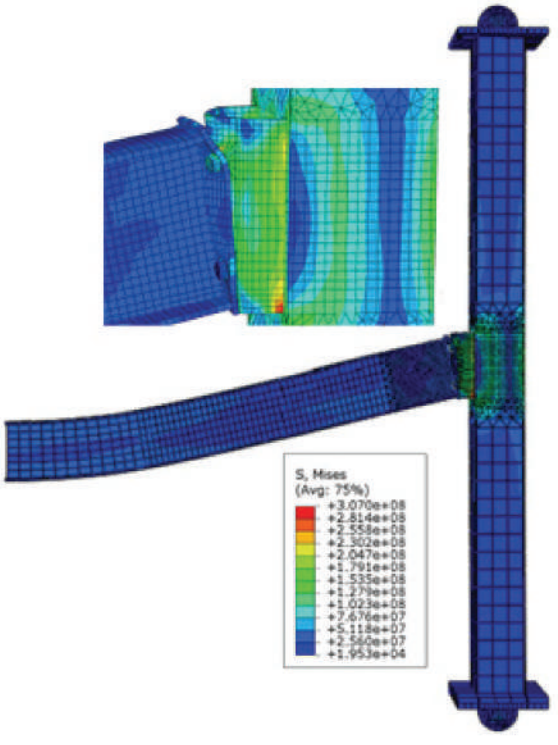

Fig. 1. Subassemblage model of steel beam and HSS composite column. (Figure courtesy of Professor Luis da Silva)

Fig. 2. Fire testing of a full-scale beam-to-column connection. (Figure courtesy of Professor Luis da Silva)

and 3, which show a connection being tested for fire temperatures (Figure 2) and the testing of an assemblage that includes the connection of Figure 2, as well as the two-span slab that is part of the original frame (Figure 3) (Haremza et al., 2011).

Fig. 3. Fire testing of a structural composite subassemblage. (Figure courtesy of Professor Luis da Silva)

Sustainable Steel and Composite Bridges in the Built Environment: This three-year project (2009–2012) is sponsored by the European Commission with a total budget of €1.5 million ($2.2 million), of which €280,000 ($400,000) is for Coimbra. The budget is shared among the University of Stuttgart in Germany as the lead institution; the University of Coimbra; LCPC—Laboratoire Centrale des Ponts et Chaussées, France; SETRA, France; BAST, Germany; ArcelorMittal, Luxembourg; Dillinger Hüttenwerke, Germany; Ramböll, Sweden; and Brisa, Portugal. The project director is Professor Ulrike Kuhlmann, University of Stuttgart.

The project focuses on the development and presentation of well-defined sustainability benefits of composite highway bridges, including highly effective and advanced structures and systems and cost-effective and environmentally friendly construction with long-life structures. A holistic approach is used, combining life-cycle assessment, life-cycle costing and life-cycle performance analyses to demonstrate the advantages of steel for bridges. As an example, Figure 4 gives a flowchart for the various operations of a life-cycle analysis (Gervásio and da Silva, 2010).

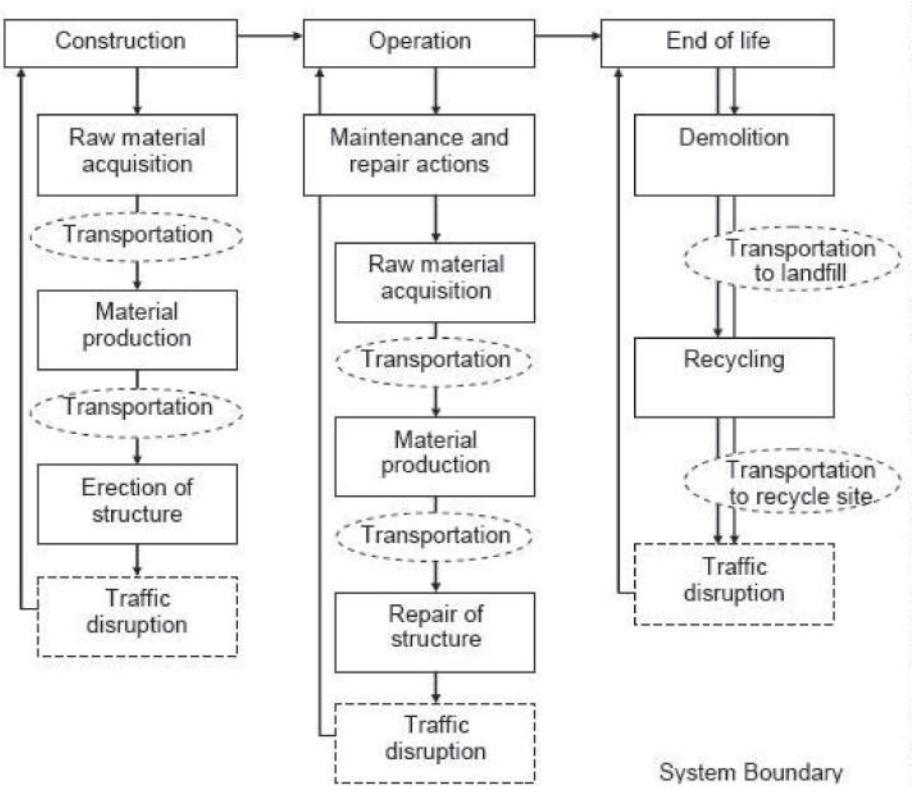

Fig. 4. Flowchart for life-cycle analysis. (Figure courtesy of Dr. Helena Gervásio)

High-Strength Steel Towers for Wind Turbines: This is a very major project that has been funded by the European Commission for two 3-year periods (2006–2009 and 2010–2013). The total financial support is €2.7 million ($3.9 million), with €434,000 ($630,000) allocated for Coimbra, with the Technical University of Luleå of Sweden as the lead institution. The other project participants are the University of Aachen in Germany; the University of Coimbra; the University of Thessaloniki, Greece; Martifer Energy Systems, Portugal; Rautaruukki, Finland, and Germanischer Lloyds, Germany. The project director is Professor Milan Veljkovic of the Technical University of Luleå.

The overall objective of the projects has been to demonstrate and improve the competitiveness of steel towers to support multi-megawatt wind turbines. The optimized design of a steel tower is based on an analysis of the criteria that govern wind tower design. Specifically, fatigue is a major consideration, and a more economical design would involve the use of high strength steel. One solution provides for an improvement of the flange detail that has traditionally been used to splice tower segments. Another suitable splice solution would be to use a friction type (slip-critical) joint to allow higher strains in the shell (Veljkovic et al., 2010; Matos et al., 2011). Another design limitation is the potential for the shell buckling that may take place in the tower wall, for which the strength is strongly related to geometric imperfections. New solutions for steel and hybrid tower stability and using foundations with steel micropiles are being developed. A bolted connection for the tower splice will be used, as illustrated in Figure 5.

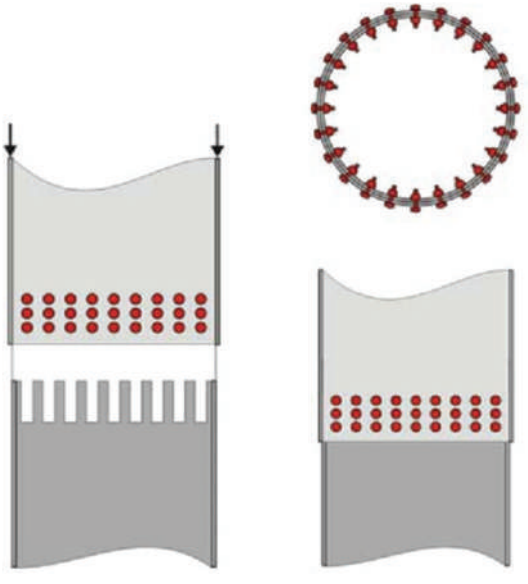

Fig. 5. Bolted slip-critical splice for a wind tower. (Figure courtesy of Professor Luis da Silva)

SOME CURRENT RESEARCH WORK AT KARLSRUHE INSTITUTE OF TECHNOLOGY IN KARLSRUHE, GERMANY

The University of Karlsruhe, one of the old, excellent German universities, educated large numbers of engineers and conducted extensive research in all areas of engineering and science. A few years ago, the government of Germany conducted an evaluation of its universities and identified certain institutions as being particularly capable. The University of Karlsruhe was one of a very small number of schools that was designated as an *elite university,* and thus the name of the institution was changed to Karlsruhe Institute of Technology (KIT). The research teams of some of the engineering departments subsequently changed their names to specific centers, and the KIT Research Center for Steel, Timber and Masonry (RCSTM) is now the unit that addresses all study subjects in these areas. Professor Thomas Ummenhofer is the director of the RCSTM.

The research and laboratory staffs are substantial, without giving a number of positions here. Laboratory and computing facilities are excellent, including a very high-capacity universal testing machine.

Detection of Cracks in Steel Components by Means of Ultrasound Excited Thermography: This project has been sponsored by the German Research Foundation. The director is Professor Thomas Ummenhofer; the primary researcher has been Dipl.-Ing. Robin Plum.

Detection of cracks in steel members and connections is a significant issue for many types of structures, whether the cracks have been caused by fatigue-type loading, fabrication techniques or other effects. Once the cracks have been identified, the possible solutions are generally fairly well defined, whether specific repairs are needed (or not, as the case may be) or whether changes in design methods and approaches may be warranted.

Developments over the last several years have indicated that active thermography methods—specifically, ultrasound applications of the technique—may be particularly suitable for structural purposes. Rubbing or "clapping" of crack surfaces as prompted by sound waves in the medium produces heat, which can be detected by an infrared camera. The equipment and applications of the procedure are illustrated in Figure 6. This is the primary focus of the current KIT project, to be applied to heavy structural members. Figure 7 shows an application of the method to detect a fatigue crack in a heavy rolled shape (IPE 500).

The primary objective is to determine the depth of the crack. In addition, it is important to determine the ultrasound frequency and the crack opening displacement, which can then be correlated to the state of prestressing (Plum and Ummenhofer, 2009). Finally, finite element simulations of the thermographic structural problem are developed to assess

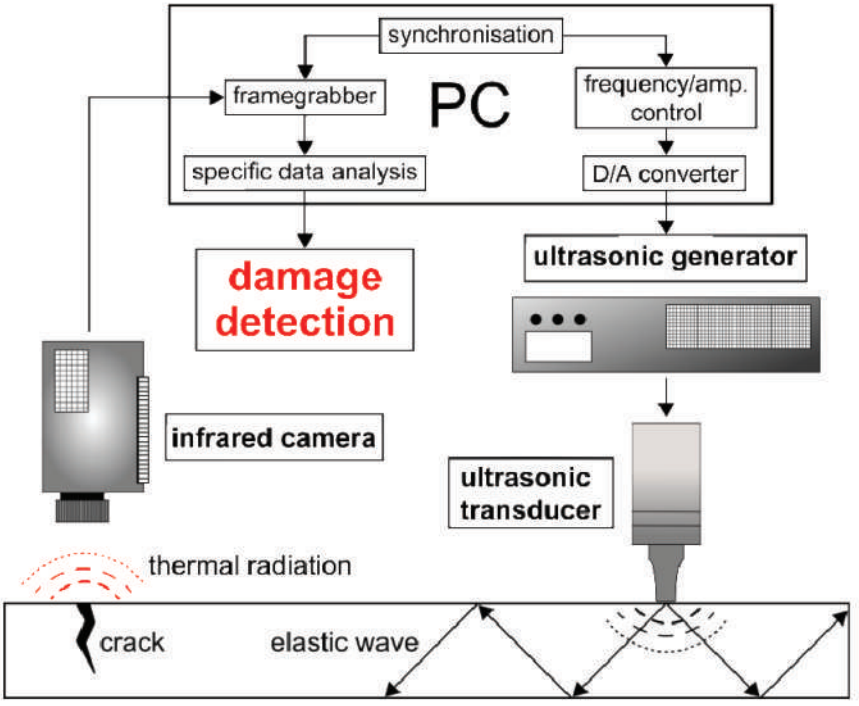

Fig. 6. The principle of ultrasound excited thermography. (Figure courtesy of Professor Thomas Ummenhofer)

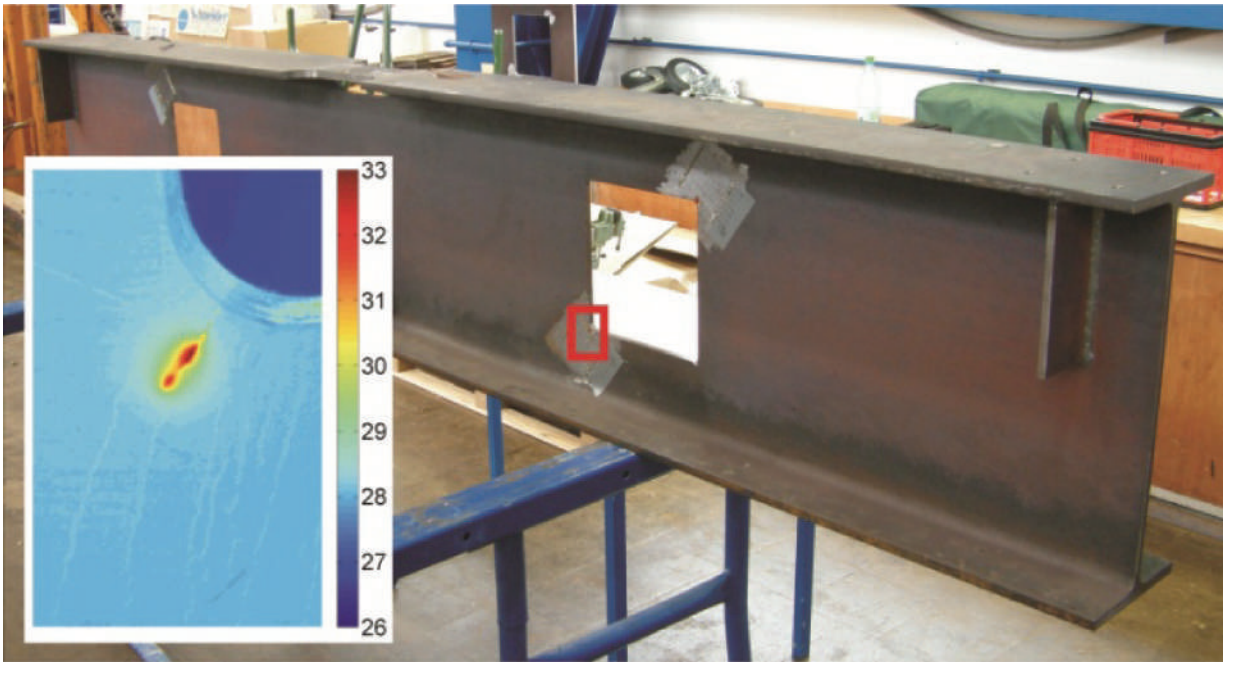

Fig. 7. Thermographic detection of a fatigue crack in a heavy-girder IPE 500. (Photograph courtesy of Professor Thomas Ummenhofer)

the accuracy of the experimental results and to improve the understanding of the physical effects of the process (Plum and Ummenhofer, 2010).

Adhesive Bonded Cast Steel—Structural Steel Connections: This project has been sponsored by the German Federation of Industrial Research Associations. It has been managed by KIT in cooperation with the University of Applied Sciences of Munich and the Fraunhofer Institute for Manufacturing Technology and Advanced Materials. The director is Professor Thomas Ummenhofer; the primary researcher has been Dipl.-Ing. Matthias Albiez.

Tubular members are being used for many structural applications, and the connections are often very complex and almost always have to be welded. For bridges and certain industrial applications, the complexity of the welded joints may promote fatigue cracking, and the cracks are often discovered only after the structure has been completed. Attempting to avoid complex welds, the project aims to develop connection solutions that utilize cast details of tubes and other shapes, and welds will be replaced by adhesive connections. This avoids the high temperatures associated with welding as well as the shrinkage that accompanies weld cooling. Providing cast steel details that allow for more uniform stress distributions and gradual force transfers between the connection elements, the solution with adhesives is likely to resolve a number of fabrication and structural performance issues.

The project will address the following subjects:

1. The adhesives currently available will be evaluated to determine their ability to satisfy the "boundary conditions" for the joints, including conditions for curing, strength and force transfer across the joint. The long-term stability of the adhesive will also be examined, including any organic effects.
2. A manufacturing process will be developed that uses a semi-automatic injection device that is suitable for the deposit of the adhesive in the (often narrow) gap between a cast node and the HSS. It is anticipated that the HSS sizes will range from 100 to 500 mm in diameter (4 to 20 in.).
3. The strength and behavior of the adhesively bonded joint will be determined for static, dynamic and thermal loads, including aging effects.
4. Above all, a joint will be developed that provides the necessary redundancy and alternate load paths in the case of a local failure.
5. Practical design approaches will be developed.

An example of a potential joint is shown in Figure 8.

Optimization of Supporting Structures for Offshore Wind Energy Converters: This project has been sponsored by the German Federation of Industrial Research Associations. It has been managed by KIT in cooperation with the Federal Institute for Materials Research and Testing (BAM) of Germany. The director is Professor Thomas Ummenhofer; the primary researcher has been Dipl.-Ing. Philipp Weidner.

Foundation structures for offshore structures in general and now also for the wind farms that are being developed in many areas of the world need novel evaluations of their strength and behavior. The structures have to be designed for all of the relevant offshore effects, including fatigue, for the often very heavy, elaborate and complicated joints. The project will examine all of these procedures, including tower construction and methods of maintenance. Underwater repair of welds must also be taken into account; it is anticipated that such will often be conducted using the HiFIT device developed at KIT. The device uses post-weld high-frequency hammer peening of the weld toe to reduce residual stresses and thus improve the performance of the weld. Material thicknesses in the range of 30 to 60 mm (1¼ to 2⅜ in.) are anticipated for the structures; the analysis and repair procedures will be evaluated for short- and long-term performance. Figure 9 shows various typical tower support and mast solutions.

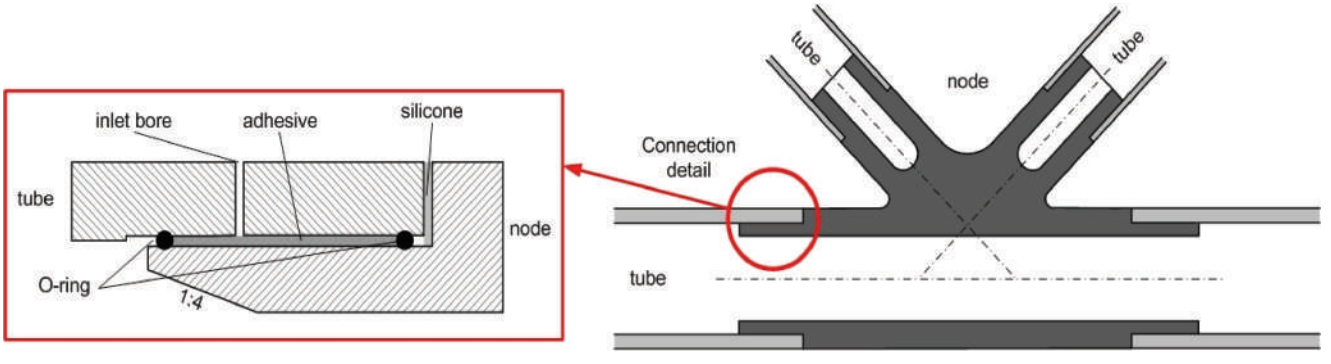

Fig. 8. Potential connection detail with cast steel elements and adhesive joints. (Figure courtesy of Professor Thomas Ummenhofer)

SOME CURRENT RESEARCH WORK AT THE UNIVERSITY OF NAPLES, FEDERICO II, IN NAPLES, ITALY

The University of Naples, Federico II, is one of the premier universities in Europe for the study of seismic effects. For many years Professor Federico Mazzolani conducted extensive evaluations of the seismic performance and strength of steel connections and frames as well as bridges; he has also done major studies of aluminum structures. For all practical purposes, he was the "father" of Eurocode 8 (CEN, 2004), the seismic design code for European countries, and has provided numerous links with industry and the code developers in North and South America as well as Asia. Now retired, his successor is Professor Raffaele Landolfo, who continues to lead an aggressive research and development effort.

High-Strength Steel in Seismic-Resistant Building Frames: This is a major three-year (2009–2012) project that has been funded by the Research Fund for Coal and Steel of the European Commission. The work is carried out as a joint effort among numerous European universities, led by the University of Naples, Federico II. The partners are the University of Timisoara, Romania; the University of Liège, Belgium; the University of Stuttgart, Germany; and the University of Ljubljana, Slovenia, along with a number of industry participants from various European countries. The project director is Professor Raffaele Landolfo.

Using typical multi-story frames in mild steel and high-strength steel, the mild steel is used for elements and connections that will serve as the major sources of ductility and energy absorption for the frames. The high-strength elements are used for members that will supply the principal portions of the elastic strength of the frames. The major activities of this project can be summarized as follows:

1. Select suitable structural systems and provide the designs of the frames.
2. Evaluate the seismic performance of the frames.
3. Assess the welding needs for the connections and other elements of the structures, taking into account the seismic performance requirements.
4. Perform prequalification tests of moment-resistant bolted beam-to-column connections.
5. Perform prequalification tests of moment-resistant welded beam-to-column connections.
6. Develop guidelines for conceptual design and performance-based design of the steel frames with members and connections in two steel grades.
7. Evaluate the technical and economical efficiency of the designs with two steel grades as compared to designs using a single grade of steel.

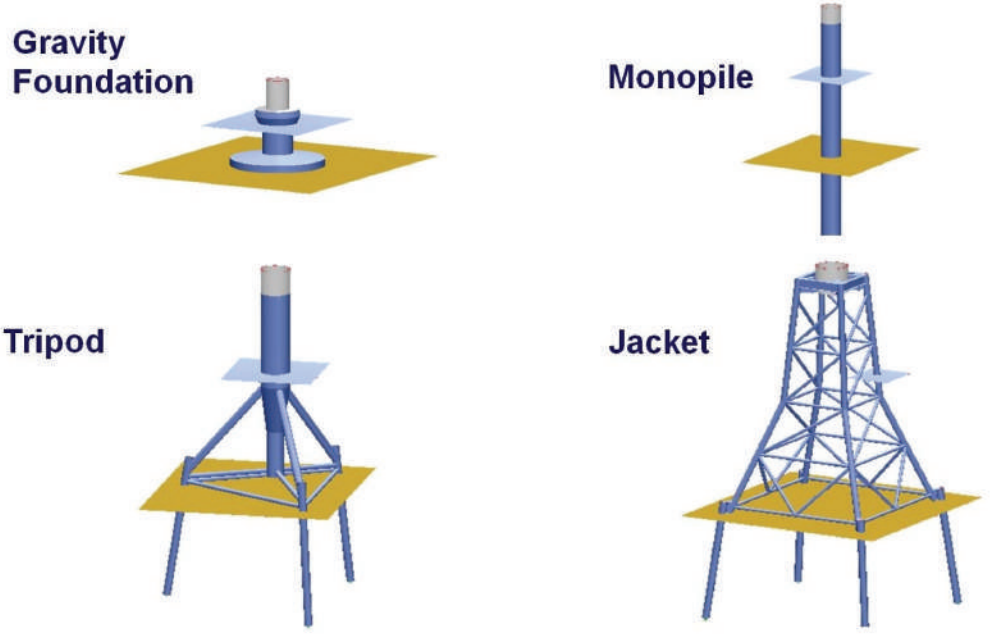

Fig. 9. Various offshore wind tower underwater structures. (Figure courtesy of Professor Thomas Ummenhofer)

The primary efforts of the University of Naples, Federico II, focus on the design and numerical analyses of a comprehensive set of frames combining two grades of steel. The performances of moment-resistant frames (MRF), concentrically braced frames (CBF), eccentrically braced frames (EBF) and dual MRF and CBF as well as dual MRF and EBF are examined.

The designs have been force-based, using the criteria of Eurocode 8, with special evaluations where the designs fail the requirements of EC8 (CEN, 2004): (1) the influence of ground-motion characteristics on ductility demands and (2) estimating the strength requirements for the nondissipative (elastic) structural members. It is anticipated that improved design procedures will be developed for frames with multiple grades of steel, taking into consideration the performance abilities of the various elements of the frames (Tenchini et al., 2011; Cermelj and Beg, 2011; Comeliau et al., 2011).

Displacement-Based Seismic Design of Steel Structures: This is a major three-year (2010–2013) project that has been funded by the Research Fund for Coal and Steel of the European Commission. The work is carried out at the University of Naples, Federico II. The project director is Professor Raffaele Landolfo.

The use of displacement-based design (DBD) methods and codes has been explored by numerous researchers over the years (Priestley et al., 2007). It is felt that a successful implementation offers the best approach to arrive at practical performance-based design criteria—in lieu of the force-based approaches that are common today. The DiSTEEL project, as it is called at the University of Naples, Federico II, aims at developing a suitable DBD procedure and performance criteria for moment-resisting frames with various types of beam-to-column connections. Thus, full-strength moment (rigid) connections, full-strength flexible connections and partial strength bolted connections will form the original basis, as illustrated in Figure 10. The connection classifications will be done in accordance with the criteria of Eurocode 3 (CEN, 2005a).

Figure 11 illustrates the fundamental characteristics of the DDBD method (Priestley et al., 2007). Significant additional research work is being conducted, but much must still be explored for the most suitable approaches (Della Corte et al., 2010).

The DiSTEEL project is organized in accordance with four primary areas:

1. A detailed review of the literature will be performed to collect experimental data. The data will be classified such that it will be possible to identify how the hysteretic behavior is influenced by the connection details.
2. The experimental data will be examined and codified according to Eurocode 3 and by finite element models. This information will be used to develop simple design-oriented equations that can be used to determine the magnitudes of the connection rotations at the yield and ultimate limit states.
3. Sample moment-resisting frames will be designed in accordance with the codified force-based procedures and the direct DBD (DDBD) method that has been developed. The results will be used to validate the DDBD.
4. Nonlinear dynamic analyses will be performed for the sample frames in order to determine the reliability and efficiency of the DDBD method as contrasted with current force-based procedures.

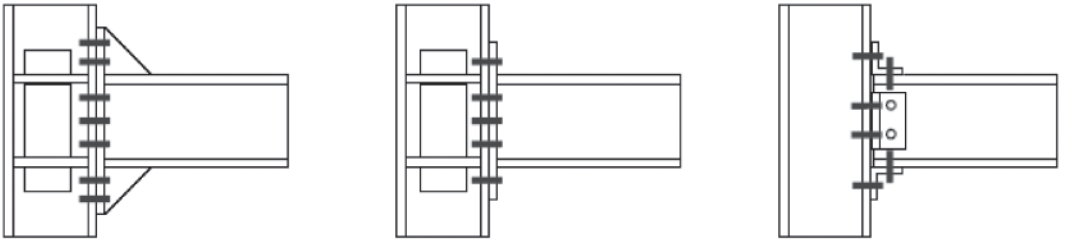

Fig. 10. Beam-to-column connections to be used in the DiSTEEL analyses: (a) full-strength rigid joints; (b) full-strength flexible joints; (c) partial-strength joints. (Figure courtesy of Professor Raffaele Landolfo)

Laboratories University Network of Seismic Engineering: This is a major three-year (2010–2013) project that has been funded by the Civil Protection Department of the government of Italy.

The network is a consortium of 10 Italian universities that conduct research in seismic engineering. The aim is to provide advice to various government and other institutions with regard to seismic issues, dealing with all aspects of new and old construction, seismic risk and damage following earthquakes, and to assess the efficiency of new tools of design and construction.

The consortium involves several research units; the operation headed by Professor Landolfo focuses on extending the current seismic regulations and codes to cold-formed steel systems (Landolfo et al., 2010). The following are the principal areas of effort:

1. Numerical and experimental studies will be performed to assess the local behavior of cold-formed profiles, connections, panels and walls.
2. The results of the numerical analyses will be evaluated by a parametric study to determine the seismic behavior of elements of various geometries, materials and seismic input.
3. Upgraded specifications and design tools that are suitable for use by designers will be developed. For example, seismic design procedures that will allow shear wall components to be defined in a few steps are likely to be very useful to industry.

ACKNOWLEDGMENTS

Significant assistance has been provided by International Structural Steel Research Advisors (ISSRA) members Professors Luis da Silva, University of Coimbra, and Dinar Camotim, Technical University of Lisbon. In addition, the efforts of Professors Raffaele Landolfo and Federico Mazzolani of the University of Naples, Federico II, and Professors Thomas Ummenhofer and Ram Puthli of the Karlsruhe Institute of Technology have been sincerely appreciated.

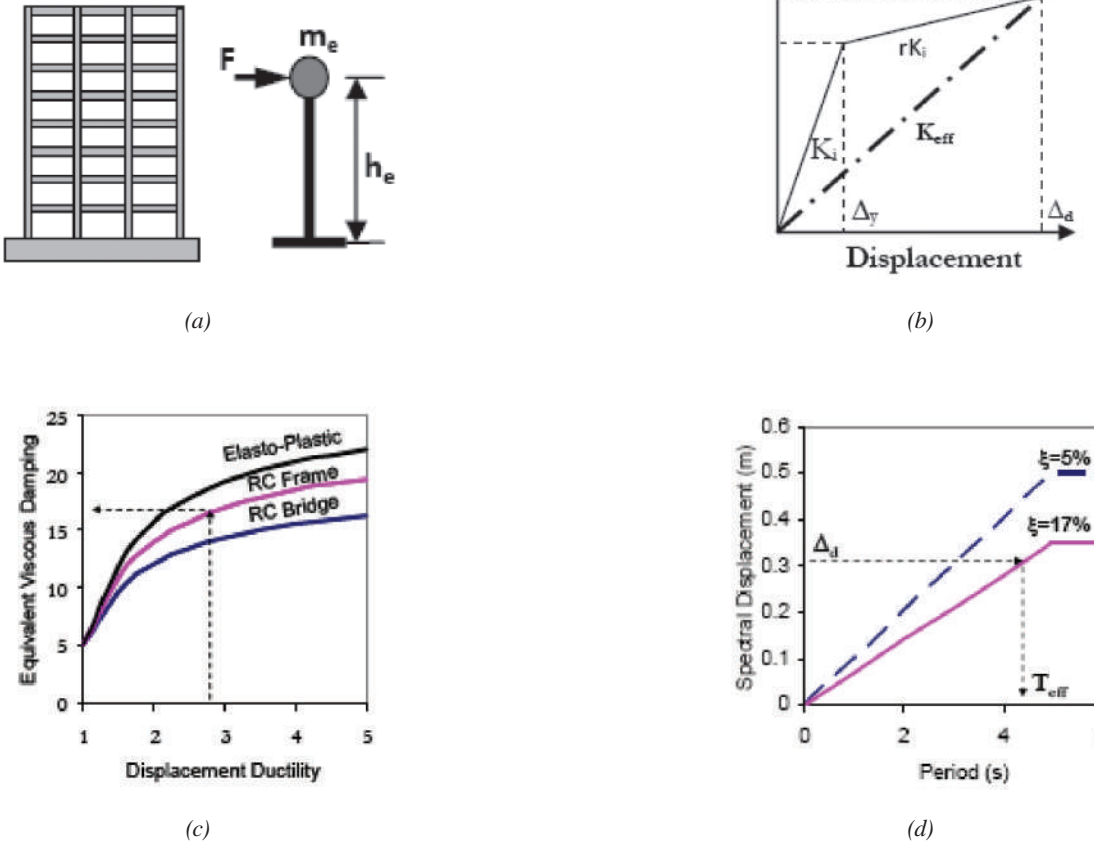

Fig. 11. Characteristic features of the direct displacement-based design method: (a) SDOF representation; (b) effectiveness, k_{eff}*; (c) equivalent viscous dampling; (d) dispacement spectrum. (Figure courtesy of Professor Raffaele Landolfo)*

REFERENCES

Carvalho Lopes, F.R., Santiago, L., Simões da Silva, L. and Santos da Silva, J.G. (2010), "Numerical Assessment of Structural Assembly between Steel Beam and CFT Column under Fire," *Proc. Urban Habitat of Constructions under Catastrophic Events* (COST C26 Workshop, Naples, Italy), CEN, Brussels, Belgium.

CEN (2004), *Eurocode 8: Design of Structures for Seismic Resistance—Part 1: General Rules, Seismic Actions and Rules for Buildings*, Comité Européen de Normalisation, Brussels, Belgium.

CEN (2005a), *Eurocode 3: Design of Steel Structures—Part 1-1: General Rules and Rules for Buildings*, Comité Européen de Normalisation, Brussels, Belgium.

CEN (2005b), *Eurocode 3: Design of Steel Structures—Part 1-2: Structural Fire Design*, Comité Européen de Normalisation, Brussels, Belgium.

Cermelj, B. and Beg, D. (2011), "Numerical Analysis of Welded Stiffened and Welded Cover-Plate Beam-to-Column Joints with Fully Encased Wide-Flange Columns," *Proc. Eurosteel 2011,* August 30–September 2, Budapest, Hungary.

Comeliau, L., Demonceau, J.F. and Jaspart, J.F. (2011), "Non-Dissipative Joints in Seismic Resistant Building Frames Bolted Beam-to-Column Joints," *Proc. Eurosteel 2011,* August 30–September 2, Budapest, Hungary.

Della Corte, G., Landolfo, R. and Mazzolani, F.M. (2010), "Displacement-Based Seismic Design of Braced Steel Structures," *Steel Construction—Design and Research*, Vol. 3, September, pp. 134–139.

Franssen, J.-M. and Vila Real, P. (2010), *Fire Design of Steel Structures*, Eurocode Design Manuals, European Convention for Constructional Steelwork (ECCS), Brussels, Belgium.

Gage-Babcock & Associates (1973), "Automobile Burn-Out Test in an Open-Air Parking Structure," Report No. 7328, Gage-Babcock and Associates, Westchester, IL.

Gervásio, H. and Simões da Silva, L. (2010), "Lifetime Analysis of Highway Composite Bridges," *Proc. International Symposium on Steel Structures: Culture and Sustainability,* September 21–23, Istanbul, Turkey.

Haremza, C., Santiago, A. and Simões da Silva, L. (2011), "Experimental Behaviour of Heated Composite Joints Subject to Variable Bending Moments," *Proc. Eurosteel 2011,* August 31–September 2, Budapest, Hungary.

Harris, Leslie (January 1979), "1979 Update of the Survey of Fire Experience in Automobile Parking Structures in the United States and Canada," Marketing Research Associates, Teaneck, New Jersey.

Landolfo, R., Fiorino, L. and Iuorio, O. (2010), "A Specific Procedure for Seismic Design of Cold-Formed Steel Housing," *Advanced Steel Construction*, Vol. 6, No. 1, pp. 603–618.

Matos, R., Fontoura, B., Rebelo, S., Jesus, A., Veljkovic, M. and Simões da Silva, L. (2011), "Fatigue Behaviour of Steel Friction Connections—Experimental and Numerical Results," *Proc. Eurosteel 2011,* August 31–September 2, Budapest, Hungary.

Plum, R. and Ummenhofer, T. (2009), "Ultrasound Excited Thermography of Thick-Walled Steel Load-Bearing Members," *QIRT Journal*, Vol. 6, No. 1, pp. 79–100.

Plum, R. and Ummenhofer, T. (2010), "Structural-Thermal FE Simulation of Vibration and Heat Generation of Cracked Steel Plates due to Ultrasound Excitation Used for Vibrothermography," *Proc. QIRT Conference 2010,* Quebec, Canada, pp. 763–770.

Priestley, M.J.N., Calvi, G.M. and Kowalski, M.J. (2007), *Displacement-Based Design of Structures*, IUSS Press, Pavia, Italy.

Tenchini, A., Rebelo, C., da Silva, L., Serra, M., Landolfo, R. and D'Aniello, M. (2011), "Seismic Performance of High Strength Steel Building: Dual-Frame Analysis," *Proc. Eurosteel 2011,* August 31–September 2, Budapest, Hungary.

Veljkovic, M., Feldmann, M., Naumers, J., Pak, D., Rebelo, C. and Simões da Silva, L. (2010), "Friction Connections in Tubular Towers for Wind Turbines," *Stahlbau*, Vol. 79, No. 9, pp. 660–668, in German.

GUIDE FOR AUTHORS

SCOPE: The ENGINEERING JOURNAL is dedicated to the improvement and advancement of steel construction. Its pages are open to all who wish to report on new developments or techniques in steel design, research, the design and/or construction of new projects, steel fabrication methods, or new products of significance to the uses of steel in construction. Only original papers should be submitted.

GENERAL: Papers intended for publication may be submitted by mail to the Editor, Keith Grubb, ENGINEERING JOURNAL, AMERICAN INSTITUTE OF STEEL CONSTRUCTION, One East Wacker Drive, Suite 700, Chicago, IL, 60601, or by email to grubb@aisc.org.

The articles published in the *Engineering Journal* undergo peer review before publication for (1) originality of contribution; (2) technical value to the steel construction community; (3) proper credit to others working in the same area; (4) prior publication of the material; and (5) justification of the conclusion based on the report.

All papers within the scope outlined above will be reviewed by engineers selected from among AISC, industry, design firms, and universities. The standard review process includes outside review by an average of three reviewers, who are experts in their respective technical area, and volunteers in the program. Papers not accepted will not be returned to the author. Published papers become the property of the American Institute of Steel Construction and are protected by appropriate copyrights. No proofs will be sent to authors. Each author receives three copies of the issue in which his contribution appears.

MANUSCRIPT PREPARATION: Manuscripts must be provided in Microsoft Word 2003 format. A laser-quality proof or high quality PDF must accompany your submittal. Download our complete author guidelines at **www.aisc.org/ej**.

There's always a solution in steel.

ENGINEERING JOURNAL
American Institute of Steel Construction
One East Wacker Drive, Suite 700
Chicago, IL 60601

312.670.2400 www.aisc.org